Western Australia Salt Lakes

ΕΛΛΗΝΙΚΗ
ΕΠΙΣΤΗΜΟΝΙΚΗ
ΕΤΑΙΡΕΙΑ
ΕΔΑΦΟΜΗΧΑΝΙΚΗΣ
& ΓΕΩΤΕΧΝΙΚΗΣ
ΜΗΧΑΝΙΚΗΣ

Τα Νέα της Ε Ε Ε Ε Γ Μ

144

Αρ. 144 – ΝΟΕΜΒΡΙΟΣ 2020

SIMSG ISSMGE

ISRM

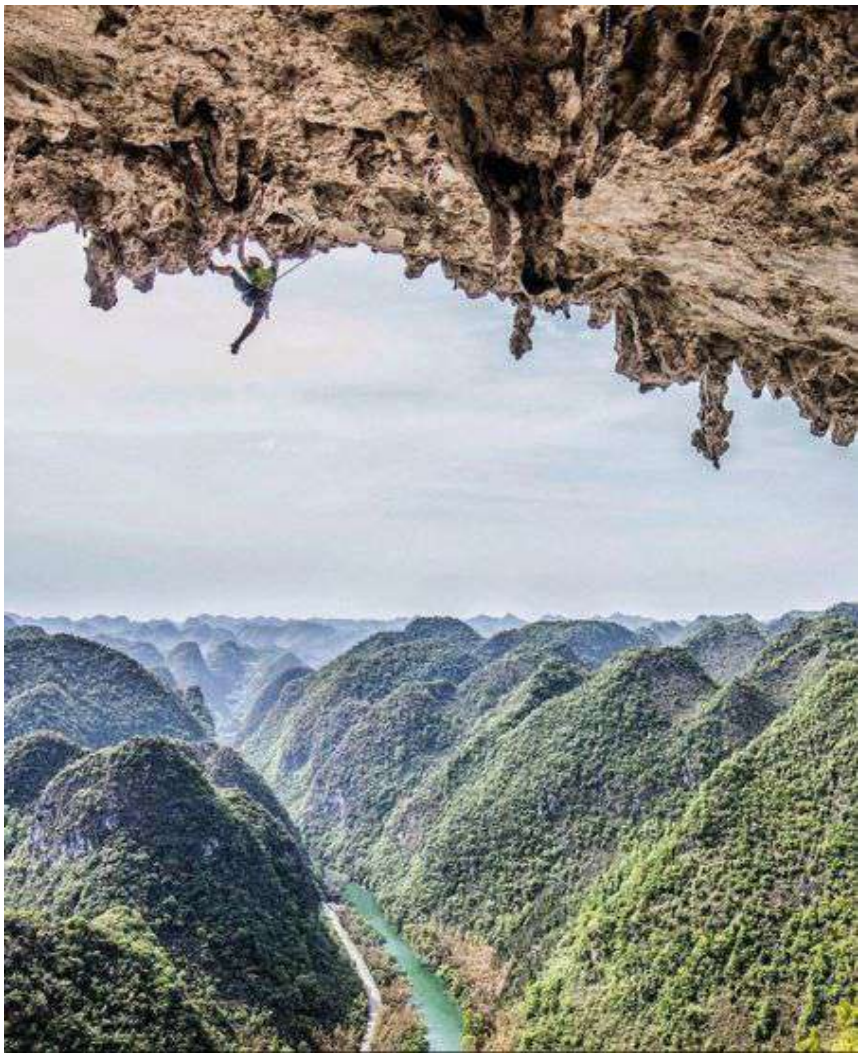

Getu, China, home of one of the longest, hardest cave climbing routes in the world

Π Ε Ρ Ι Ε Χ Ο Μ Ε Ν Α

ΣΕΙΣΜΟΣ ΣΑΜΟΥ - ΣΜΥΡΝΗΣ

Fault responsible for Samos earthquake identified

Preliminary data indicate that the fault that ruptured in the Samos earthquake slipped 6 feet (1.8 meters)

Athanassios Ganas, Panagiotis Elias, Pierre Briole, Varvara Tsironi, Sotiris Valkaniotis, Javier Escartin, Ilektra Karasante, Eirini Efstathiou

Summary

On October 30, 2020 11:51 UTC, a strong shallow earthquake rocked the eastern Aegean Sea. The epicenter was located offshore of the Greek island of Samos, about 160 miles (260 kilometers) to the East of Athens. The earthquake was a magnitude-6.7 on the Richter Scale according to the National Observatory of Athens (NOA). The effects of the earthquake were devastating in Greece and Turkey. In Greece, two young children lost their lives from a wall collapse in the town of Vathy, eastern Samos. In Turkey, more than 100 people died from multiple building collapses in the city of Izmir about 40 miles (60 kilometers) to the north of the epicenter.

Here we present a first analysis of the geodetic data that were gathered and processed as of Nov. 4, 2020 15:00 UTC. Our preliminary modeling indicates that the rupture occurred on a 23-mile long (37 kilometer) north-dipping tensional ('normal') fault located off the northern shore of Samos.

InSAR is a form of imagery collected by repeating passes of a radar satellite over an area. The technique is used to measure how much the ground has moved roughly vertically between each pass of a satellite and can give scientists a clue as to how much slip occurred on a fault beneath the surface. In this case, the fault that ruptured in the Samos earthquake slipped 6 feet (1.8 meters). The upper edge of the fault rupture — the part of the fault that slipped closest to the surface, is at a shallow depth of 0.9 miles (1.5 kilometers) near the northern shore of Samos.

Introduction

The Samos area is located in eastern part of the Aegean (Eurasia) microplate, a well-known extensional, back-arc area behind the Hellenic subduction (McKenzie, 1978; Ganas and Parsons, 2009). The kinematics of the plate motions are determined by the subduction of the African oceanic plate under the Aegean and the westwards motion of the Anatolian microplate. Crustal extension is accommodated by a combination of normal-slip and strike-slip motions along active faults, especially in central Aegean and western Anatolia (Mascle and Martin, 1990; Taymaz et al. 1991; Tan et al. 2014). In terms of strain, the amount of crustal extension between Samos and western Anatolia (the broader Izmir area) is 7.4 mm/yr according to Vernant et al. (2014) based on GNSS data modeling.

The Mw=7.0 earthquake of Oct. 30, 2020 11:51 UTC occurred north of the island of Samos (Fig. 1), along a E-W striking normal fault as indicated by the moment tensor solutions of both regional and teleseismic data (compiled by EMSC). Through Nov. 2, 2020 more than 776 aftershocks (with 2.0≤ML≤5.2) were recorded by EMSC (Fig. 2). Three hours after the mainshock, a moderate-size Mw = 5.2 aftershock struck at 15:14 UTC. The moment tensor solutions of the mainshock indicate E-W to ESE-WNW normal faulting in agreement with the regional, extensional tectonics. The aftershock sequence extends over a distance of 70-km east-west with most of events occurring to the east of the mainshock (Fig. 2). The EMSC aftershock data (the longitude vs time plot; in days from main shock) show that the sequence is spatially constrained between 26.4°E – 27.2°E (Fig. 2 middle panel).

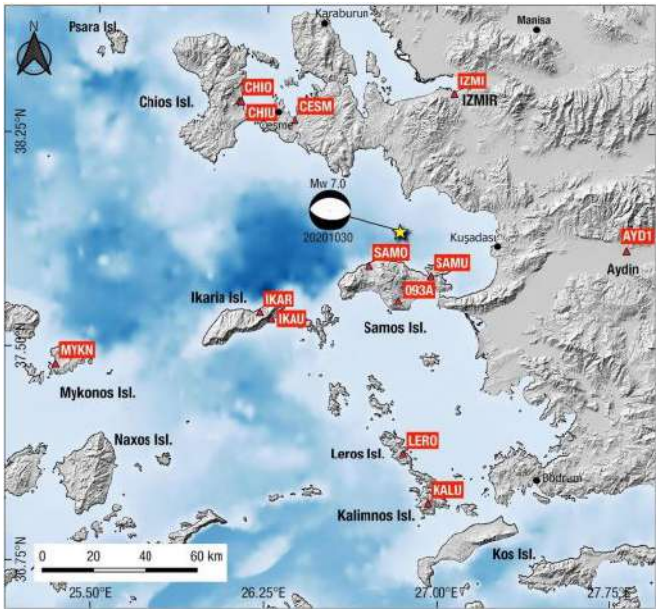

Fig.1: Location map showing shaded topography/bathymetry, the focal mechanism (beachball; GCMT solution) and the epicenter of the Samos October 30, 2019 earthquake. Triangles indicate permanent GPS (GNSS) station locations.

Sentinel-1 Interferogram

We used the ascending images acquired by the European satellites Sentinel-1 on October 24 and October 30, 2020 on the track 131. The interferogram (Fig. 3) was made on the Geohazards Exploitation Platform using the SNAP software. The digital elevation model (DEM) used for the processing is the Shuttle Radar Topography Mission (SRTM) 1 Arc-Second Global. We enhanced the signal to noise ratio by applying the adaptive power spectrum filter of Goldstein and Werner (1998) with a coherence threshold of 0.3. The quality of the interferogram is good, both in terms of coherence and tropospheric noise. The interferogram shows fringes corresponding to ground deformation onshore Samos. The absolute value of the interferometric fringes is estimated by the tie to the GNSS stations SAMO and SAMU (Fig. 1) that captured the co-seismic displacement. All fringes correspond to motion towards the satellite except the short northern one located by the coast where the motion is away from the satellite. We extracted the line of sight (l.o.s) displacements by picking the six fringes on Fig. 3 at 64 locations in total. The uplift is interpreted a result of co-seismic motion along an offshore normal fault, running E-W and dipping to the North.

Co-seismic motion of the GNSS stations

We analyzed the data of eleven GNSS stations belonging to two Greek private networks, SmartNet and Uranus, and from the Turkish network CORS (Fig. 1). The processing was made using two different Precise Point Positioning (PPP) software: the GIPSY/OASIS II software (ver. 6.4) developed by the Jet Propulsion Laboratory (JPL), and the Canadian online processing PPP service. The coseismic displacements are listed in Tab. 1, and Fig. 4 shows the time series at SAMO (Karlovasi). We could not see in the GNSS data evidence for any rapid post-seismic deformation, and in particular there is no

offset at the time of the large aftershock on Oct. 30, 2020 15:14 UTC (M=5.2). Consequently, because the second Sentinel-1 image was acquired in the afternoon of Oct. 30, shortly after the event, we assume that the interferogram (Fig. 2) contains coseismic signal only with insignificant post-seismic fault slip.

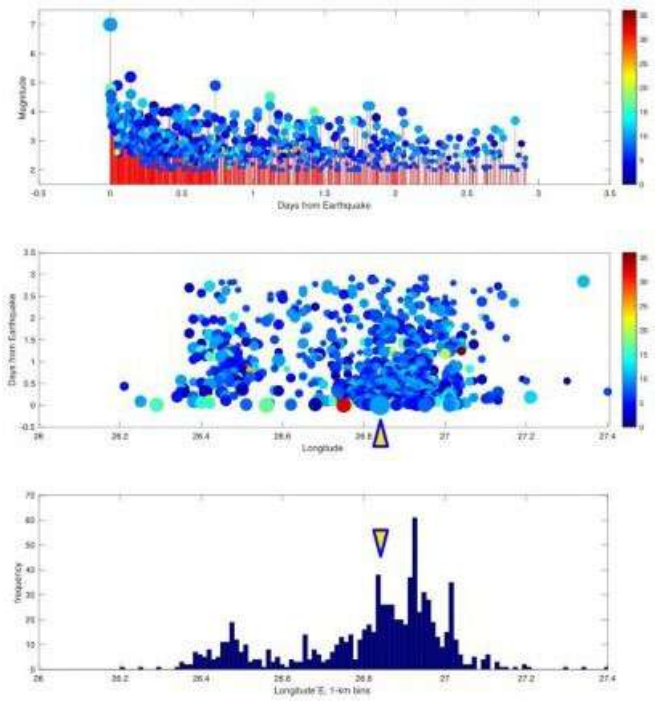

Fig. 2. Spatiotemporal evolution of the Samos aftershock sequence (source of data: EMSC). Circle colours correspond to depth, and size to the magnitude. Bottom panel shows frequency of occurrence with respect to longitude (east-west).

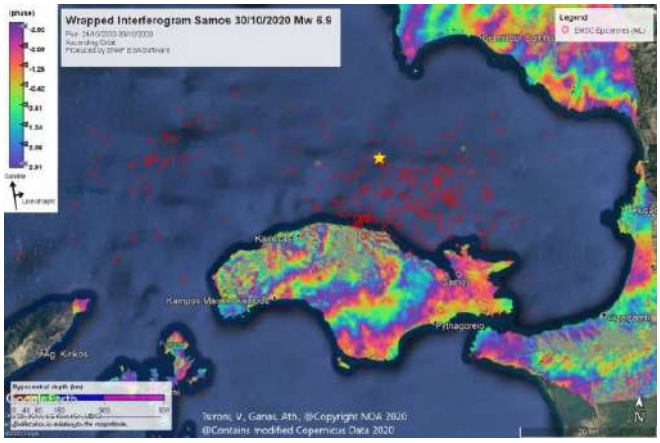

Fig. 3. The coseismic interferogram (wrapped phase; cropped swath) over Samos island for image pair Oct. 24-Oct.30, 2020.

Fault model

We use the InSAR l.o.s. displacements and the GNSS offsets to estimate the fault parameters assuming a rectangular source buried in a homogeneous elastic half-space and homogeneous slip. Our inversion approach finds the geometry and kinematics (strike and dip-angle) of best-fitting fault model. We invert jointly the l.o.s InSAR ground motions and the GNSS co-seismic displacements using the code *inverse6* (Briole, 2017). The modelling allows us to constrain seven parameters: the 3D location of the fault-top center, the fault azimuth, length and width and the amount of slip. We assume pure normal faulting and do not invert for a component of rake, as this parameter is coupled with the fault azimuth in the inversion of geodetic data. We also fix the fault dip-angle of 37° given by the seismological moment tensors, as the geodetic data does not have the capacity to resolve this angle. The fault width is also only loosely constrained because there are no GNSS points in the near field on the Turkish shore in front of Samos. Our best fitting model is with a fault of 36 km length and 18 km width, striking N276°E, (Fig. 5).

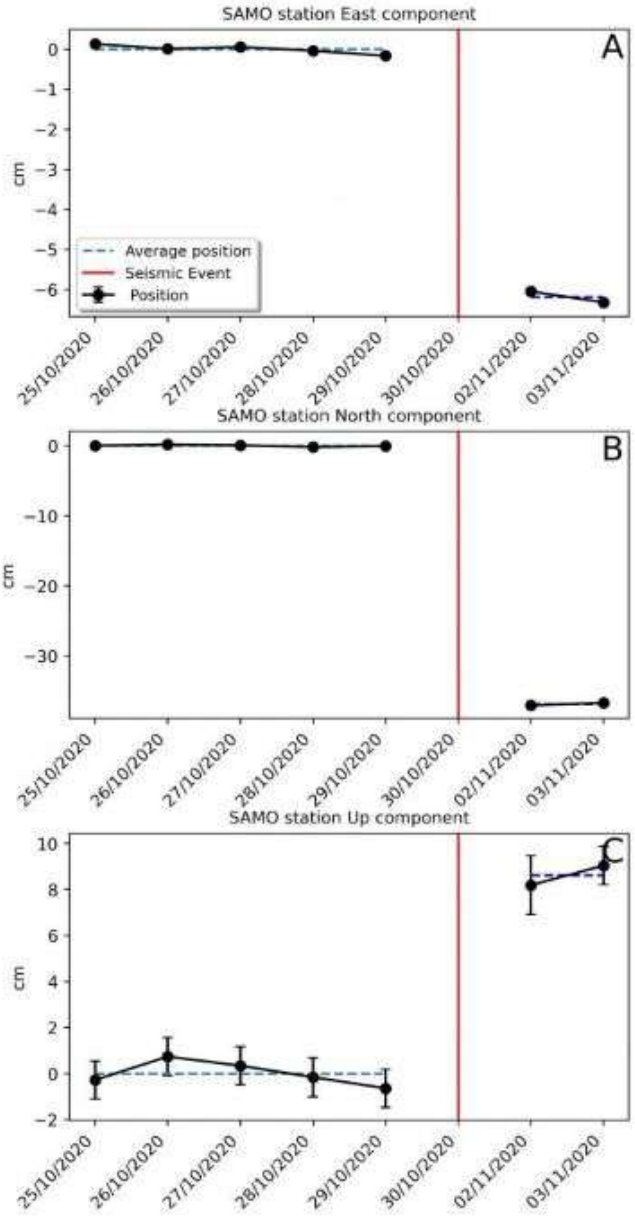

Fig. 4. Position time series (E, N, Up) of station SAMO (see location in Fig.1). The co-seismic offsets are the following: dE = -6 cm, dN = -37 cm and dU = +8 cm. The red vertical lines indicate the timing of the main shock.

Analyzing the solution space, we find that all lengths between 32 and 42 km are possible, all widths between 14 and 19 km, and all slips between 1.5 and 2.2 m, with the product of the three being constant (to comply with the derived geodetic moment). The possible range of depths of the base of the fault slip is 10 to 13 km, thus slightly deeper that the 10 km found for the Mw = 6.6 July 2017 Kos-Bodrum earthquake (Ganas et al. 2019). We also verified the impossibility of the south dipping fault model, as such model cannot jointly fit the GNSS vectors and the InSAR fringes.

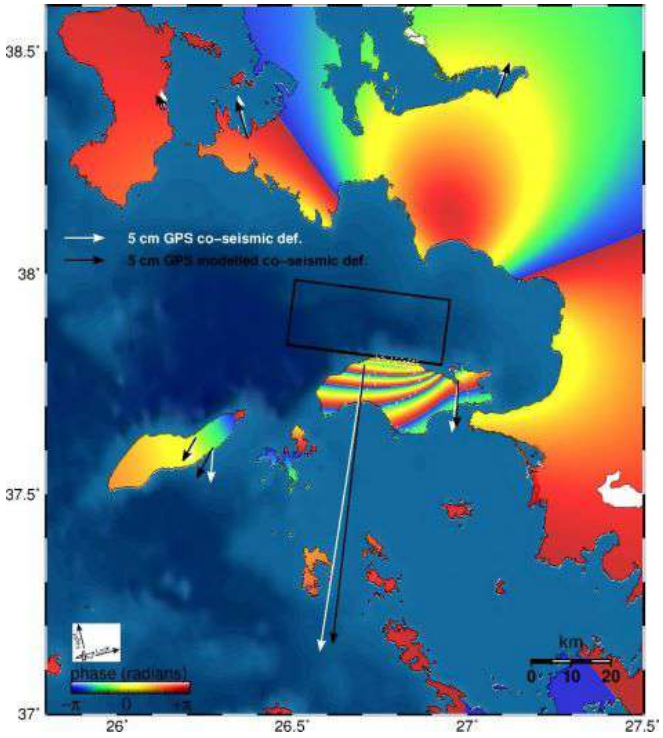

Fig. 5: Synthetic interferogram corresponding to our best fitting fault model (projection of the fault in black). The fault dip-direction is towards north thus Samos comprises the footwall block. The white arrows indicate the observed GNSS displacements and the black ones the model.

Acknowledgements: We thank Brendan Crowell, Simon Bufféral, Nicolas Chamot-Rooke, Marco Meschis, Tuncay Taymaz, Diego Melgar, Evi Nomikou, Margarita Segou and Efthimios Lekkas for comments and discussions. We are indebted to ESA, Geohazards Lab and Terradue for providing access to Geohazards Exploitation Platform (GEP) for InSAR cloud processing. GNSS data were provided by Hexagon SmartNET and Uranus (Tree) networks of Greece. We thank Tuncay Taymaz and Semi Ergintav for sharing Turkish GNSS data.

References

Briole, P. 2017. Modelling of earthquake slip by inversion of GNSS and InSAR data assuming homogenous elastic medium. Zenodo, http://doi.org/10.5281/zenodo.1098399

Ganas, A., Parsons, T., 2009. Three-dimensional model of Hellenic Arc deformation and origin of the Cretan uplift. J. Geophys. Res.: Solid Earth 114 (B6) https://doi.org/10.1029/2008JB005599

Ganas, A., et al, 2019. The July 20, 2017 M6.6 Kos Earthquake: Seismic and Geodetic Evidence for an Active North-Dipping Normal Fault at the Western End of the Gulf of Gökova (SE Aegean Sea), Pure and Applied Geophysics, 176 (10), 4177-4211 https://doi.org/10.1007/s00024-019-02154-y

Goldstein, R. M.; Werner, C. L. 1998. Radar interferogram filtering for geophysical applications. Geophys. Res. Lett. 25(21), 4035-4038

Mascle, J., and L. Martin, 1990. Shallow structure and recent evolution of the Aegean Sea: A synthesis based on continuous reflection profiles, Marine Geology, 94, 4, 271-299.

McClusky, S., et al. 2000, Global Positioning System constraints on plate kinematics and dynamics in the eastern Mediterranean and Caucasus, J. Geophys. Res. 105, B3, 5695-5719, DOI: 10.1029/1999JB900351.

McKenzie, D. 1978. Active tectonics of the Alpine–Himalayan belt: the Aegean Sea and surrounding regions, Geophys. J. Roy. Astr. Soc. 55, 1, 217-254, DOI: 10.1111/j.1365-246X.1978.tb04759.x.

Tan, O., Papadimitriou, E.E., Pabucçu, Z. et al. 2014. A detailed analysis of microseismicity in Samos and Kusadasi (Eastern Aegean Sea) areas. Acta Geophys. 62, 1283–1309. https://doi.org/10.2478/s11600-013-0194-1

Taymaz, T., J. Jackson, and D. McKenzie 1991. Active tectonics of the north and central Aegean Sea, Geophys. J. Int. 106, 2, 433-490, DOI: 10.1111/j.1365-246X.1991.tb03906.x

Vernant, P.; R. Reilinger, S. McClusky, 2014. Geodetic evidence for low coupling on the Hellenic subduction plate interface, Earth and Planetary Science Letters, 385, 122-129, https://doi.org/10.1016/j.epsl.2013.10.018.

The SAR images acquired by the SENTINEL-1 satellites are distributed routinely by the European Space Agency (ESA) free of charge. The GNSS data from stations surrounding the epicenter were provided by the Greek private GNSS networks (SmartNet and Uranus) and the Turkish CORS network.

Citation: Ganas, A., Elias, P., Briole, P., Tsironi, V., Valkaniotis, S., Escartin, J., Karasante, I., and Efstathiou, E., 2020, Fault responsible for Samos earthquake identified, Temblor, http://doi.org/10.32858/temblor.134

Posted on November 5, 2020 by Temblor

The October 30, 2020, Mw 6.9 Samos (Greece) earthquake

Newsletter #21 του Προγράμματος Μεταπτυχιακών Σπουδών **Στρατηγικές Διαχείρισης Περιβάλλοντος, Καταστροφών & Κρίσεων** του Εθνικού & Καποδιστριακού Πανεπιστημίου Αθηνών.

Το τεύχος είναι προσβάσιμο εδώ.

Preliminary Teleseismic Finite-Fault Models for the 2020-10-30 M7.0 Greece Earthquake

+ Initial Rupture Point (Hypocenter): KOERI

+ Method: Shimizu+2020GJI

+ Two Possible Fault Planes (USGS W-Phase Moment Tensor): Indistinguishable by FFM

+ Likely bilateral shallow rupture

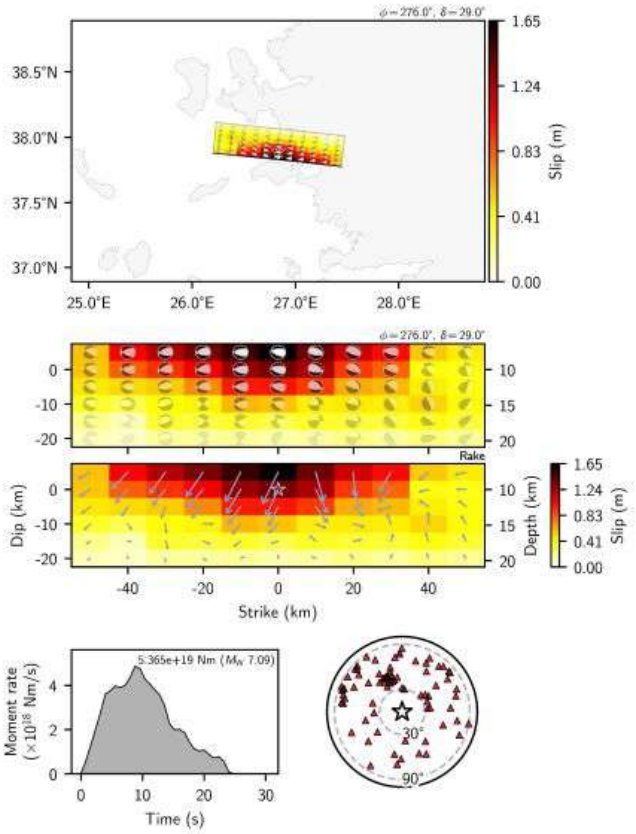

https://twitter.com/rokuwaki

Δορυφορική συμβολομετρική απεικόνιση του πεδίου εδαφικής παραμόρφωσης λόγω του σεισμού στη Σάμο της 30 Οκτωβρίου 2020 11:51 UTC

Σήμερα, η υπηρεσία geObservatory του Κέντρου Ερευνών Δορυφορικής Τηλεπισκόπησης BEYOND του Εθνικού Αστεροσκοπείου Αθηνών συνέλεξε από το Hellenic Mirror Site την πρώτη διαθέσιμη δορυφορική εικόνα ραντάρ υψηλής ανάλυσης μετά τον ισχυρό σεισμό στη Σάμο, και παρέχει τώρα την πρώτη χαρτογράφηση της εδαφικής παραμόρφωσης στην ευρύτερη περιοχή που επλήγη, με την επιφύλαξη να δώσει και νεότερους υπολογισμούς μέσα στις επόμενες ημέρες προς επιβεβαίωση των μετρήσεων του πεδίου παραμόρφωσης και των πρώτων παραμορφώσεων που διαφαίνονται στο πρώτο αυτό συμβολογράφημα.

Στο παρακάτω διαφορικό συμβολογράφημα φαίνεται το μοτίβο εδαφικής παραμόρφωσης στη διεύθυνση δορυφόρου – στόχου (line-of-sight). Στην περιοχή Κάμπος που βρίσκεται στο βόρειο κομμάτι της Σάμου και περίπου 15 χιλιόμετρα μακρυά από το επίκεντρο του σεισμού, μπορεί κανείς να διακρίνει δύο με τρεις κροσσούς συμβολής. Κάθε τέτοιος κροσσός αντιστοιχεί σε 2,8 εκατοστά παραμόρφωσης.

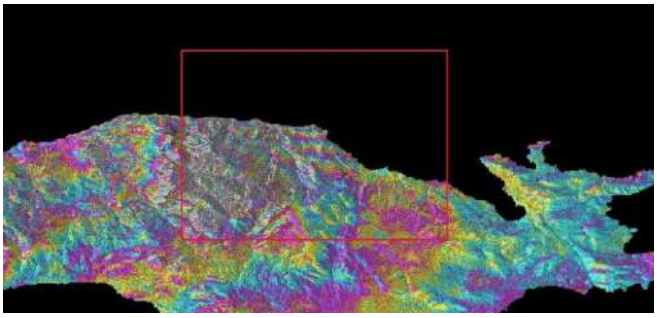

Το Hellenic Mirror Site συντηρεί και διαθέτει εικόνες υψηλής χωρικής ανάλυσης των Ευρωπαϊκών δορυφόρων Sentinels. Η συγκεκριμένη δορυφορική εικόνα είναι εικόνα ραντάρ συνθετικού ανοίγματος SAR Sentinel-1A ανοδικής τροχιάς και χωρικής ανάλυσης 10 m με ώρα λήψης 18:04:31 τοπική ώρα.

Ο σεισμός σημειώθηκε την Παρασκευή 30/10/2020 στις 11:51 UTC, είχε μέγεθος 6,7 Ρίχτερ, εστιακό βάθος 11,8 χλμ, και επίκεντρο 17 χλμ βόρεια της Σάμου, σύμφωνα με τα στοιχεία του Γεωδυναμικού Ινστιτούτου του Εθνικού Αστεροσκοπείου Αθηνών. Μέχρι στιγμής ο τραγικός απολογισμός στην Ελλάδα και στη γειτονική Τουρκία αναφέρει σε νεκρούς, μεγάλο αριθμό από τραυματίες και τεράστιες υλικές καταστροφές. Ο τραγικός απολογισμός συνεχίζεται και τα νούμερα αλλάζουν συνεχώς. Το Κέντρο BEYOND διαχείρισης φυσικών καταστροφών θα παραμείνει ανοιχτό και θα βρίσκεται στη συνδρομή των αρχών με την συνεχή ενημέρωση μέσω των παρατηρήσεων των διαστημικών αποστολών Copernicus Sentinels που συλλέγει το Hellenic Mirror Site.

Το προϊόν δημιουργηθηκε μέσω της αυτοματοποιημένης αλυσίδας geObservatory για την παραγωγή διαφορικών συμβολογραμμάτων από εικόνες Ραντάρ Συνθετικού Ανοίγματος. Η τεχνική αξιοποιεί δύο τέτοιες εικόνες, μια πριν και μια μετά τον σεισμό και υπολογίζει την διαφορά στην απόσταση δορυφόρου-γης μεταξύ των δύο διαδοχικών λήψεων.

Στην ιστοσελίδα του geObsevatory (http://geobservatory.beyond-eocenter.eu) εμφανίζονται όλα τα διαφορικά συμβολογράμματα που σχετίζονται με το σεισμικό γεγονός. Η ιστοσελίδα θα επικαιροποιείται και θα κάνει συστηματικά διαθέσιμα νέα προϊόντα μέτρησης της εδαφικής παραμόρφωσης καθώς νέα δορυφορικά δεδομένα Sentinel-1 θα γίνονται διαθέσιμα.

BEYOND Centre of EO Research & Satellite Remote Sensing, 31 October 2020, http://beyond-eocenter.eu/index.php/news-events/344-doryforiki-simvolometrikh-apikonish-edafikhs-paramorfwsis-sth-samo

Κ. Παπαζάχος: Γιατί η Σάμος γλίτωσε τα χειρότερα από τον σεισμό

Η κλίση προς Βορρά του ρήγματος στη Σάμο δείχνει να απέτρεψε μία πολύ μεγαλύτερη έκταση των καταστροφών και πιθανών συνεπακόλουθων ανθρώπινων απωλειών στο νησί, από τον ισχυρό σεισμό που σημειώθηκε το πρωί της Παρασκευής.

Ο σεισμός στοίχισε τη ζωή σε δύο νέα παιδιά, τα οποία καταπλάκωσε τοίχος από ένα ετοιμόρροπο σπίτι, την ώρα που επέστρεφαν από το μάθημά τους, ενώ στην Τουρκία προκλήθηκαν πιο εκτεταμένες καταστροφές με τον νεότερο τραγικό απολογισμό να αναφέρει 62 θύματα. Τι συνέβη όμως και πώς η εδαφική παραμόρφωση στην ευρύτερη περιοχή που επλήγη

μπορεί να εξηγεί τη διαφοροποίηση στο μέγεθος των ζημιών κατά μήκος του ρήγματος;

Ο καθηγητής Γεωφυσικής του ΑΠΘ, Κωνσταντίνος Παπαζάχος δίνει μία προκαταρκτική ερμηνεία για τη σεισμική δραστηριότητα μιλώντας στο ΑΠΕ.

«Η Σάμος βρίσκεται στο νότιο κομμάτι του ρήγματος, όπου το έδαφος ανυψώθηκε ελαφρά, βρέθηκε δηλαδή στην «πλάτη» του κανονικού ρήγματος, που συνήθως δέχεται πολύ μικρότερες σεισμικές κινήσεις» λέει

«Επειδή το ρήγμα έχει κλίση προς τον Βορρά -αυτό δείχνουν και τα επίκεντρα των μετασεισμών - το κομμάτι που βυθίστηκε βρίσκεται στη θαλάσσια περιοχή βόρεια της Σάμου. Εκεί ήταν και το τμήμα που δέχθηκε τις πιο ισχυρές σεισμικές κινήσεις», διευκρινίζει ο καθηγητής. «Αυτό εξηγεί ενδεχομένως γιατί οι καταγραφές των επιταχύνσεων στο Βαθύ ήταν 25% της επιτάχυνσης βαρύτητας g -με βάση δεδομένα από το ΙΤΣΑΚ- τιμή υψηλή, αλλά όχι πολύ υψηλή για έναν σεισμό των 7 Ρίχτερ, όπως ο σεισμός που έγινε. Αν το ρήγμα έκλινε προς τη μεριά της Σάμου, θα είχαμε ακριβώς αντίστροφη εικόνα, τις πιο σημαντικές κινήσεις στην Σάμο, με πολύ δυσμενέστερο απολογισμό. Για τον ίδιο λόγο και οι αναμενόμενες σεισμικές κινήσεις των μετασεισμών, που συνεχίζουν να σπάνε τμήματα του ρήγματος, αναμένεται να είναι ελαφρά μικρότερες από ό,τι θα περίμενε κανείς. Μέσα στην τραγωδία, η γεωμετρία του ρήγματος δείχνει να απέτρεψε τα πολύ χειρότερα για το νησί».

Οι βυθίσεις

Τα στοιχεία στον δορυφορικό χάρτη δείχνουν ότι στο βορειότερο τμήμα της Σάμου (Άγιος Κωσταντίνος – Βουρλιώτες) υπάρχει μία βύθιση έως 6-7 εκατοστά και μία υποψία βύθισης στη βορειοανατολική Σάμο (Πρασονήσι). Όμως, η Δυτική και Βορειοδυτική Σάμος παρουσιάζουν μεγάλες ανυψώσεις, άνω των δέκα εκατοστών. Την ίδια στιγμή ο θαλάσσιος πυθμένας βόρεια της Σάμου και οι βόρειες ακτές προς την Τουρκία βυθίστηκαν προς τα κάτω.

Η διάρρηξη ξεκίνησε από το υπόκεντρο (βάθος ~13km, όπως επεναπροσδιορίστηκε) και η προχώρησε και στις 2 κατευθύνσεις (Ανατολικά και Δυτικά), καλύπτοντας μία έκταση 55-60 χιλιόμετρα σε μήκος και 15 χιλιόμετρων σε πλάτος. «Το μήκος 55-60 χιλιομέτρων αντιστοιχεί σε έναν σεισμό των 7 Ρίχτερ» σημείωσε ο καθηγητής.

«Η μεγάλη ολίσθηση πάνω στο ρήγμα πιθανότατα έγινε στο δυτικό τμήμα του ρήγματος, εκεί που το ρήγμα ίσως έφτασε και στην επιφάνεια, μετατοπίζοντας σημαντικά τον θαλάσσιο πυθμένα και προκαλώντας το τσουνάμι», πρόσθεσε.

Ο κ. Παπαζάχος και η ομάδα του θα συνεχίσουν την έρευνα πάνω στα αρχικά τους συμπεράσματα, αξιοποιώντας πρόσθετες αναλύσεις των σεισμολογικών δεδομένων και των GPS, καθώς και τυχόν επιφανειακές παρατηρήσεις.

(Κέρδος online 2/11/2020, http://www.kerdos.gr/επιστήμη-τεχνολογία/376572-κ-παπαζάχος-γιατί-η-σάμος-γλίτωσε-τα-χειρότερα-από-τον-σεισμό)

Μεγάλο σεισμό στη Σάμο έδειχνε πρόγνωση από το 2004

Το σφοδρό χτύπημα των 6,7 ρίχτερ αιφνιδίασε τους κατοίκους της Σάμου και της Σμύρνης, όμως δεν αποτέλεσε «έκπληξη» για τους επιστήμονες

Ο χάρτης (της επόμενης σελίδας) απεικονίζει τα ενεργά σεισμικά ρήγματα της Σάμου όπως χαρτογραφήθηκαν από την ερευνητική ομάδα του Τμήματος Γεωλογίας του ΑΠΘ και του Τμήματος Γεωγραφίας του Πανεπιστημίου Αιγαίου. Ο καθηγητής Σπύρος Παυλίδης εξηγεί πως «είχαμε εκτιμήσει τη σεισμική δυναμικότητα του υποθαλάσσιου ρήγματος που προκάλεσε τον σεισμό της Παρασκευής στα 6,8 ρίχτερ. Οπως προκύπτει, ο σεισμός αυτός ενεργοποίησε και το ρήγμα που εκτείνεται παράλληλα με τις ακτές του Καρλοβασίου»

Την ενεργοποίηση ενός δεύτερου σεισμικού ρήγματος στη Σάμο φαίνεται ότι έχει προκαλέσει ο σεισμός της περασμένης Παρασκευής που σκόρπισε τον θάνατο και στις δύο πλευρές του Αιγαίου. Οπως εξηγούν ειδικοί επιστήμονες στα «ΝΕΑ», μετά τη δόνηση των 6,7 ρίχτερ έχει καταγραφεί πλούσια μετασεισμική δραστηριότητα, τμήμα της οποίας έχει μετατοπιστεί προς τα δυτικά· το στοιχείο αυτό, σύμφωνα με τον Σπύρο Παυλίδη, ομότιμο καθηγητή Γεωλογίας των Σεισμών στο ΑΠΘ, μαρτυρά την ενεργοποίηση ενός άλλου ρήγματος, που εκτείνεται κατά μήκος των ακτών, κοντά στο Καρλόβασι, και έχει δυναμικότητα έως και 6,4 ρίχτερ.

Λίγα στοιχεία είναι γνωστά για το ρήγμα που προκάλεσε τη φονική δόνηση της Παρασκευής, καθώς στα υποθαλάσσια ρήγματα η συλλογή αξιόπιστων δεδομένων είναι δυσχερής. Κάποιοι εκτιμούν το μήκος του στα 30 χιλιόμετρα, ενώ άλλοι θεωρούν πως υπερβαίνει τα 50 χιλιόμετρα και απεύχονται το ενδεχόμενο η μετατόπιση της σεισμικής δραστηριότητας να επιφέρει το «σπάσιμο» άλλου κομματιού του ρήγματος, προς την πλευρά της Ικαρίας.

Χαρτογράφηση

«Η επιστημονική μας ομάδα, από το Τμήμα Γεωλογίας του Αριστοτελείου Πανεπιστημίου και το Τμήμα Γεωγραφίας του Πανεπιστημίου Αιγαίου, δημοσίευσε το 2013 στο διεθνές περιοδικό "Techtonophysics" μια χαρτογράφηση όλων των σεισμικά ενεργών ρηγμάτων της Σάμου και μια εκτίμηση για το μέγεθος σεισμού που μπορεί να παραγάγει καθένα από αυτά», λέει στα «ΝΕΑ» ο καθηγητής και πρόεδρος της Ελληνικής Γεωλογικής Εταιρείας Σπύρος Παυλίδης.

«Καταγράψαμε πέντε ρήγματα, στο Καρλόβασι με δυναμικότητα 6,4 ρίχτερ, ένα κοντά στον Μαραθόκαμπο δυναμικότητας επίσης 6,4 ρίχτερ, στο Πυθαγόρειο δυναμικότητας 6,6 ρίχτερ, στο Βαθύ 6,3 ρίχτερ και αυτό που προκάλεσε τον σεισμό της Παρασκευής, του οποίου τη δυναμικότητα εκτιμήσαμε στα 6,8 ρίχτερ. Μετά την ενεργοποίησή του έχουν καταγραφεί δεκάδες μετασεισμοί, αρκετοί από τους οποίους έχουν μετακινηθεί προς τη δυτική ακτή του νησιού. Από τα δεδομένα που έχουμε στα χέρια μας θεωρούμε ότι ο σεισμός της Παρασκευής έχει ενεργοποιήσει το ρήγμα του Καρλοβασίου», καταλήγει. «Μπορεί η δυναμικότητα του συγκεκριμένου ρήγματος να έχει εκτιμηθεί στα 6,4 ρίχτερ, αυτό όμως δεν σημαίνει ότι θα έχουμε οπωσδήποτε έναν σεισμό τέτοιου μεγέθους. Μέχρι στιγμής στην περιοχή καταγράφονται δονήσεις λίγο μεγαλύτερες των 4 ρίχτερ».

Τη μετατόπιση της σεισμικής δραστηριότητας προς τα δυτικά επιβεβαιώνει και η Εύη Νομικού, αναπληρώτρια καθηγήτρια στο Τμήμα Γεωλογίας του ΕΚΠΑ. «Παρότι όλοι απευχόμαστε να υπάρξει ενεργοποίηση των υποθαλάσσιων ρηγμάτων προς τα δυτικά, φαίνεται μάλλον το αντίθετο», λέει στα «ΝΕΑ». «Στην περιοχή εντοπίζονται πολλά ρήγματα, με ακριβώς ίδια κατεύθυνση, και κατά τη γνώμη μου αποτελούν όλα επέκταση του ρήγματος που ενεργοποιήθηκε την Παρασκευή. Αρα, μπορεί να μην έχουμε ακριβώς ενεργοποίηση άλλων ρηγμάτων, αλλά ενεργοποίηση άλλων τμημάτων του ίδιου ρήγματος», σημειώνει.

Μέθοδος από την Καλιφόρνια

Οπως όλα δείχνουν, το σφοδρό χτύπημα των 6,7 ρίχτερ αιφνιδίασε τους κατοίκους της Σάμου και της Σμύρνης, όμως δεν αποτέλεσε «έκπληξη» για τους επιστήμονες. Σε αυτό συνηγορεί και μια μακροπρόθεσμη πρόγνωση που είχε δημοσιευτεί στα πρακτικά διεθνούς συνεδρίου για τη Γεωλογία της Ανατολικής Μεσογείου τον Απρίλιο του 2004 και έδινε πιθανότητα άνω του 80% για σεισμό μεγαλύτερο των 6,5 ρίχτερ στη Σάμο μέχρι το 2023.

Επικεφαλής της έρευνας ήταν ο διακεκριμένος σεισμολόγος και μέλος της επιτροπής εκτίμησης σεισμικού κινδύνου Γεράσιμος Παπαδόπουλος. «Οι περιοχές που είχαμε εξετάσει ήταν η Σάμος, η Ρόδος, τα Κύθηρα, η Κεφαλονιά, η Αθήνα και το Βόρειο Αιγαίο», λέει στα «ΝΕΑ» ο δρ Παπαδόπουλος. «Η μεθοδολογία που ακολουθήσαμε βασίζεται στην κατανομή των χρονικών διαστημάτων που μεσολαβούν ανάμεσα στους προηγούμενους ισχυρούς σεισμούς ανά περιοχή. Είναι μια μέθοδος που έχει εξελιχθεί από σεισμολόγους στην Καλιφόρνια», συμπληρώνει.

«Με τη μεθοδολογία αυτή υπολογίσαμε την πιθανότητα να γίνει μεγάλος σεισμός μέσα σε ορισμένο χρονικό ορίζοντα μετρώντας από την 1η Σεπτεμβρίου του 2003. Οι υψηλότερες πιθανότητες με βάση το προηγούμενο ιστορικό εντοπίστηκαν στη Σάμο και στο Βόρειο Αιγαίο. Στη Σάμο η πιθανότητα να γίνει σεισμός μεγαλύτερος από 6,5 ρίχτερ μέχρι το 2013 ήταν 76%, και μέσα σε 20 χρόνια, δηλαδή ως το 2023, υπερέβαινε το 80%», λέει ο Γεράσιμος Παπαδόπουλος. Επίσης, επαληθεύτηκε και η πρόγνωση για το Βόρειο Αιγαίο. «Εκεί είχαμε εκτιμήσει πιθανότητες άνω του 75% να σημειωθεί σεισμός άνω των 6,5 ρίχτερ μέχρι το 2018 και στις 24 Μαΐου του 2014 εκδηλώθηκε ισχυρός σεισμός μεγέθους 6,9 ρίχτερ».

(Κατερίνα Ροββά / ΤΑ ΝΕΑ, 3 Νοεμβρίου 2020, https://www.tanea.gr/2020/11/03/greece/megalo-seismo-sti-samo-edeixne-prognosi-apo-to-2004)

Προκαταρκτική Έκθεση του ETAM για το Σεισμό της Σάμου, στις 30 Οκτωβρίου 2020

Η Προκαταρκτική Έκθεση του ETAM για το Σεισμό της Σάμου, στις 30 Οκτωβρίου 2020, είναι διαθέσιμη στον ακόλουθο σύνδεσμο:
https://www.eltam.org/images/nltr/newsletters/20201125/etam_report_samos2020earthquake.pdf

Εντυπωσιακό video για το tsunami

https://twitter.com/search?q=samos%20tsunami&src=typed_query

Διμερής Διαδικτυακή Ημερίδα Ελλάδας - Τουρκίας

Οι συνέπειες του σεισμού Mw 6.7 της 30ης Οκτωβρίου 2020 σε Σμύρνη και Σάμο

Registration : zoom.us/webinar/register/WN_1TRPrZQBT4qf9TI1kI5Tig

Πρόγραμμα : http://www.epes.org.gr/.../3/7/7337589/webinar_programme.pdf

www.epes.org.gr

ΑΡΘΡΑ

Satellite interferometry for mapping surface deformation time series in one, two and three dimensions: A new method illustrated on a slow-moving landslide

Sergey Samsonov, Antoine Dille, Olivier Dewitte, François Kervyn, Nicolas d'Oreye

Introduction

Surface deformation information is a key parameter for characterization of natural and anthropogenic processes such as earthquakes, volcanic eruptions, landslides, glacier flows, and subsidence and uplift due to resource exploitation (e.g. Colesanti and Wasowski, 2006; Wasowski and Bovenga, 2014; Elliott et al., 2016; Bayer et al., 2017; Dong et al., 2018; Li et al., 2019). To this end, space-borne Differential Interferometric Synthetic Aperture Radar (DInSAR) allows the derivation of surface deformation with wide spatial coverage, millimetre precision, high temporal and spatial resolutions and all-day and all-weather working capabilities (Massonnet and Feigl, 1998; Rosen et al., 2000).

However, conventional DInSAR technique measures only one component of the surface deformation – in the satellite's line-of-sight (LOS) (Wright et al., 2004; Hu et al., 2014). This makes interpretation of DInSAR measurements challenging and narrows the understanding of the mechanisms and dynamics of the deformation processes at work. Different methods were therefore developed to provide direct measurements of the two (2D, east and vertical) (e.g. Samsonov and d'Oreye, 2012, Samsonov and d'Oreye, 2017) or the three (3D, north, east and vertical) components of surface deformation at one point in time (e.g. Wright et al., 2004; Gourmelen et al., 2011; Ng et al., 2012; Raucoules et al., 2013; Shi et al., 2018). The most straightforward strategy for deriving 3D surface deformation is to combine multiple DInSAR LOS measurements with different viewing geometries. However, trying to derive 3D deformation from multi-orbit satellite SAR observations alone poorly constrains the north component of motion (Fuhrmann and Garthwaite, 2019). Indeed, due to the small inter-satellite variation in SAR satellite orbits (i.e. near-polar orbit), this approach may be applied solely for a very specific case – in high latitude areas where the azimuth angle diversity is higher (e.g. Gray, 2011; Hu et al., 2014). Larger diversity in acquisition geometry can be obtained using airborne DInSAR, that allows acquisition with any desired azimuthal direction (e.g. Delbridge et al., 2016; Handwerger et al., 2019). However, the cost of such acquisitions limits the temporal sampling. As a results of these difficulties, the retrieval of 3D surface deformation therefore commonly consists of merging conventional DInSAR LOS measurements with other types of measurements, that may rely either on SAR imagery or ancillary data, such as GNSS measurements (e.g. Samsonov and Tiampo, 2006; Samsonov et al., 2007, Samsonov et al., 2008; Hu et al., 2014).

East and vertical deformation components are often derived from conventional DInSAR applied to two (or more) different satellite tracks, that are then combined with outputs from either speckle tracking Wright et al., 2004; De Michele et al., 2010; Raucoules et al., 2013; Shi et al., 2018) or Multiple Aperture Interferometry (MAI) (e.g. Gourmelen et al., 2011) to retrieve the north component of deformation (Hu et al., 2014). With the speckle tracking technique, range and azimuth deformation are calculated from the offset of a given point on the ground using local correlation analysis between two images (Michel et al., 1999; Leprince et al., 2007). This method is applied to either the amplitude (Michel et al., 1999; Pathier et al., 2006) or the phase information (Gray et al., 2001; Pattyn and Derauw, 2002) of the SAR images. While it is not affected by signal saturation with high deformation gradient, speckle tracking precision is much lower, with values between 1/30th to 1/10th of the image pixel size, than the millimetre-scale precision that can be achieved with DInSAR (Leprince et al., 2007; Raucoules et al., 2013; Hu et al., 2014). This implies that the use of the speckle tracking technique is often limited to the case of relatively large deformation. The other method, MAI, aims at extending the applicability of DInSAR to along-track deformation based on split-beam DInSAR processing (Bechor and Zebker, 2006; Jung et al., 2009; Gourmelen et al., 2011). Bechor and Zebker (2006) found that for interferograms with coherence of 0.4 and higher, MAI outperforms speckle tracking analysis in precision. However, such high coherence is relatively uncommon, particularly in vegetated regions. Pepe et al. (2016); Pepe and Calo (2017) proposed to derive 3D deformation from ascending and descending data by applying higher order regularizations; this technique was used for mapping 3D deformation time series at the Big Island of Hawaii.

Another strategy used to overcome the constraint originating from the geometry of SAR observation is to make assumptions about deformation processes being studied (Hu et al., 2014). In the case of landslides and glacier flows, a reasonable assumption is that motion occurs parallel to the surface, although not necessarily downslope. By reducing the degrees of freedom from three to two, with this assumption one may resolve the three components of motion from (at least) one ascending and one descending DInSAR datasets. This approach has been demonstrated on glaciers in polar regions using single or few ascending and descending interferograms from the ERS-1/2 tandem mission (e.g. Joughin et al., 1998; Mohr et al., 1998; Gourmelen et al., 2011; Kumar et al., 2011). Notti et al. (2014); Kalia (2018); Hu et al., 2018, Hu et al., 2019 applied a similar principle on landslides, here projecting measured LOS velocity along the steepest downslope (one step further from assuming a movement parallel to the surface) to obtain estimates of the landslide motion. Assumption of motion along the steepest downslope may however be seen as too strict, as it does not allow consideration of lateral motion.

Time series are essential for studying surface deformation processes, which ideally calls for an integrated multi-sensor, multi-track and multi-temporal DInSAR measurements approach (Hu et al., 2013, Hu et al., 2014). However, all the previous methods discussed above, derived 3D surface deformation from either individual interferograms, or separate or interpolated ascending and descending datasets. Because of the mismatch in the acquisition times of ascending and descending datasets, these methods cannot be used to merge all available DInSAR data for producing a single set of temporally dense, 3D surface deformation time series (Samsonov and d'Oreye, 2012).

Here, we propose a novel version of the Multidimensional Small Baseline Subset (MSBAS) method (Samsonov and d'Oreye, 2012, Samsonov and d'Oreye, 2017), MSBAS-3D, that is able to produce 3D (north, east, and vertical) surface deformation time series from multi-track and multi-sensor DInSAR data. This new method aims at measuring surface deformation for processes involving motion parallel to the surface, such as landslides and glacier flows. The ability of MSBAS-3D to capture the full 3D deformation pattern and the benefits for the understanding of the processes at work are illustrated for a large, slow-moving, deep-seated landslide for which long DInSAR and dGNSS time series, as well as ground truth data, are available.

Methodology

The Multidimensional Small Baseline Subset (MSBAS) meth-

odology is developed for simultaneous post processing of the hundreds to thousands of individual interferograms produced by a conventional DInSAR processing (Samsonov and d'Oreye, 2012, Samsonov and d'Oreye, 2017). Depending on the number of datasets, their acquisition parameters and specified control flags, the technique produces line-of-sight (MSBAS-1D), east and vertical (MSBAS-2D), and now north, east, and vertical (MSBAS-3D) surface deformation time series. The output of processing consists of cumulative time series for each acquisition epoch and linear deformation rate for each pixel that remains coherent throughout the entire time span. A brief derivation of all three techniques is provided below, with an emphasis on the new MSBAS-3D technique.

MSBAS-1D

In case of a single DInSAR dataset computed from data acquired by a sensor with an azimuth angle θ and an incidence angle φ, the LOS surface deformation time series is computed by applying the Small Baseline Subset (SBAS) technique (Berardino et al., 2002; Usai, 2003). The SBAS technique implemented in MSBAS-1D software is called when one or more DInSAR datasets with similar incidence and azimuth angles are provided. In matrix form MSBAS-1D can be written as

$$AV_{los} = \Phi, \quad V_{los} = A^{+}\Phi, \quad d_{los}^{i+1} = d_{los}^{i} + V_{los}^{i}\Delta t^{i} \tag{1}$$

where A is a matrix constructed from the time intervals between consecutive SAR acquisitions, V_{los} is a vector of the unknown LOS deformation velocities, Φ is a vector of observed DInSAR values, A^{+} is a pseudo-inverse of matrix A found by applying the Singular Value Decomposition (SVD), and dlosi is a cumulative LOS deformation at the time t^{i}.

The LOS deformation velocity V_{los} is related to the three components of the deformation velocity vector V with components VN, VE, VV through the following equation

$$V_{los} = \mathbf{SV} = S_N V_N + S_E V_E + S_V V_V \tag{2}$$

where S = {S_N, S_E, S_V} = {sinθ sinφ, − cosθ sinφ, cosφ} is a LOS unit vector with north, east and vertical components S_N, S_E, S_V.

MSBAS-2D

When both, ascending and descending DInSAR datasets acquired over the same area and time period are available, the MSBAS-2D technique computes east and vertical components of surface deformation time series. This solution is approximate because the contribution of the third, north component is neglected for the reason that $S_N < S_E$, V and $V_N \simeq V_E$, V. In matrix form MSBAS-2D can be written as

$$\begin{pmatrix} \widehat{A} \\ \lambda L \end{pmatrix}\begin{pmatrix} V_E \\ V_V \end{pmatrix} = \begin{pmatrix} \widehat{\Phi} \\ 0 \end{pmatrix}, \quad \begin{pmatrix} V_E \\ V_V \end{pmatrix} = \begin{pmatrix} \widehat{A} \\ \lambda L \end{pmatrix}^{+}\begin{pmatrix} \widehat{\Phi} \\ 0 \end{pmatrix}, \quad d_{E,U}^{i+1} = d_{E,U}^{i} + V_{E,U}^{i}\Delta t^{i} \tag{3}$$

where the matrix consists of the matrix A (described above) multiplied by the east and vertical components of the LOS unit vector S.

The Tikhonov regularization matrix L multiplied by the regularization parameter λ is used for regularizing time series (Tikhonov and Arsenin, 1977). The effect of regularization is similar to applying a low-pass filter and it is recommended when the acquisition times of ascending and descending datasets do not match. The matrix A, as well as the regularization matrices L of zeroth, first and second orders were explicitly derived in (Samsonov, 2010; Samsonov and d'Oreye, 2017). As in the previous case, the unknown east and vertical components of deformation velocities VE and VV for each acquisition epoch and pixel are solved by applying SVD and the 2D surface deformation time series are reconstructed from computed deformation velocities by the numerical integration.

MSBAS-3D

In certain cases, the contribution of the north-south component of displacement is too large to be neglected (SN < SE, V, VN ≃ VE, and VN > VV). By assuming that the motion occurs parallel to the surface, we can however reduce the degrees of freedom from three to two, allowing resolving all three components of motion from (at least) one ascending and one descending DInSAR datasets. This assumption is for instance suited for characterizing gravity-driven processes such as landslides and glacier flows. The constraint can be written in terms of deformation velocities in the following form

$$V_V = \frac{\partial H}{\partial X_N} V_N + \frac{\partial H}{\partial X_E} V_E \tag{4}$$

where H is the topographic height and are first derivatives in the north XN and east XE directions. The and values can be computed from DEM using, for example, the Generic Mapping Tools (GMT) grdmath -M DDY/DDX command. Prior low-pass filtering of DEM (e.g. using GMT grdfilter command) is recommended for reducing sensitivity to surface features that do not affect the ground motion originated at some (shallow) depth. It is likely that sliding surface at depth is smoother than DEM. The magnitude of a low-pass filter needs to be sufficiently strong so the resulting surface has a slope equal to an overall slope of the form that host the landslide.

The MSBAS-3D technique that computes constrained 3D surface deformation time series can be written in matrix form as

$$\begin{pmatrix} \widehat{A} \\ H \\ \lambda L \end{pmatrix}\begin{pmatrix} V_N \\ V_E \\ V_V \end{pmatrix} = \begin{pmatrix} \widehat{\Phi} \\ 0 \\ 0 \end{pmatrix}, \quad \begin{pmatrix} V_N \\ V_E \\ V_V \end{pmatrix} = \begin{pmatrix} \widehat{A} \\ H \\ \lambda L \end{pmatrix}^{+}\begin{pmatrix} \widehat{\Phi} \\ 0 \\ 0 \end{pmatrix}, \quad d_{N,E,V}^{i+1} = d_{N,E,V}^{i} + V_{N,E,V}^{i}\Delta t^{i} \tag{5}$$

where the matrix consists of the matrix A (described above) multiplied by the north, east and vertical components of the LOS unit vector S. The matrix represents the motion parallel to the surface constraint. The unknown north, east and vertical components of deformation velocities V_N, V_E and V_V for each acquisition epoch and pixel are solved by applying SVD and the surface deformation time series are reconstructed from the computed deformation velocities by the numerical integration.

For some combinations of acquisition parameters and topographic gradients, (5) may become ill-conditioned, which can be assessed by computing condition number for all possible topographic gradients for given acquisition parameters.

Computational aspects

Matrices in Eqs. (1), (3), (5) typically have hundreds of columns and thousands of rows, corresponding to the total number of SAR images and DInSAR interferograms, respectively. Computation of the Singular Value Decomposition (SVD) of such large matrices is intensive. In case of the 1D analysis, viewing geometry S is irrelevant so SVD computation is performed only once. In case of the 2D analysis, constant viewing geometry S is assumed. This allows performing SVD computation only once, which results in a slight reduction of precision. In case of the 3D deformation analysis, SVD inversion is performed for each coherent pixel in order to account for the spatially varying constraint so varying viewing geometry is implemented as well. The typical processing time of MSBAS-1D and MSBAS-2D is only a few tens of minutes,

while the typical processing time of MSBAS-3D can reach several hours (for a typical grid of a few thousand pixels in each dimension) due to the large number of SVD computations required.

Unlike other advanced methods such as StaMPS (Hooper, 2008), MSBAS processing is incremental. The addition of new SAR images requires computing of only the few interferograms satisfying user-defined baseline criteria before executing MSBAS processing.

Test case and data

The ability to unravel surface deformation pattern using the different level of processing of the MSBAS method is illustrated on a large landslide, for which long DInSAR and dGNSS time series, as well as ground truth data, are available (Nobile et al., 2018).

Funu landslide

Funu landslide (2°31'S, 28°50'E, Fig. 1) is located in the densely populated City of Bukavu, situated in the Kivu Rift (western branch of the East African Rift System) in eastern Democratic Republic of the Congo. This region is characterised by a high susceptibility to landslides due to a combination of natural predisposing and triggering factors (e.g., high rainfall intensities, moderate to high seismicity, deep weathering and steep landscapes) (Jacobs et al., 2016; Monsieurs et al., 2018; Depicker et al., 2019; Dille et al., 2019). Located in the tropics, the region is affected by persistent cloud cover over most of the year, making DInSAR a key remote sensing tool for the study of landslides in this area (Nobile et al., 2018).

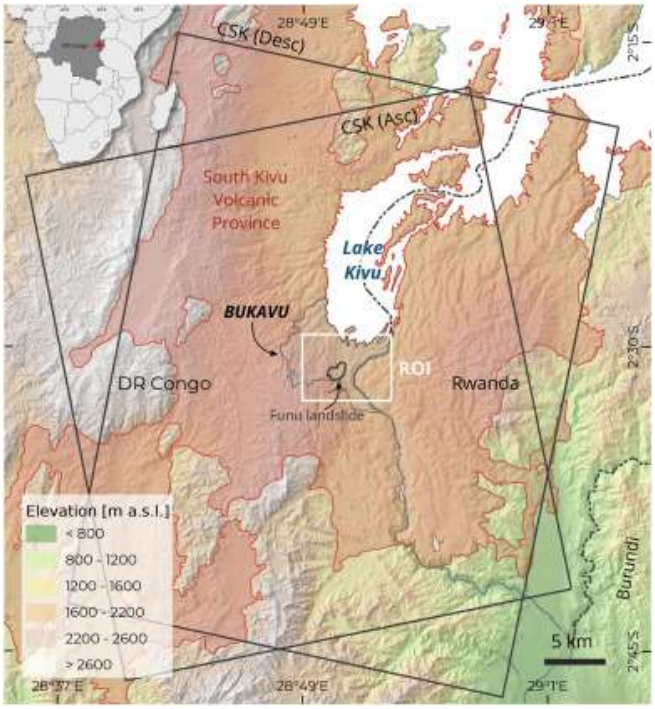

Fig. 1. Funu landslide is located in the city of Bukavu, eastern DR Congo. It lies within the South Kivu Volcanic Province that is formed of sequences of late Miocene to Pleistocene sub-horizontal basaltic lava layers. Outlined in white is shown the area processed with MSBAS. The footprints of the ascending and descending COSMO-SkyMed SAR images used in this study are outlined in black.

This 1.5 km2 slow-moving slope instability was formed thousands of years ago (Moeyersons et al., 2004). The depth of this bedrock landslide can be estimated to be of at least 100 m, i.e. the average height of its main scarp (Dewitte and Demoulin, 2005; Larsen et al., 2010). The landslide developed in sequences of late Miocene to Pleistocene sub-horizontal basaltic lava layers (Fig. 2b) that make up the South Kivu Volcanic Province (Fig. 1). An accurate delineation of the layers does not exist. However, the presence of springs at different elevations shows that their permeability varies, attesting to perched water tables. Weathering of some layers can be very intense with a regolith thickness that can be more than 10 m (Fig. 2c). The distribution of the weathering is highly uneven, sometimes having important changes over short distances of a few tens of meters (Moeyersons et al., 2004). The landslide is currently prone to surface deformation as attested to by continuous damage to infrastructure and buildings (Moeyersons et al., 2004; Balegamire et al., 2017). This landslide is also densely populated, with approximately 80 thousand people living directly on it (Michellier et al., 2016).

Nobile et al. (2018) provided a first analysis of the Funu landslides kinematics and mechanisms by combining one year of DInSAR measurements from 70 Cosmo-SkyMed SAR images acquired between 21 March 2015 and 19 April 2016, processed using the StaMPS SBAS approach (Lanari et al., 2007; Hooper, 2008) and on-site dGNSS measurements. They measured deformation of up to 70 mm/yr in the ascending and descending LOS directions. These measurements were in good agreement with dGNSS, except for one zone of the landslide that corresponds to a recent, smaller subsequent landslide. There, dGNSS measurements showed deformation an order of magnitude larger than DInSAR (up to 500 mm/yr while converted to LOS). The limit in the maximum detectable deformation resolvable by the X-band DInSAR was reached (Nobile et al., 2018). The study by Nobile et al. (2018) confirmed that the Funu landslide is mostly driven by a rotational mechanism with a prominent main scarp and a characteristic back-tilted bench. Several minor scarps, probably linked to secondary shear surfaces, are present in the zone of depletion and delimit individual blocks. From rotational in the depletion zone, the main movement develops a more planar behaviour with flow-like features in its runout and accumulation zones (as suggested from its morphometry). They concluded that the dense urban fabric, the relatively low velocity of the ground deformation, and the general eastward topography with the average slope of about 6.5 degrees (vs 45 degree SAR incidence angle) that avoids shadowing and foreshortening effects make the Funu landslide a particularly interesting site for DInSAR analysis.

COSMO-SkyMed images

We used 176 ascending and 166 descending COSMO-SkyMed images that were acquired between 24 March 2015 and 3 January 2019 (Table 1). Ascending images were acquired with the incidence angle of 41 degrees, range pixel spacing of 1.3 m and azimuth pixel spacing of 2.3 m. Descending images were acquired with the incidence angle of 50 degrees, range pixel spacing of 1.7 m and azimuth pixel spacing of 2.1 m.

Each COSMO-SkyMed set was processed independently with the GAMMA software (Wegmuller and Werner, 1997). Ascending image acquired on 5 February 2017 and descending image acquired on 5 May 2017 were selected as masters for respective sets and remaining images were re-sampled into the master geometry. Multilooking factor of 2 in range and azimuth were used, as well as a maximal perpendicular baselines of 600 m (Fig. 3). The topographic phase was removed using the 1 arc-second (~30 m) resolution Shuttle Radar Topography Mission Digital Elevation Model (SRTM DEM, Fig. 1).

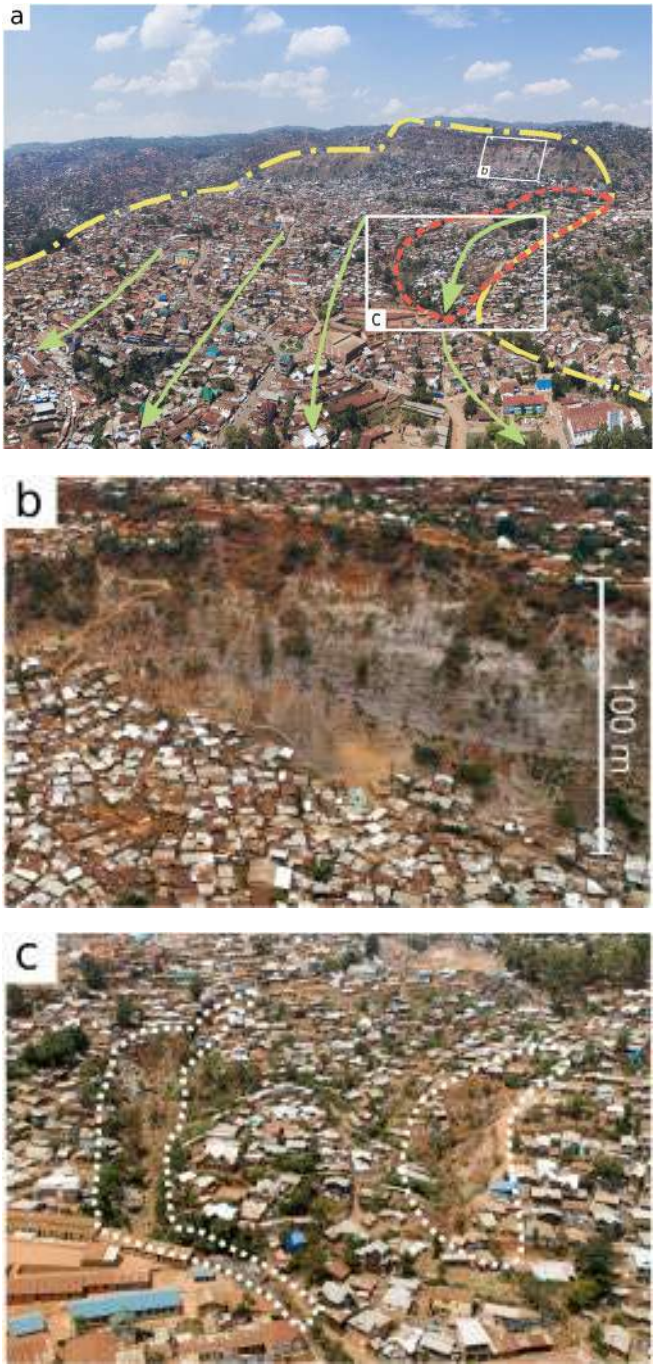

Fig. 2. Drone photographs of Funu landslide acquired in September 2018. a) General view of the landslide, with its extent outlined in yellow and green arrows indicating principal direction of movement. The fastest moving region, where discrepancies between DInSAR and dGNSS are observed, is outlined in red. Note constraints from topography and apparent divergent motion at landslides bottom. The total landslide height is about 400 m while the height of the main scarp is up to 100 m. b) Sequences of late Miocene to Pleistocene sub-horizontal basaltic lava layers apparent over the main scarp. c) Gullies delineating the toe of the fastest landslide unit. Their presence highlights the deep weathering of some basaltic layers, with a regolith thickness that can easily exceed 10 m. (For interpretation of the references to colour in this figure legend, the reader is referred to the web version of this article.)

DInSAR data set	θ	ϕ	Temporal coverage	N	M
COSMO-SkyMed (asc)	−12	41	20,150,324–20,190,103	176	963
COSMO-SkyMed (dsc)	−168	50	20,150,324–20,190,103	166	924
Total			20,150,324–20,190,103	342	1887

Table 1. COSMO-SkyMed SAR data used in this study, θ is azimuth angle and φ is incidence angle, N is number of SLC images and M is number of DInSAR interferograms computed for each data set. 2D and 3D time series span 24 March 2015–3 January 2019 interval when both ascending and descending data are available.

Differential interferograms were filtered using the adaptive filter with a filtering function based on local fringe spectrum (Goldstein and Werner, 1998) and unwrapped using the minimum cost flow algorithm (Costantini, 1998). The residual orbital ramp was corrected by applying baseline refinement algorithm implemented in the GAMMA software that utilizes unwrapped phase and topographic height at selected coherent pixels to solve for a refined baseline. Minor interpolation of each interferogram was performed in order to improve the spatial coverage reduced by decorrelation. Then, ascending and descending interferograms were geocoded and resampled using the Geospatial Data Abstraction Library (GDAL) program to a common lat/lon grid with a uniform spatial sampling of 5 m.

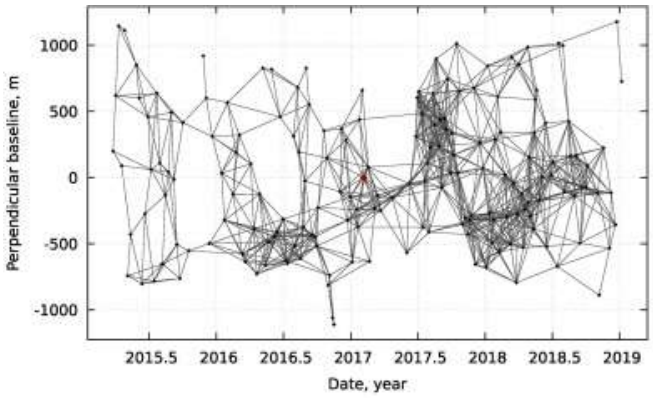

(a) Ascending

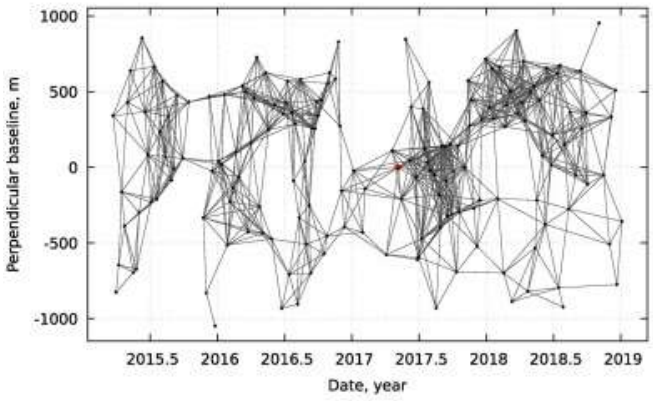

(b) Descending

Fig. 3. Spatial and temporal baselines of COSMO-SkyMed ascending and descending interferograms used in this study. Brown points mark ascending and descending master images.

Geocoded to a common grid, ascending and descending interferograms with an average coherence after filtering above 0.5 were processed with the MSBAS techniques to produce deformation time series and annual linear deformation rates over Funu landslide and its close surroundings.

dGNSS measurements

The DInSAR-derived deformation rates are validated through a comparison with the dGNSS measurements acquired by repeated measurement campaigns. The dGNSS measurements were captured in a static acquisition mode with Leica GX1230 dual-frequency receivers and post-processed with Leica Geosystems post-processing software. The dGNSS measurements were acquired over already in place benchmarks that are solid concrete structures, such as a water fountains, concrete sewers or street curbs. Measurement duration (5 min) at roving sites was constrained by the safety of operators and equipment in this area, although position accuracy would have benefited from longer sessions. The accuracy achieved for the dGNSS locations was estimated as 7.5 mm for the horizontal and 16.5 mm for the vertical components. These uncertainties refer to the internal precision of the measurement, field conditions, and data post-processing. It was also assumed that all benchmarks and the reference station move at the same rift opening rate of about 2 mm/year (Delvaux et al., 2017).

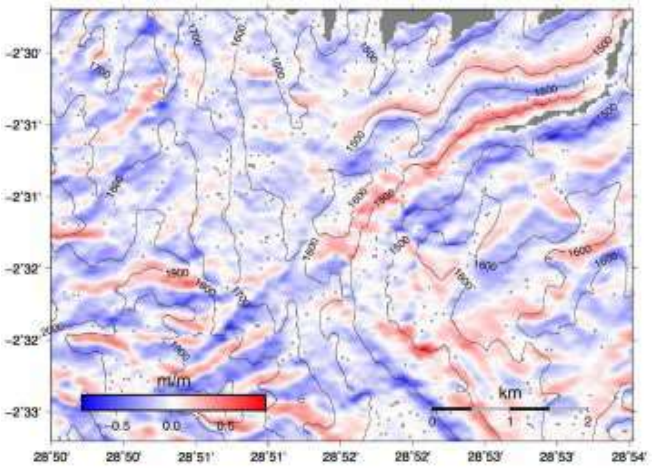

(a) First derivative along north direction

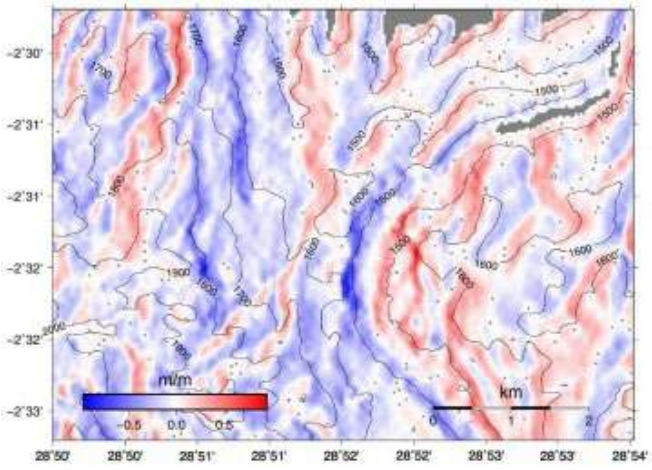

(b) First derivative along east direction

Fig. 4. Central first derivatives of 1 arc-second (~30 m) resolution SRTM DEM in north direction (a) and in east direction (b) used in the computation of the three-dimensional deformation with MSBAS-3D.

DEM derivatives

The and values (Fig. 4) were computed from SRTM DEM using the Generic Mapping Tools (GMT) grdmath -M DDY/DDX command. Prior low-pass filtering of DEM was applied using GMT grdfilter command to computed average values in 65 m window and therefore removing surface features that are not expected to affect the ground motion at depth.

Results

Fig. 5, Fig. 6, Fig. 7 show annual linear deformation rates for the city of Bukavu computed with the 1D, 2D, and 3D MSBAS techniques. For all methods, the deformation signal of the large Funu landslide clearly stands out.

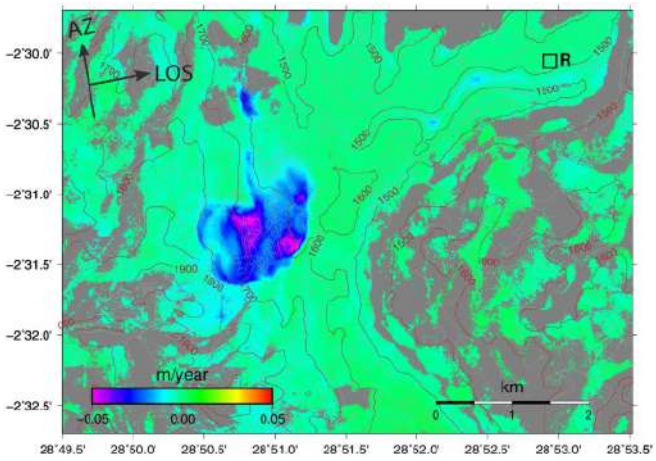

(a) Ascending line-of-sight

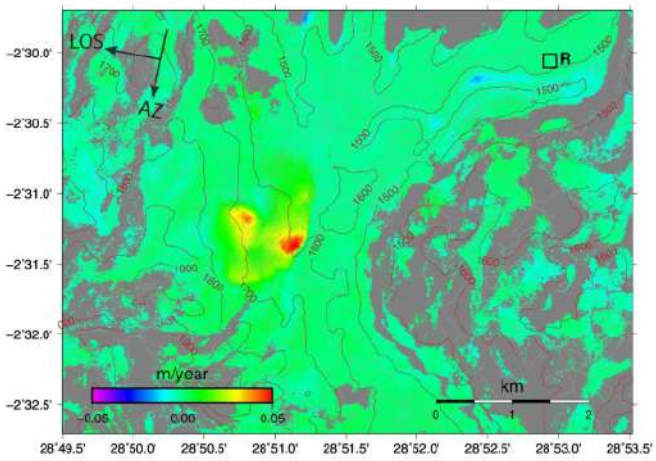

(b) Descending line-of-sight

Fig. 5. Maps of linear deformation rate in the radar line-of-sight (LOS) geometry computed using MSBAS-1D from COSMO-SkyMed ascending (a) and descending (b) SAR data. Displacements along LOS direction have to be interpreted as a one-dimensional component of the full 3-D displacement vector. Red colour represents motion towards satellite and blue colour represents motion away from satellite. 100 m elevation contour lines are plotted in brown. R is reference region. Streets are plotted in gray (downloaded from http://overpass-turbo.eu/). Average SAR backscatter intensity is exposed in decorrelated areas.

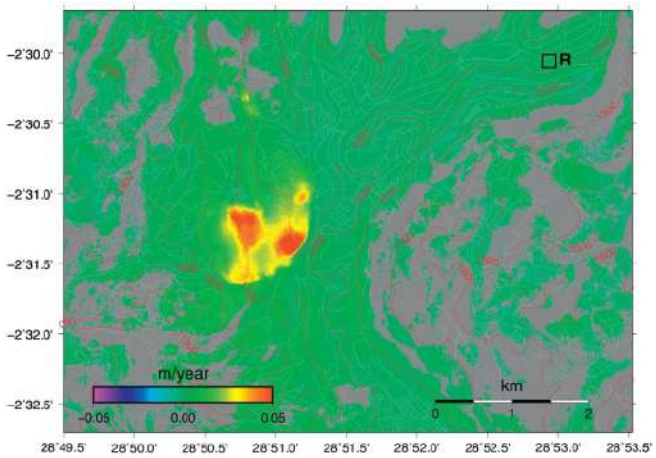

(a) East

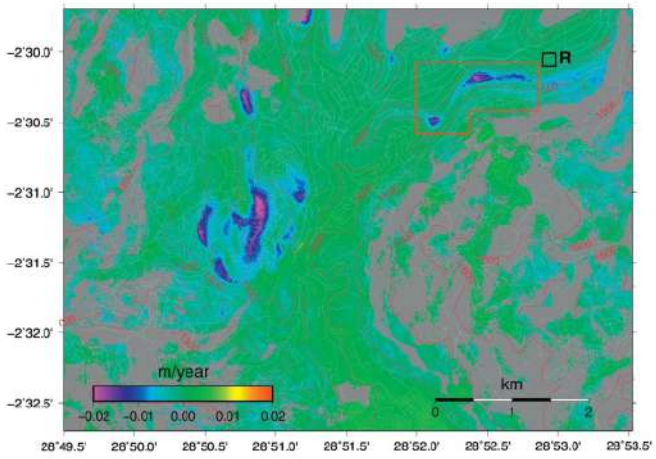

(b) Vertical

Fig. 6. East (a) and vertical (b) components of linear deformation rate computed using MSBAS-2D from combined COSMO-SkyMed ascending and descending SAR datasets. 100 m elevation contour lines are plotted in brown. R is reference region. Subsiding area that does not deform according to (4) is outlined in red. Streets are plotted in gray (downloaded from http://overpass-turbo.eu/). Average SAR backscatter intensity is exposed in decorrelated areas.

The 1D ascending and descending linear deformation rates computed with (1) show distance to satellite (line-of-sight) displacements. Absolute maximal rates of displacement are similar (0.05 m/year) between ascending (Fig. 5(a)) and descending (Fig. 5(b)) datasets, but the extent of the deformation measured over the Funu landslide in the descending map is significantly lesser than in the ascending map.

The 2D east and vertical linear deformation rates computed with (3) show eastward motion with a maximum magnitude of 0.05 m/year (Fig. 6(a)) and downward motion with a magnitude up to 0.02 m/year (Fig. 6(b)). Only the signal of the landslide is shown in the eastward component deformation map, while the vertical displacement map highlights also other deforming regions within the city.

The 3D north, east and vertical linear deformation rates computed with (5) are shown in Fig. 7. The north deformation rate map (Fig. 7(a)) highlights areas with both northern and southern motion with a maximum rate of 0.02 m/year over different places within the city. The east map (Fig. 7(b)) shows eastward deformation with a maximum rate of 0.05 m/year that is nearly identical to the 2D case (Fig. 6(a)) and

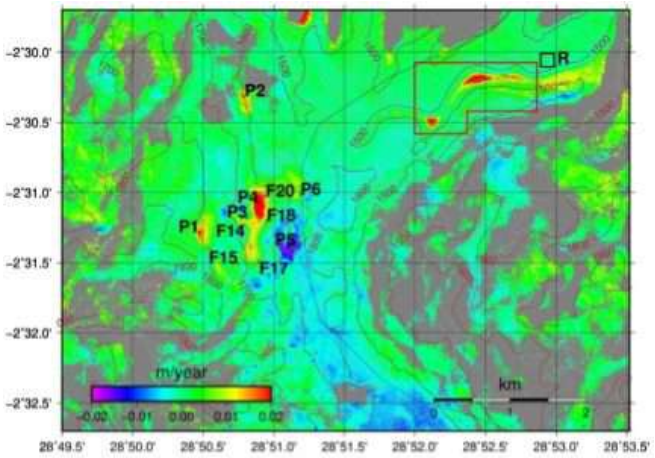

(a) North

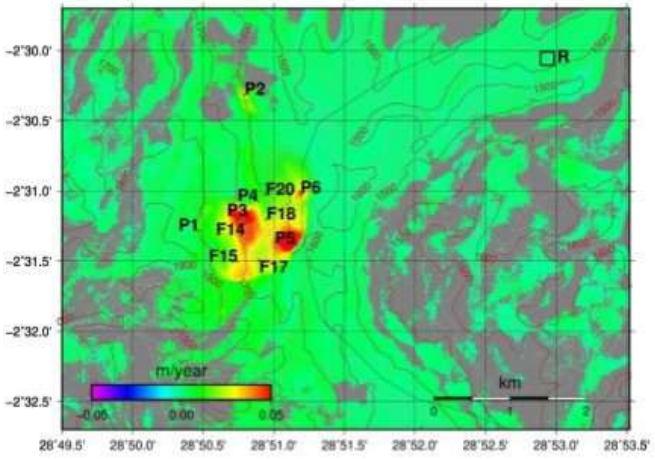

(b) East

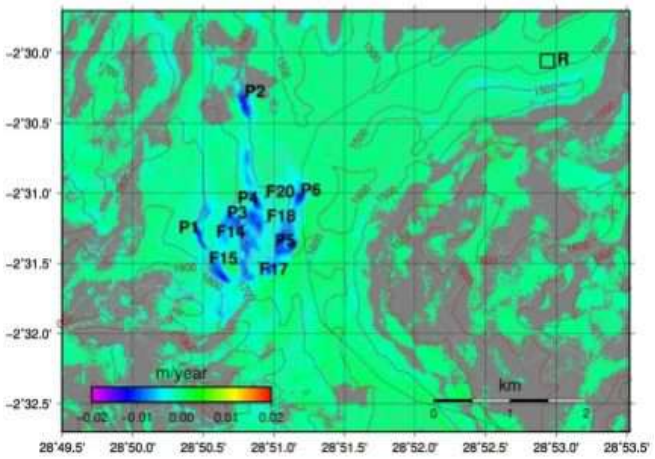

(c) Vertical

Fig. 7. North (a), east (b), and vertical (c) components of linear deformation rate computed using MSBAS-3D from combined COSMO-SkyMed ascending and descending SAR datasets. 100 m elevation contour lines are plotted in brown. R is reference region. Subsiding area that does not deform according to (4) is outlined in red. Streets are plotted in gray (downloaded from http://overpass-turbo.eu/). Average SAR backscatter intensity is exposed in decorrelated areas. Points F14, F15, F17, F18, F20 mark location of campaign GNSS sites. For points P1-P6 that approximately correspond to regions of fastest motion time series are provided in Fig. 9.

is dominated by the signal of the large Funu landslide. The vertical map (Fig. 7(c)) highlights only downward motion with a maximum rate of 0.02 m/year. Similarly as with the 2D case (Fig. 6(a)), signals of other deforming regions are captured within the city. The overall scale of the deformation measured with the 3D case is however of lower magnitude.

Annual horizontal displacements measured with MSBAS-3D method are plotted as vectors in Fig. 8, along with the dGNSS deformation vectors. It clearly highlights an advancing landslide lobal front, as well effect of lateral constraints from the surrounding non-moving topography. The directions of movement measured by dGNSS and DInSAR are in general in good agreement at F14, F15, F17, F18 and F20 dGNSS sites, for which the coefficient of determination R2 is greater than 0.75 for north and east deformation components.

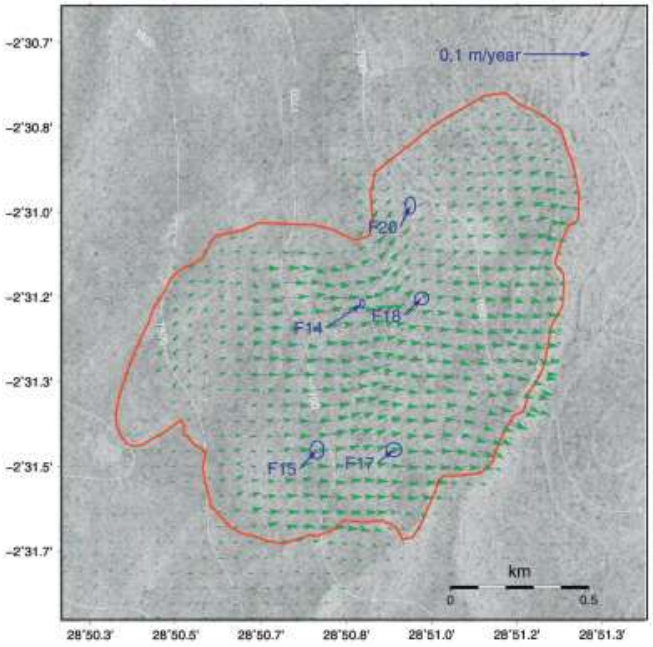

Fig. 8. Horizontal deformation rate vectors computed from COSMO-SkyMed ascending and descending DInSAR data with MSBAS-3D technique are in green. Horizontal deformation vectors with 2σ (i.e 95%) confidence interval elipses computed from campaign GNSS data for selected sites F14, F15, F17, F18, F20 are in blue. Funu landslide outline is in red. 100 m elevation contour lines are in white. Background is SAR intensity.

The 3D surface deformation time series for points P1-P6 (marked in Fig. 7) that approximately correspond to regions of fastest motion within the landslide are shown in Fig. 9. Standard deviation, computed in 5×5 pixels (~25×25 m) window, measures deviation from a mean value rather than precision of the measurement technique because deformation signal and measurement noise cannot be separated. Standard deviation over a larger 33×33 pixels (~165×165 m) window at a region that does not experience observable ground deformation allows measuring precision of this measurement technique. The estimated precision is better than 2.8, 1.4, and 0.5 mm for north, east and vertical components respectively.

Deformation produced by the Funu landslide clearly stands out in all deformation maps. Discrimination between vertical and horizontal movements provided by MSBAS-2D and MSBAS-3D (Fig. 6, Fig. 7) show that, overall, Funu landslide movement is mostly horizontal (to the east). Half-moon deformation patterns highlight rotational movements at the head of the landslide that could not be directly observed from the LOS measures obtained with MSBAS-1D (Fig. 5).

Fig. 5, Fig. 6, Fig. 7 also highlight other ground deformation processes outside of the Funu landslide. At point P2 is observed the deformation associated with another old, deep-seated landslide, as already stressed in Nobile et al., 2018. Deformation observed at the northern limit of the city is probably associated to subsidence of recently urbanized river delta deposits. As similar origin is inferred for documented subsidence over the flat valley bottom east of the study area (red insert). These patterns of deformation were also observed in the field (Kalikone Buzera et al., 2017). Even though the purpose of our research was not to focus on those areas, this further confirms the reliability of the DInSAR processing.

Discussion and conclusions

Working on ascending and descending interferograms computed prior to the MSBAS analysis and geocoded to a common grid, the MSBAS method computed 1D, 2D, and constrained to the parallel surface flow 3D surface deformation time series. From those time series, MSBAS computed map of linear deformation rates for a large, slow-moving, deep-seated landslide in the city of Bukavu. The advantages and disadvantages of each MSBAS and similar methods are summarized in Table 2.

	Resolved deformation components	Assumptions and disadvantages
MSBAS-1D	Exact 1D (line-of-sight)	Individual contributions of north, east and vertical deformation components cannot be determined
MSBAS-2D	Approximate 2D (east and vertical)	Negligible north component
MSBAS-3D	Exact 3D	Motion parallel to the surface
De Michele et al. (2010); Gourmelen et al. (2011)	Exact 3D	Requires combination of high (DInSAR) and low (speckle tracking and MAI) precision measurements; can be used for mapping only large deformation
Pepe et al. (2016)	Approximate 3D	Minimum acceleration constraint
Hu et al. (2018)	Exact 3D	Negligible cross-slope component; Motion is allowed in vertical plane in direction of slope aspect

Table 2. Comparison of methods for resolving deformation components from DInSAR and other SAR-derived data.

The LOS measures of deformation obtained with the MSBAS-1D method (Fig. 5) are consistent with the multi-temporal DInSAR SBAS results obtained over a one-year period by Nobile et al., 2018. Overall, the MSBAS results are in agreement with dGNSS measurements with the exception of one zone of the landslide that corresponds to a recent subsequent landslide within the large landslide (Fig. 2b); here, dGNSS measurements show deformation of up to 500 mm/yr (Nobile et al., 2018). These high deformation rates as well as the sharp velocity contrast with the zone directly surrounding it (with a deformation rate nearly an order of magnitude lower), lead to either a loss of coherence or an underestimation of the deformation during the unwrapping of the interferograms. Those are however associated with the intrinsic limitations of DInSAR technique with respect to measure of rapid displacements. Speckle offset analysis performed with the GAMMA software on selected long-timespan pairs did not detect these large deformation rates neither.

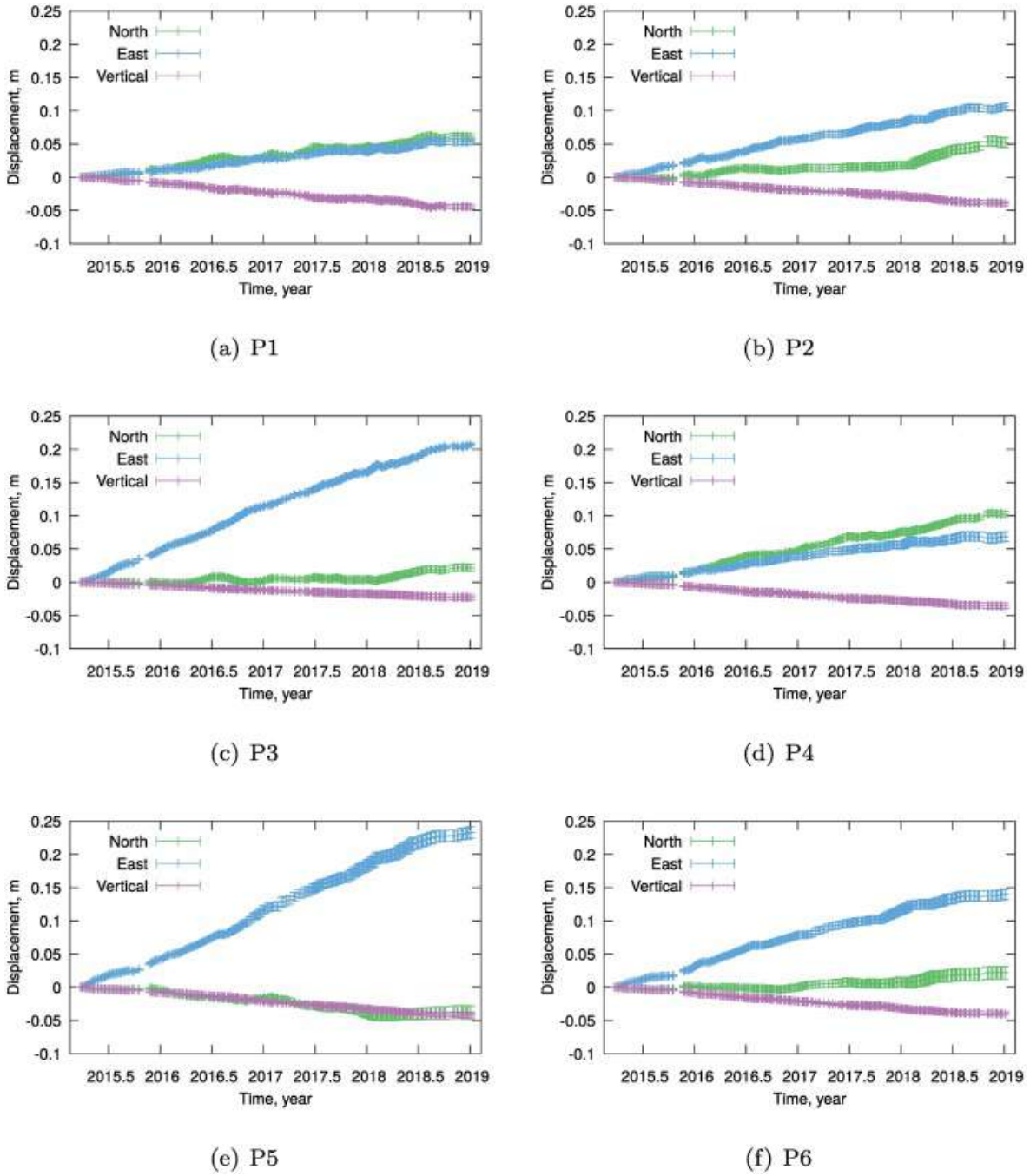

Fig. 9. Three-dimensional time series of ground deformation for points P1-P6 (marked in Fig. 7) that approximately correspond to regions of fastest motion. Standard deviation is computed in 5×5 pixels (~25×25 m) window.

The benefits provided by decomposing the deformation components were illustrated in Fig. 5, Fig. 6, Fig. 7, Fig. 8. Compared to MSBAS-2D and 3D, the limitations associated to the traditional 1D LOS analysis (Fig. 5) are clear. While difficult to interpret and communicate to stakeholders unfamiliar with the concept of 1D LOS viewing geometry (Fuhrmann and Garthwaite, 2019), deformation measured on those maps may also lead to misconception about the underlying processes. For instance, individual north, east and vertical deformation components may cancel each other out when the contribution of horizontal components is equal in magnitude but opposite in sign to the contribution of the vertical component. In extreme cases, deformation may appear entirely absent in one (i.e. either ascending or descending) of LOS deformation maps (e.g. Samsonov et al., 2013, Samsonov et al., 2014). The 2D and 3D results (Fig. 6, Fig. 7, Fig. 8) are much easier to interpret thanks to the direct discrimination between horizontal and vertical deformation components. The information gathered about the north component provides additional, non-negligible keys for the understanding of processes at work (see Fig. 8). The 3D solution highlights the presence of an active, advancing landslide front, as well effect of lateral constraints from the surrounding non-moving topography. If this behaviour was anticipated from morphometric analysis of high resolution DEMs and the presence of a large bulge at the landslide toe, this pattern of displacement was completely missed by traditional DInSAR measures (Nobile et al. 2018). With the increase of the understanding of the mechanisms of the landslide (interaction with surrounding topography, future evolution and interaction with downslope stream, etc.), such knowledge also bring information on environmental controls, temporally and spatially-variable external forcing conditions and characteristics of future deformation patterns.

In our example, while the magnitude of the horizontal deformation remains similar between MSBAS-2D and MSBAS-3D, the information about the north component provides clear insights for the understanding of the landslide deformation pattern. The decision of whether to use one or the other will depend on the validity of the Surface Parallel Flow constraint (4) and is case-specific. For many gravity-driven processes, such as landslides and glacier flows, making such an assumption of motion parallel to the surface is a valid approximation. However, even when the assumption of motion parallel to the surface is not strictly correct, the approximate 3D analysis may still provide valuable clues for the understanding of the processes at work that may otherwise go undetected. With our example applied on the city of Bukavu, we also show measure of displacement were expected movement clearly not comply with the assumption of motion parallel to the surface. Besides Funu landslide, the study area encompasses for instance a flat valley bottom that corresponds to an old marsh, recently urbanized and that is subjected to subsidence (Nobile et al., 2018). There, MSBAS-3D incorrectly classifies ground movement as horizontal (Fig. 7(a)), while it is perfectly well grasped with MSBAS-2D (Fig. 6(b)).

In comparison to the method used in Notti et al. (2014); Kalia (2018); Hu et al., 2018, Hu et al., 2019 (Table 2), where the LOS velocity is projected along the steepest downslope to obtain estimates of the landslide motion, MSBAS-3D computes a more general solution. It does not require the motion to occur along the steepest downslope, but only parallel to the surface; which allows to capture lateral motion. The drawback of MSBAS-3D approach is that slope-normal displacements are not allowed. The slope-normal displacements can be produced by mass depletion/accumulation, hydrological loading/unloading, and soil swell/shrink. The magnitude of slope-normal displacements of slow-moving landslides, however, is usually smaller than the magnitude of parallel to the surface displacements. In case of large slope-normal displacements, the Hu et al. (2018) methodology may provide more accurate results.

Other methods commonly used to measure azimuthal deformation have other drawbacks (Table 2). Speckle tracking (e.g. Wright et al., 2004; De Michele et al., 2010; Raucoules et al., 2013; Shi et al., 2018) or Multiple Aperture Interferometry (MAI) (e.g. Gourmelen et al., 2011) approaches are for instance best suited for measuring meter-scale deformation (Fuhrmann and Garthwaite, 2019). When the measured deformation is of lower magnitude (e.g., millimetre- to decimetre-scale displacement associated to slow moving landslides (Hungr et al., 2014), the north-south displacement component accuracy provided is much lower to what can be reached with conventional DInSAR. Also, the competing techniques presented in the introduction commonly work on individual (or a series of disconnected) interferograms to derive the 3D deformation. By potentially missing controls of temporally and spatially-variable external forcing on the process kinematic, they are more adapted to the study of sudden deformation events such as earthquakes or volcanic eruptions (Hu et al., 2014). Here lie the strengths of the MSBAS method: producing 3D deformation time series with the accuracy of conventional DInSAR and the spatio-temporal resolution of modern SAR sensors, it can provide unrivalled insights for studying both long and short-term kinematics of surface processes. Those benefits associated to the 3D decomposition of surface deformation were demonstrated here on a large slow-moving landslide, but this method can be applied to studying many other gravity-driven processes producing motion parallel to the surface.

(Engineering geology, November 5, 2020, https://geologyengineering.com/2020/11/satellite-interferometry-for-mapping-surface-deformation-time-series-in-one-two-and-three-dimensions-a-new-method-illustrated-on-a-slow-moving-landslide)

Deep learning based classification of rock structure of tunnel face

Jiayao Chen, Tongjun Yang, Dongming Zhang, Hongwei Huang, Yu Tian

Introduction

Structural health monitoring (SHM) and intelligent damage image recognition technology during the construction period have been the subject of intense research in rock tunnel engineering (Gao and Mosalam, 2018). In this regard, the complex and variable nature of geological structures, difficulty in prediction, and frequency of the construction process in the tunnel face have made the research problem very prominent. Moreover, if rock mass structure is not accurately predicted, the tunnel face encounters collapse problems and construction obstacles, which will undoubtedly present serious challenges to the tunnel construction, operation, and maintenance.

In recent years, with the rapid development of artificial intelligence (AI) and machine learning (ML) technologies (Krizhevsky et al., 2012), especially in the application of in-depth learning in the computer vision, rock structure information of tunnel face based on the image recognition has received the attention of scholars and builders in the construction and maintenance process (Huang et al., 2018). So far, several researchers have used the classical field research methods (Aksoy et al., 2012, Zhang and Goh, 2012, Rehman et al., 2019), mechanics deduction (Goh and Zhang, 2012, Song et al., 2018, Li et al., 2019, Su et al., 2019), and numerical simulation (Manouchehrian and Cai, 2018, Schreter et al., 2018, Xiang et al., 2018, Lee et al., 2019) to identify the mechanism of different rock mass structures. Starting from the exploration of structural mechanisms, many internal characteristics of the project could be solved and the project risk is greatly reduced. However, most of the studies have been carried out for the specific rock structure ignoring the macroscopic judgment and analysis of the whole rock structure. Hence, the automatic recognition of rock image cannot be realized. In accordance with the National Standard for Engineering Classification of Rock Mass (GB50218-2014), five rock structure categories were defined based on the description of the form and feature of discontinuities in Table 1, including Mosaic Structure (MS), Granular Structure (GS), Layered Structure (LS), Block Structure (BS), and Fragmentation Structure (FS). In the study of rock features of the whole category, due to the limited sample size, researchers (Fekete and Diederichs, 2013, Chen et al., 2016, Pittam et al., 2016, Riquelme et al., 2016, Sarro et al., 2018; Zhang et al., 2020) mainly have concentrated on traditional rock feature extraction methods. For instance, Chen et al. (2016) proposed a photogrammetry method for extracting the discontinuity orientation automatically from the rock mass surface 3D point cloud based on the K-means clustering and the random sample consistency. Fekete et al. (2013) presented a workflow from data collection and analysis to design outputs for integrating the Lidar-derived point-cloud data into the rock mass stability modeling. Riquelme et al. (2016) proposed the low-cost remote sensing and manual collection techniques to gather all the accessible discontinuities of a slope. These results provided valuable ideas for the structural stability analysis of rock tunnel

Feature description	Block structure	Layered structure	Mosaic structure	Fragmentation structure	Granular structure	Define priority
Discontinuity form	Block	Layered	Rock block mosaics	Rock fragmentation	Cuttings and mud	1st
Integrity degree	Integrity	Middle integrity	General integrity	General fracture	Fracture	3rd
Discontinuity spacing (cm)	>30	>10	10–30	<30	–	2nd

Table 1. Definition of rock structure based on the National Standard for Engineering Classification of Rock Mass

Nevertheless, compared with the state-of-the-art deep learning techniques, the traditional machine learning methods have lower efficiency and accuracy for the feature extraction. As an important sector of deep learning in the computer vision applications, the convolutional neural networks (CNNs) have been widely used in the field of infrastructure health monitoring in civil engineering; e.g., identifying concrete cracks (Cha et al., 2018, Chaiyasarn et al., 2018, Dorafshan et al., 2018, Bang et al., 2019), detection of damaged buildings (Cha and Buyukozturk, 2015, Gao and Mosalam, 2018), monitoring of damaged walls (Beckman et al., 2019), and detection of corroded pipes (Cheng and Wang, 2018, Kumar et al., 2018). These methods not only have high accuracy and efficiency but also have been widely used because of the simple scenes and convenient image acquisition. However, due to the lack of lighting conditions, complex construction procedures, and poor photography environment, it is difficult to obtain image samples in the areas close to the rock tunnel face. In addition, deep learning is dependent on huge training samples (Gu et al., 2018) and there is scarce research on the tunnel face image at present.

In this paper, an adaptive digital photography system (ADPS) is utilized to acquire an image database of the tunnel working face in batches using the on-site lighting system during the construction process. Based on the statistics obtained from the Mengzi-Pingbian Highway Tunnel (MPHT) in Yunnan Province, China, five rock structure categories (i.e., MS, GS, LS, BS, and FS) were labelled based on the National Standard in China (GB50218-2014). In addition, by combining Inception and ResNet, a comprehensive CNN, namely Inception-ResNet-V2 (IRV2), was proposed to classify the dataset. The recognition accuracy, precision, F-score, and execution time of the proposed method were then analyzed compared with other deep learning methods such as ResNet-50 (Szegedy et al., 2015), ResNet-101 (He et al., 2016), and Inception-v4

(Szegedy et al., 2017). Finally, the application of deep learning framework in the face image recognition of rock tunnel was systematically evaluated.

Data collection

Image acquisition of rock tunnel face

The ADPS used in the image acquisition consists of a Canon 750D camera, tapeline, tripod, measuring equipment (laser rangefinder, thermo hygrometer, and illuminometer), and light source (two LED dropout lamps with 1000 W adjustable power). As shown in Fig. 1, ADPS was manually used to record the temperature, humidity, illumination information, and the distance between the shooting point and the surface of each tunnel face in Mengzi-Pingbian Highway Tunnel (MPHT) in Yunnan, China. In the photography process, it is ensured that the illumination is uniform and parallel, the distance between the two lights is within 1.5–2 m, and the camera is horizontally placed on the tripod.

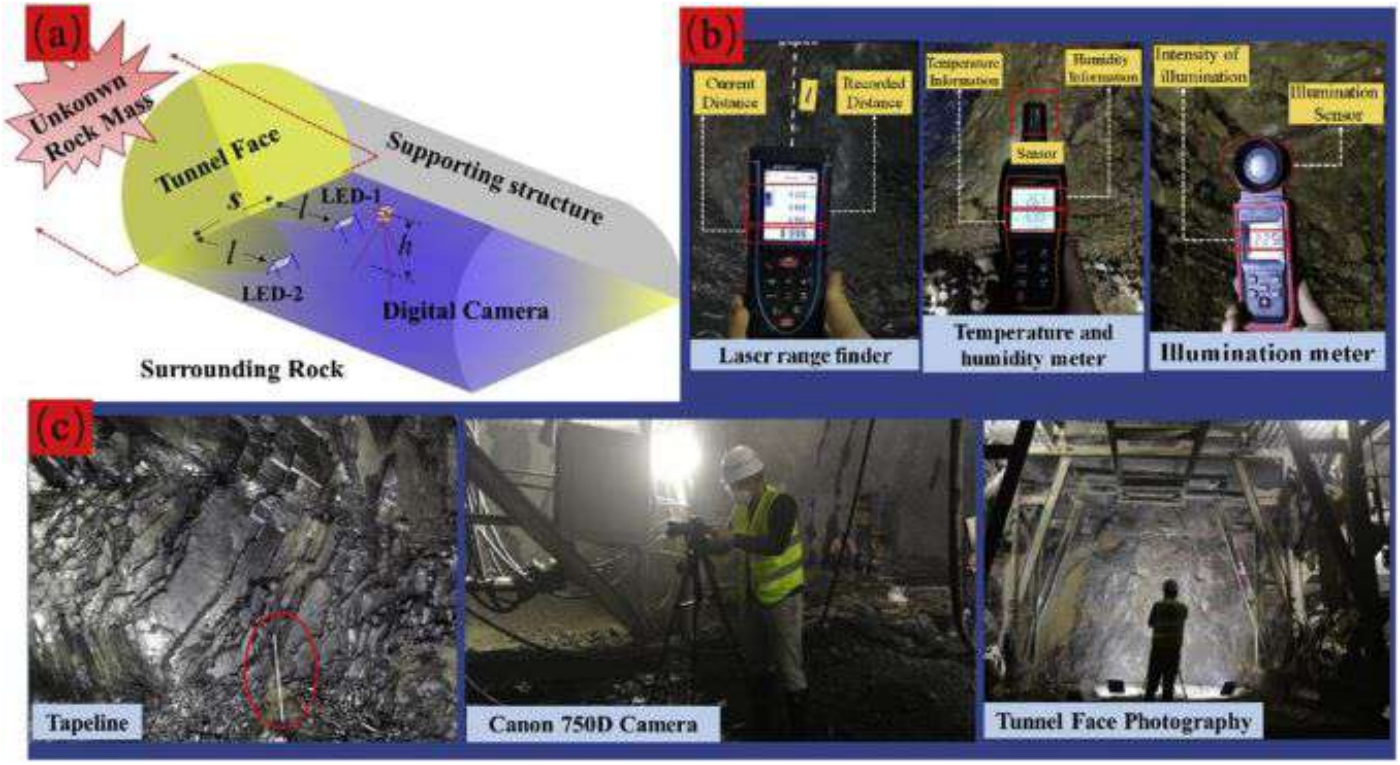

Fig. 1. The ADPS including (a) global schematic, (b) main tunnel face measuring equipment (i.e., laser ranging, thermo hygrometer, and illuminometer), and (c) in-site tunnel face image acquisition screen.

To determine the most suitable image acquisition time, six main construction processes are present and compared in Fig. 2, mainly including: (1) drilling with pneumatic leg rock-drilling trolley, (2) pre-blasting preparation (a detonator is used to connect multiple detonators, in which the red quadrilateral represents the connection), (3) tunnel ventilation (ventilation and risk elimination of working face by draught fans and ventilation pipes), (4) slag extraction from working face (removing blasting residues with excavation and transportation equipment), (5) building the first lining trolley, and (6) the best time for tunnel face image acquisition (after the first lining trolley was built, the safety of personnel was ensured and the shooting time was guaranteed). It is concluded that the best time for the face image acquisition is when the first liner trolley is built, which not only protects the safety of personnel but also ensures the shooting time. Furthermore, the face images in different construction processes are taken under different lighting conditions at a distance of 1.0–1.5 m from the camera to enrich the compiled dataset. As a result, more than 3000 images were captured from 150 tunnel faces occupying 20 GB of storage space.

Data preprocessing

In this study, 42,400 geological structure images randomly cut from 3000 raw images from various tunnel faces were tagged by 5 labels including MS, GS, LS, BS, and FS structures. In order to promote the image processing efficiency, the rock face images were cropped from the original sizes of 3968 × 2240 pixels into smaller images of 396 × 448 pixels, meaning that each original image is divided into 50 sub-images (10 × 5). The number of images in each label is listed in Table 2. The samples of the dataset are shown in Fig. 3. It can be seen that due to the complex geological conditions in Yunnan Province, China, the tunnel face textures affected by the faults, rock interlayers, and rock category, are hard to distinguish with a relative high accuracy and inefficiency by the traditional feature extraction methods (i.e., edge detection, threshold segmentation). In addition, the texture differences of rock structures with different labels decrease with the increase of database diversity. Therefore, the fast capture of key texture features is a significant challenge for the big data-based rock classification. Meanwhile, deep learning model have been characterized by the acquisition capacity of deep-features for the classification task, it is thus urgent to use deep learning model for pre-training.

Proposed method

Basic CNN model

The architecture of CNNs consists of several unique layers, including the convolutional, activation, pooling, dropout, and Softmax layers with different functions. Each of these layers is briefly explained below (Krizhevsky et al., 2012, Huang et al., 2017). Meanwhile, the framework of IRV2 is present in Fig. 4.

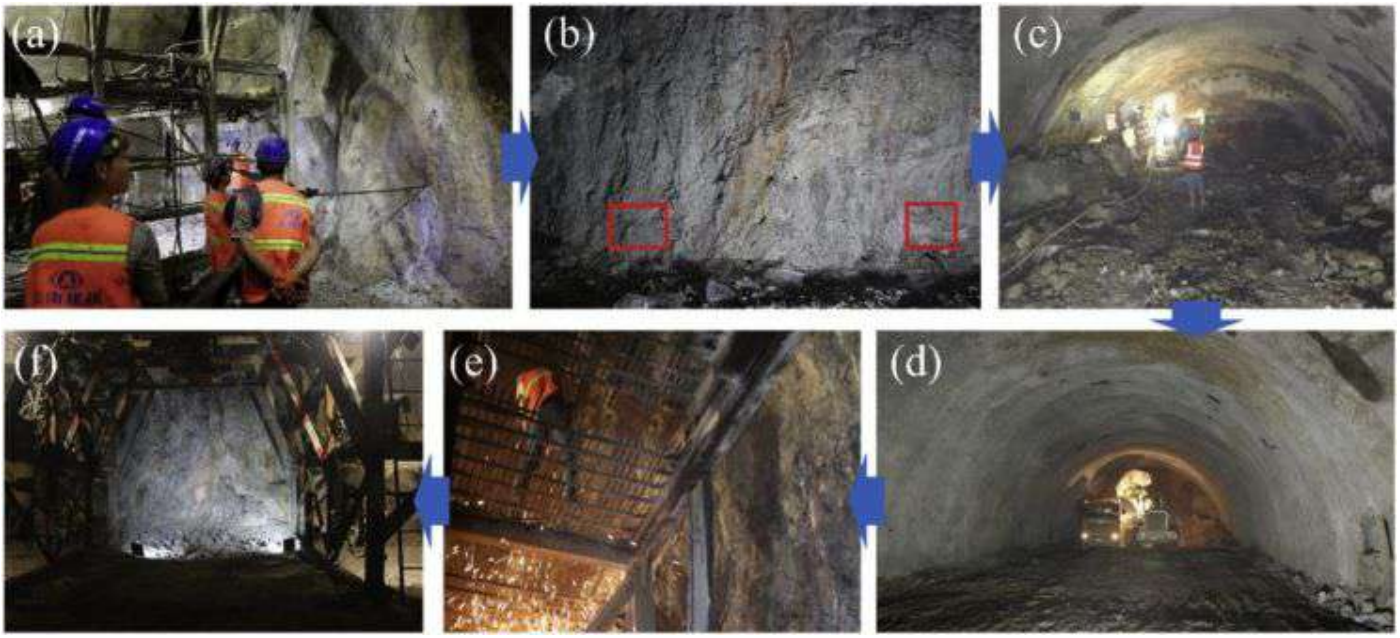

Fig. 2. Selection diagram of shooting time under different construction procedures.

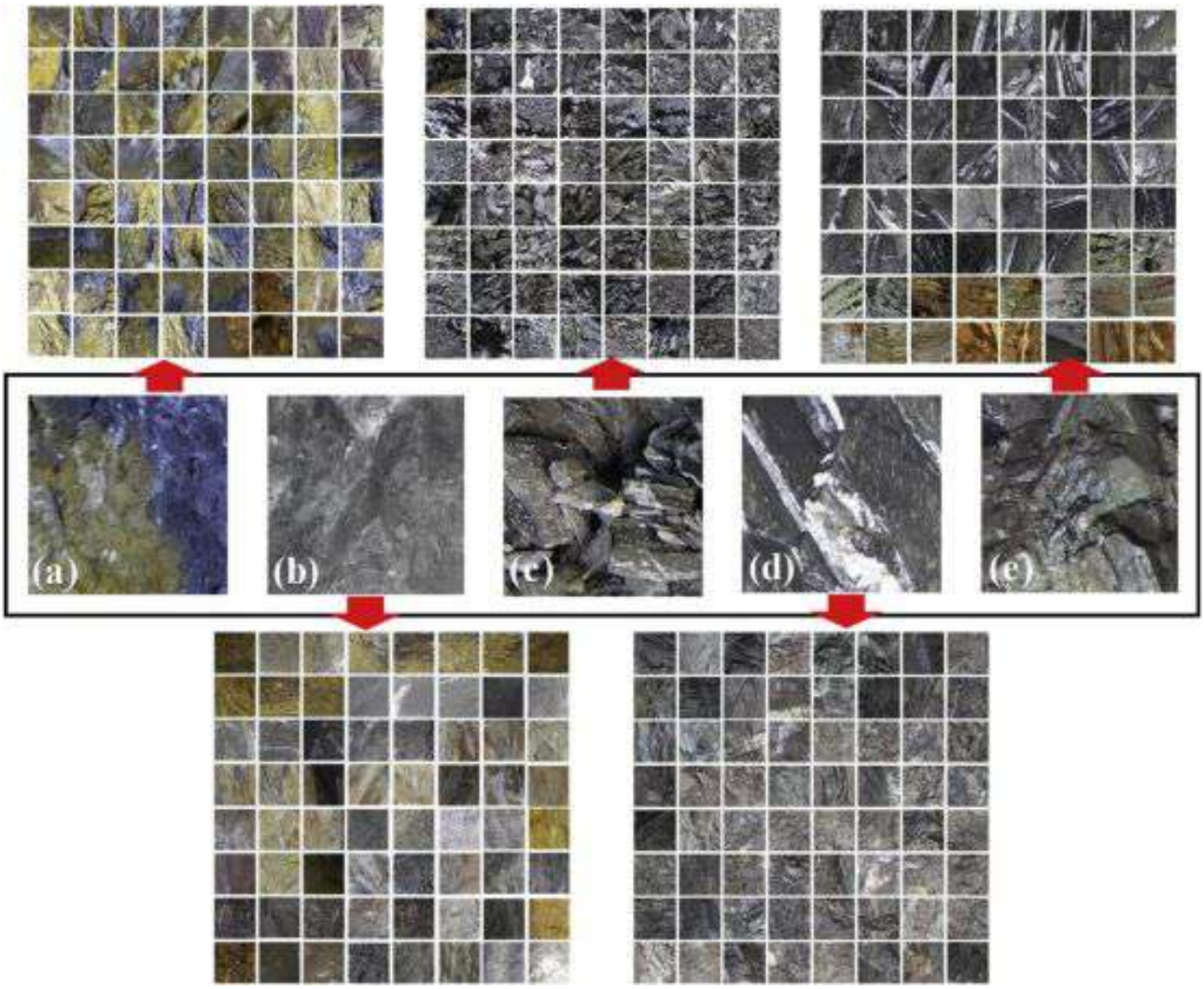

Fig. 3. Samples from different types of geological rock structures: (a) MS; (b) GS, (c) LS, (d) BS, and (e) FS.

No.	Rock structure type	Number of images
1	Mosaic Structure (MS)	7956
2	Granular Structure (GS)	9177
3	Layered Structure (LS)	7885
4	Block Structure (BS)	7962
5	Fragmentation Structure (FS)	9420
	Total number	42,400

Table 2. The number of images per rock structure type.

Convolutional layer

Convolutional layers are widely used as the feature generators. Each convolution kernel of CNNs slides across the input matrix with a definite stride. The element-by-element multiplications are conducted between the input RGB matrix and the kernel at each sliding position, and all the multiplication values are added together to form the output plus a bias. The output size is determined by the convolutional kernel and the stride size. The weights and biases of convolution kernels are the unknown parameters waiting for the optimization.

Activation layer

The role of the activation layer is to increase the nonlinearity of the convolution output. According to statistics, the Rectified-Linear-Unit (ReLU) as an activation function outperforms the traditional sigmoid function in terms of calculating the reasonable gradient. The nonlinear ReLU activation function avoids the gradient dispersion (gradient explosion) caused by too large gradient and the disappearance of gradient caused by too small gradient, while maintaining a relatively fast calculation speed. Therefore, it is widely used in the CNNs. In the Inception-ResNet-V2 algorithm shown in Fig. 4, ReLU function is implemented in all activation layers.

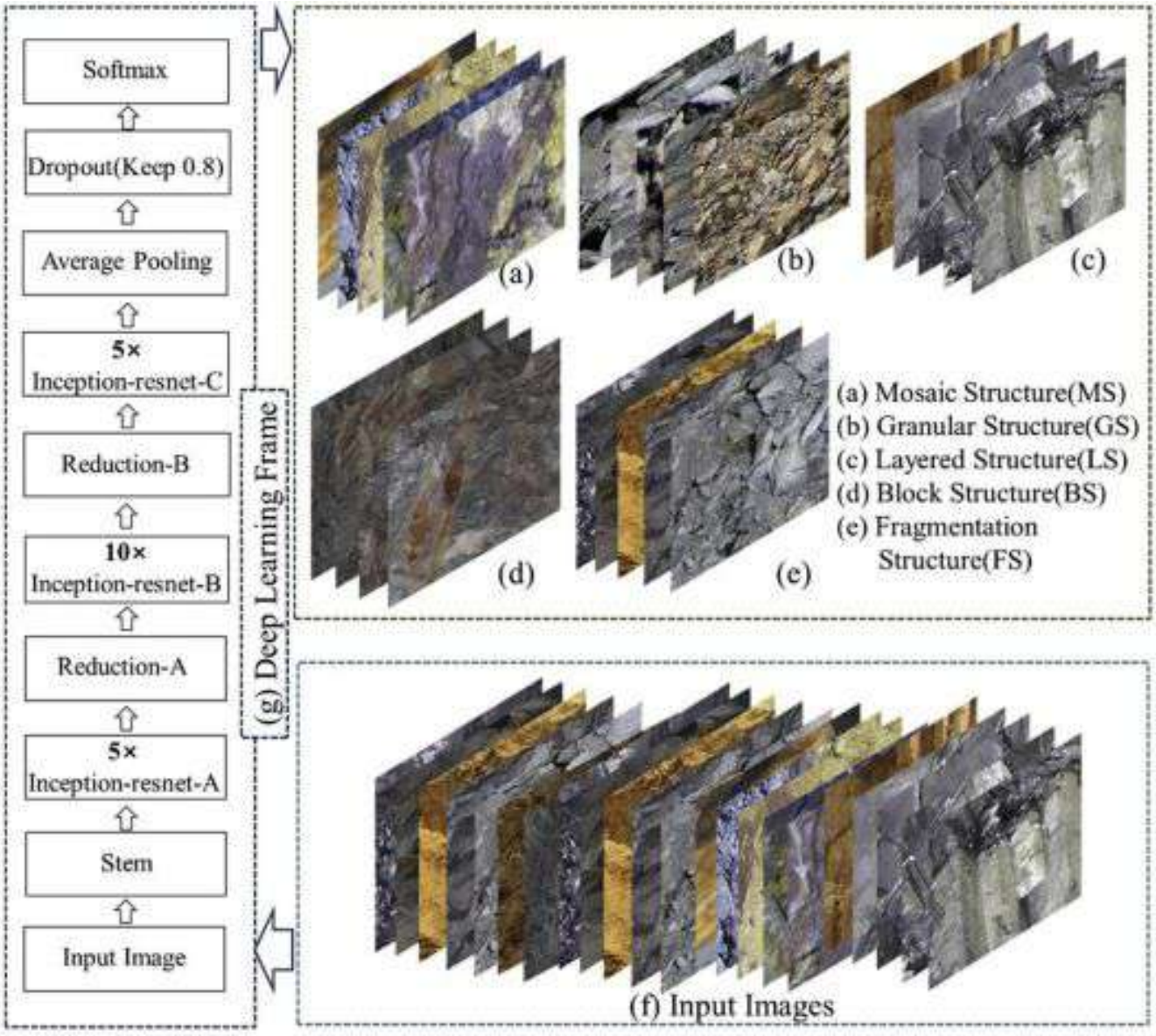

Fig. 4. Samples of rock structure type including (a–e) output samples of rock structure type, (f) input images, and (g) deep learning frame (IRV-2).

Pooling layer

The pooling layer generates the output through a sliding window similar to the convolutional layer and reduces the dimension of the feature map, number of parameters, and spatial size of the upper layer. There are two common pooling layers (i.e., the max pooling and the average pooling), whose values are calculated by the max or mean operators, respectively. As shown in Fig. 5, both of these two pooling layers are adopted in Inception-ResNet-V2 to keep the framework invariant to distortion, transformation, and translation.

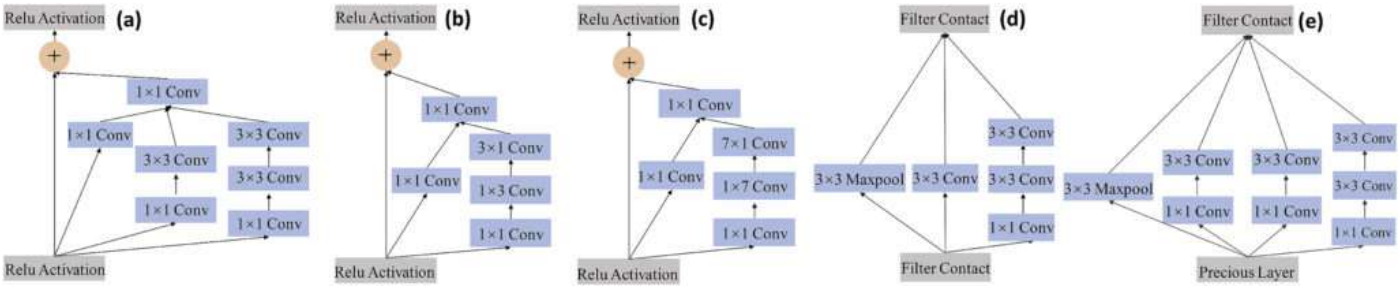

Fig. 5. The main core framework of Inception-ResNet-V2 including (a) Inception-ResNet-A, (b) Inception-ResNet-B, (c) Inception-ResNet-C, (d) Reduction-A, and (e) Reduction-B.

Dropout layer

Due to the large number of parameters in the CNNs, over-fitting problems may occur in these networks through the dropout process. Dropout is a random disconnecting technique that can randomly isolate the connections between different nodes with a dropout probability of 1-p. The dropout layer reduces the number of model parameters and increases the robustness of the algorithm. The random inactivation layer allows the model to avoid over-fitting occurrence and improves the robustness of the network structure.

Softmax layer

The Softmax layer is basically a combination of multinomial logistic losses, that is used in the multi-classification process to normalize the classification vector of a certain weight. The CNNs can transform the abstract matrix into the concrete classification, namely the rock structure of tunnel face (i.e., MS, GS, LS, BS, and FS structures in this paper).

Inception-ResNet-V2

Inception-ResNet-V2 (IRV2) (Szegedy et al., 2015, Szegedy et al., 2017, He et al., 2016) proposed first by Google company in 2018 (shown in Fig. 4) is employed as a state-of-the-art model to classify the rock structure images. It is mainly a combination of GoogLeNet (Inception) (Szegedy et al., 2015) and ResNet (He et al., 2016). The algorithm consists of 10 parts, each with its own role orientation and function. Inception is a typical network with a parallel layer structure that was first applied in GoogleNet. It includes parallel connections of filters with different sizes of 1 × 1, 3 × 3, and 5 × 5. The smaller size causes the convolution kernel to extract the image features more efficiently and greatly reduces the model parameters. Among them, the large-scale convolution kernel will increase the parameters of the model matrix, thus multiple small-scale convolution kernels will be replaced in parallel to reduce the function parameters in the case of the same receptive field. As a result, the model becomes wider and more accurate than the previous network with Inception. Presently, Inception v1–v4 (Szegedy et al., 2017) is the typical framework of GoogleNet. However, the residual learning-based ResNet is the winner of ILSVRC 2015, which can go deeper into 152 layers (Szegedy et al., 2015). The main idea of ResNet is to add a direct link to the framework, which is referred to as the idea of Highway Network. The previous network structure is a nonlinear transformation of performance input, while Highway Network allows a certain proportion of the output of the previous network layer to be retained. It allows the original input information to be transmitted directly to the next layer. Meanwhile, ResNet can protect the integrity of information by directly transmitting the input information to the output. The whole network only needs to learn the difference between input and output, which simplifies the learning objectives and difficulties. ResNet-50, ResNet-101, and ResNet-152 are the typical frameworks of ResNet.

In the Residual-Inception network (Fig. 5), the Inception module was used because it involves less computational complexity than the original Inception module. Fig. 5a–c represents the layers of Inception-ResNet, i.e., Inception-ResNet-A, Inception-ResNet-B, and Inception-ResNet-C. The number of layers in the total framework for each module is 5, 10 and 5, respectively. Fig. 5d and e demonstrates the Reduction Layer of IRV2, i.e., Reduction-A and Reduction-B. Each Inception block is connected to a filter layer (1 × 1 convolution without activation function) for the dimension transformation to achieve the input matching. This system compensates for the dimensionality reduction in the Inception block. According to a previous research (Szegedy et al., 2017), Inception-ResNet-V2 (IRV2) developed from Inception-ResNet-V1 (IRV1) matches the raw cost of Inception-v4 network. In this regard, one small technical difference between residual and non-residual Inception, in case of Inception-ResNet, is that only the batch normalization (BN) is used at the top of traditional layers. Since the experiments (Szegedy et al., 2017) showed that using a larger activation size may consume more GPU memory, more Inception modules can be added by omitting the BN layer after the activation. It also makes the model more efficient and concise. Moreover, if the number of filters exceeds 1000, the residual network will be unstable, and an early "death" issue will appear in the network training process. In other words, after tens of thousands of training data, the layer before the average pooling begins generating zeroes. This situation cannot be avoided by reducing the learning rate and adding additional BN layers. Furthermore, to compare the results of our proposed IRV2 model, ResNet-50, ResNet-101, and Inception-v4 models are implemented to classify the rock structure.

Evaluation metrics

Accuracy, precision, recall, and F-score are indispensable metrics for classification tasks, which are frequently employed to evaluate the applicability and superiority of the framework. As a simple dichotomy example, Table 3 displays the definition of True Negative (TN), True Positive (TP), False

Negative (FN), and False Positive (FP), from which the relationship between evaluation metrics and Judgment elements are obtained in Eqs. (1), (2), (3), (4).

$$\text{Accuracy} = \frac{TP+TN}{TP+TN+FP+FN} \quad (1)$$

$$\text{Precision} = \frac{TP}{TP+FP} \quad (2)$$

$$\text{Recall} = \frac{TP}{TP+FN} \quad (3)$$

$$F_\alpha = \frac{(\alpha^2+1)\text{Precision}\times\text{Recall}}{\alpha^2(\text{Precision}+\text{Recall})} \quad (4)$$

where accuracy answers the following question: out of all the images in the dataset, what fraction of images are correctly judged as true? Precision answers the following question: out of all the images that the classifier labelled as positive, what fractions of images are correctly judged as positive (i.e., true positives)? Recall answers the following question: out of all positive images, what fractions of images are correctly judged as positive? The F-score metric is a comprehensive indicator by weighing the importance between recall and precision. The α value is set as 1 in this study, which reflects the significance of recall and precision is the same.

True Value	Prediction Value	
	Positive	Negative
True	True Positive (TP)	True Negative (TN)
False	False Positive (FP)	False Negative (FN)

Table 3. Definition of True Negative (TN), True Positive (TP), False Negative (FN), and False Positive (FP

Experiment and results

The generated benchmark dataset was trained in Tensorflow framework made by Google and implemented with Intel Core i7-8700 processor, 32G RAM, Nvidia GTX 1080 Ti 11 GB GPU, Windows 10 operating system.

According to the performance of different frame models (i.e., ResNet-50, ResNet-101, Inception-v4, Inception-ResNet-V2), the experiment mainly includes the following aspects: (1) training, validation, and test results of database; (2) cross-validation, accuracy evaluation, and presentation of testing images, and (3) evaluation of execution time.

Training, validation, and test results

In the CNN simulation, the database is randomly divided into three parts of training, validation, and testing groups, each with a certain proportion. The number of each rock structure is shown in Table 4. In the table, proportion of training, validation, and testing images in each label is set to 60%, 25%, and 15%, respectively. The training and validation processes can be implemented in the same application code. Validation does not participate in the training process but is used to correct the weights and biases in the training process. Accordingly, the accuracy is improved and the probability of occurrence for overfitting and non-convergence is sharply reduced.

Total loss and accuracy are two commonly used indicators to evaluate the convergence and fitting effect of training and validation processes by using deep learning methods. Total loss is a non-negative real value function used to estimate the inconsistency between the predicted value and the real value of the model. The smaller the loss function, the better the robustness of the model. Fig. 6, Fig. 7 illustrate the changes of total loss and accuracy by increasing the experiment steps for the four different deep learning methods (i.e., ResNet-50, ResNet-101, Inception-v4, and Inception-ResNet-V2), respectively. It can be seen in Fig. 6, Fig. 7 that all four algorithms converge in the training and validation processes of the rock structure classification. Additionally, it can be observed from Fig. 6a and b that the total loss order from small to large is Inception-ResNet-V2, Inception-v4, ResNet-101, and ResNet-50 in both training and validation sets. In terms of accuracy ranking prediction (Fig. 7a and b), the relationship between the prediction accuracy and the total loss is exactly opposite to the last case. From small to large losses, they are ranked as ResNet-50, ResNet-101, Inception-v4, and Inception-ResNet-V2 in both training and validation set. Meanwhile, the convergence value of total loss in the training step is smaller than that in the validation process while the prediction accuracy in the training is higher than the validation. In summary, the IRV2 model outperforms the other models in rock structure classification.

Rock structure type	Training and validation		Testing
	Number of training images	Number of validation images	Number of testing images
MS	4357	2247	1352
GS	4862	2873	1442
LS	4018	2170	1697
BS	4033	2387	1542
FS	5161	2893	1367
Total number	22,431	12,570	7400

Table 4. The proportion of training, validation, and testing sets.

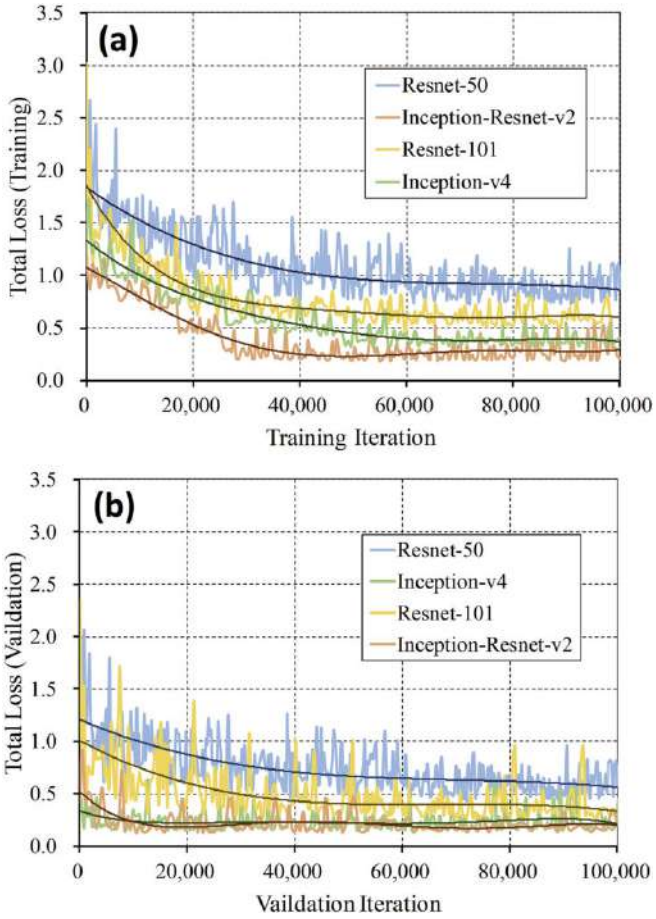

Fig. 6. Performance of four different deep learning methods for total loss in different processes including (a) training and (b) validation.

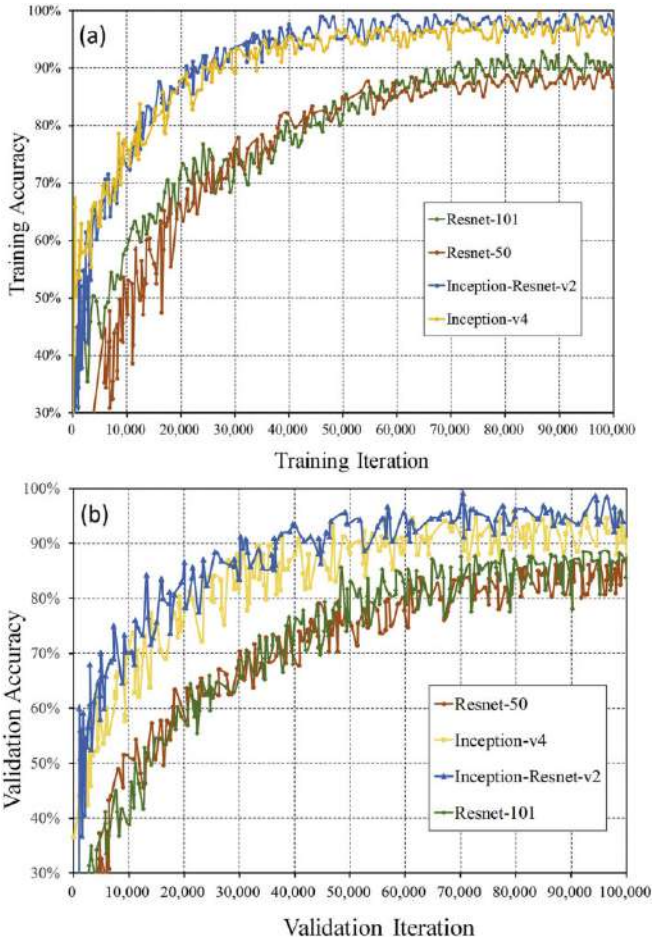

Fig. 7. Performance of four different deep learning methods for accuracy in different processes including (a) training and (b) validation.

Cross-validation and accuracy evaluation of testing images

In this study, four evaluation metrics were selected to determine the performance of the model applied in the image identification process. According to the data distribution in Table 2, 7400 images (untrained data) were randomly selected from the database for the classification testing. Additionally, the comparisons between the four methods in terms of accuracy, precision, recall value, and F-score for testing dataset are plotted in Fig. 8. It can be seen that all the evaluation metrics of CNN models present a similar trend. The values of the metrics from the highest to the lowest always follow the same order: BS, LS, MS, FS, and GS. Since the texture features and distinct appearance of the BS images, it makes the DCNN methods corresponding more prominent in BS identification. Therefore, the proposed method can improve the classification accuracy on the rock tunnel face image dataset. The FS and GS images in the dataset do not have distinct features compared with the other three water in flow categories. Therefore, the classification of FS and GS images suggest relatively poor performance, as the evaluation metrics of these two categories present rather low values.

To further explore the IRV2 classification algorithm, the confusion matrix was used to evaluate the recognition results. Confusion matrix is a standard format for classification evaluation, which is expressed in the matrix form of N rows and N columns. Each column represents the forecast category, and the total number of each column represents the number of data classified as the category; each row represents the real belonging category of data, and the total number of data in each row represents the number of data instances of the category. The calculation of a confusion matrix is to sum up the total number of observed accuracy values of both the wrong and correct categories in the statistical classification model, and then display the results in a tabular form. Table 5 shows the confusion matrix obtained from 7400 images of rock structure dataset using the Inception-ResNet-V2 model. It can be seen that the proportions of five rock structure types in the database are 18.08%, 19.29%, 22.84%, 20.89%, and 18.89%. The classification of Granular Structure (GS) shows an accuracy level of up to 93.90%. Furthermore, it can be inferred that among the 5 categories, FS has a higher probability to be misclassified as GS, since it is located closer to GS. Similarly, MS has a higher probability of being misjudged as FS. In general, BS is the easiest one to be accurately recognized in the rock structure determination, with an accuracy of 98.12%, followed by LS, MS, FS, and GS with accuracies of 97.05%, 95.93%, 94.80%, and 93.90%, respectively. Therefore, using the IRV2 model, the GS class has the poorest classification performance, while the BS class has the strongest one.

To visualize the results of image classification, a fraction of images is randomly selected out of 7400 testing images (Fig. 9), and the last fraction of each line was considered for the misclassification cases. It can be seen from Fig. 9 that the prediction of the framework IRV2 provided excellent results in five categories of classification problems. In terms of error recognition, the results of Fig. 9 are consistent with those of the confusion matrix. In the deep learning process, errors may occur in two similar categories including GS and FS. Therefore, to improve the robustness of data, it is necessary to increase the number of related categories and the texture morphology in the training process.

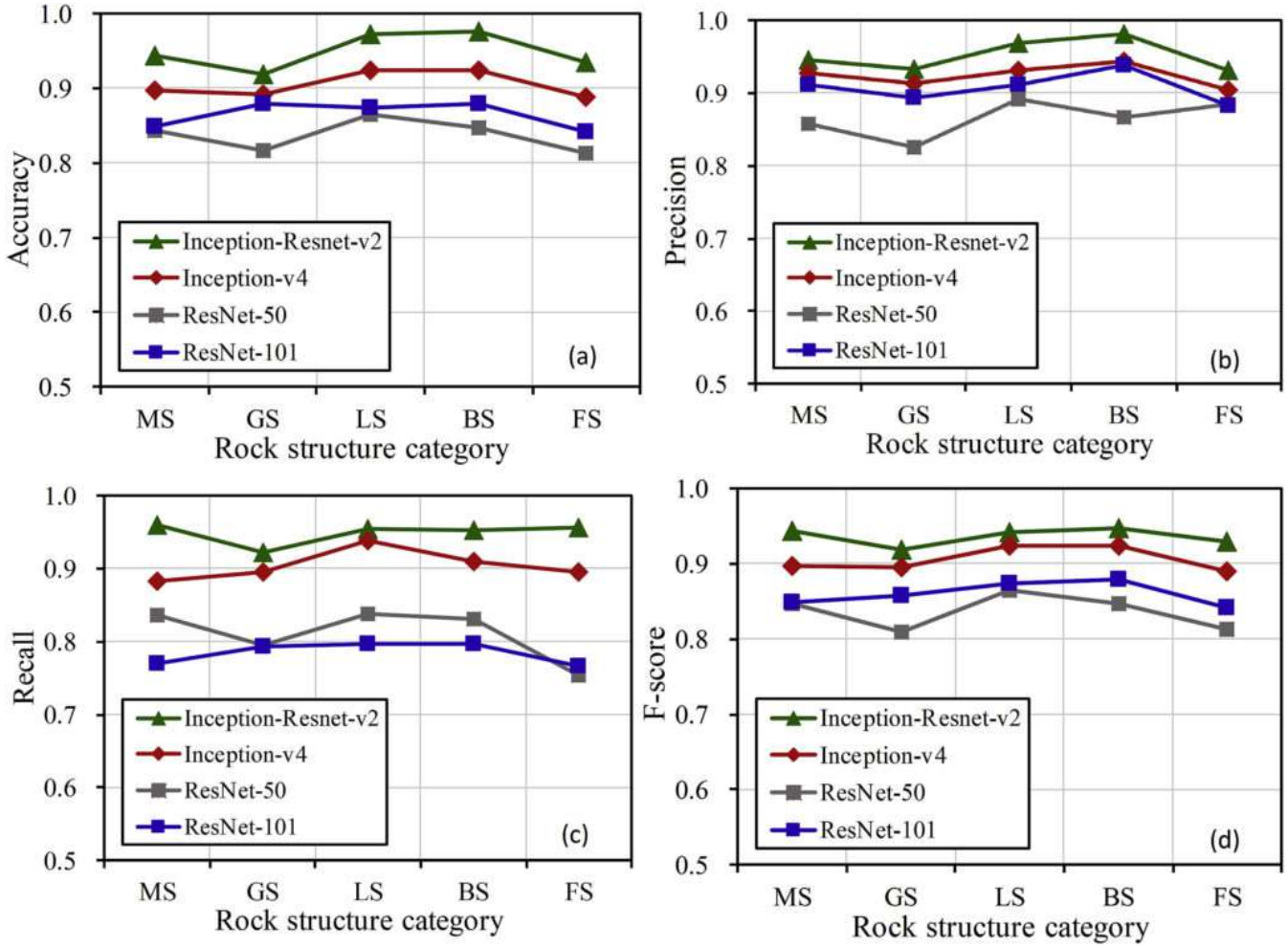

Fig. 8. Performance of various rock structure categories evaluated by different metrics including (a) accuracy, (b) precision, (c) recall, and (d) F-score.

Rock structure type	MS	GS	LS	BS	FS	% of data
Mosaic Structure (MS)	95.93%	0.30%	1.18%	1.04%	1.55%	18.08%
Granular Structure (GS)	0.21%	93.90%	0.76%	0.55%	4.58%	19.29%
Layered Structure (LS)	0.77%	0.88%	97.05%	0.47%	0.82%	22.84%
Block Structure (BS)	0.78%	0.52%	0.45%	98.12%	0.13%	20.89%
Fragmentation Structure (FS)	0.95%	3.37%	0.66%	0.22%	94.80%	18.89%

Table 5. Confusion matrix of classification results with rock structure dataset using the IRV2 model.

Evaluation of execution time

The execution time of different frameworks using different processors (CPU and GPU) is shown in Table 6. The results show that the computing time of the Graphics Processing Unit (GPU) is much shorter than that of the Central Processing Unit (CPU) in different running processes (i.e., validation and testing) and models. However, some traditional machine learning methods are CPU-based (Cha and Buyukozturk, 2015). In these approaches, it takes much time and storage space when the algorithm is complex. Thus, using the GPU for solving the classification problems has an important reference value for the current research. In addition, by employing the GPU, the average validation time of the proposed Inception-ResNet-V2 algorithm is 2.163 s per image, while this time for ResNet-50, ResNet-101, and Inception-v4 is 2.78 s, 3.02 s, and 2.25 s, respectively. In other words, the validation time of the IRV2 framework model is about 1.28, 1.39, and 1.04 times shorter than ResNet-50, ResNet-101, and Inception-v4, respectively. In addition, the IRV2 method takes 0.325 s per image in terms of test time, which is 1.57, 1.95, and 1.48 times shorter than ResNet-50, ResNet-101, and Inception-v4, respectively. Therefore, it can be concluded that IRV2 is computationally more efficient than the other three algorithms.

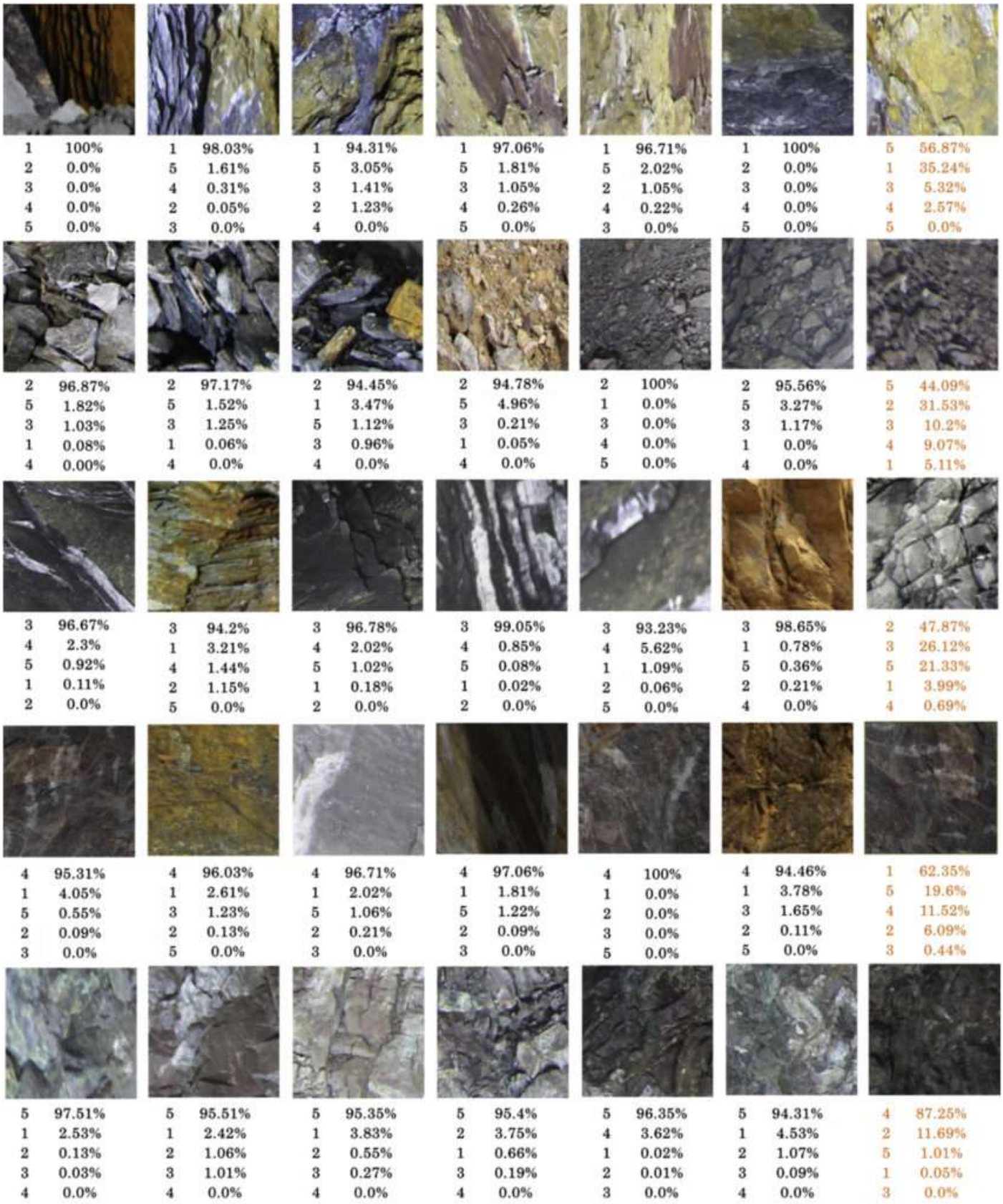

Fig. 9. Fraction identification of geological structure images results.

Processor	Execution time (s)	ResNet-50	ResNet-101	Inception-v4	Inception-ResNet-V2
CPU (i7-8700 K)	Validation time	97.354	105.667	81.144	77.394
	Testing time	20.468	25.634	19.387	13.024
GPU (Nvidia-1080Ti)	Validation time	2.782	3.021	2.254	2.163
	Testing time	0.512	0.636	0.482	0.325

Table 6. Execution time per image.

Discussion

To further evaluate the recognition effect of the tunnel face image in the MPHT project, an original image was selected as the raw material (Fig. 10). The image was segmented into 25 sub-images (5 × 5) and labelled according to the corresponding locations. All sub-images were fed to the IRV2 framework in batches for testing. The advantage of substituting the sub-images for the original image is to avoid the influence of local recognition errors on the overall recognition rate and one-time determination of tunnel face structure and, subsequently, to analyze the rock mass structure by the probabilistic and statistical methods.

Fig. 10. Schematic diagram of rock tunnel face structure classification processes based on the proposed method.

Fig. 11 displays the category statistics of each sub-image trained according to the segmentation results of Fig. 10. In this figure, the red rectangular box is the error recognition item. As can be seen, although the rock mass structure of the sub-image 5-1 is actually the Layered Structure (LS), 35.2% of the misjudgment rate still classifies it as Block Structure (BS).

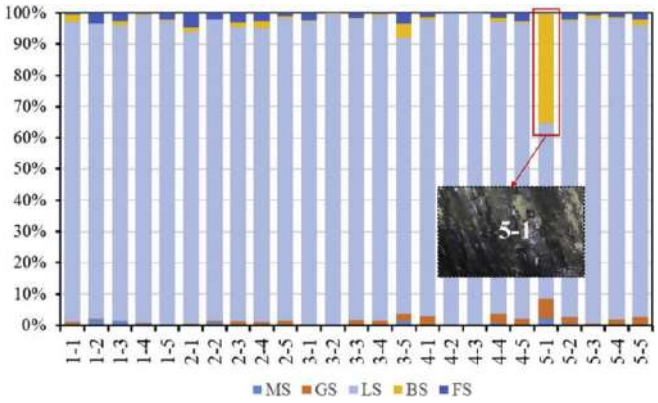

Fig. 11. Statistical results of rock structure classification.

To further analyze the difference between the sub-image statistical recognition method and the overall recognition method, Table 7 summarizes the average value of the statistical data in Fig. 11 and the testing probability of the original image classification. The table shows that both methods can accurately identify the classification results. In the LS classification, the probability of the sub-image method and original image method is 94.27% and 93.25%, respectively. However, the two methods are different in the error recognition labels. The sub-image method further concentrates on BS and FS, while the original image method mainly focuses on FS and MS. From the manual error recognition view, the probability of occurrence in BS and FS is higher than that in FS and MS; and thus the sub-image method is closer to the human recognition. Therefore, from the perspective of recall accuracy and error divergence, the sub-image method is a more reasonable workaround.

Conclusion

In this paper, a vision-based framework model known as Inception-ResNet-V2 network was proposed for the classification of rock mass structure in the tunnel face. To capture the database orderly and quantitatively, an adaptive digital photography system (ADPS) system consisting of a Canon 750D

camera, tapeline, tripod, measuring equipment and the light source was used in the image acquisition process. The Inception-ResNet-V2 network was trained by over 35,000 images extracted from 150 tunnel faces in Mengzi-Pingbian Highway Tunnel (MPHT) in Yunnan Province, China, and then tested by additional 7400 images. Compared with ResNet-50, ResNet-101, and Inception-v4, the proposed network can reduce the validation and testing time, increase the accuracy of rock structure classification, and facilitate the future condition assessment.

Method	Rock structure type				
	MS	GS	LS	BS	FS
Sub-image	0.45%	1.30%	94.27%	2.30%	1.68%
Original image	2.35%	0.00%	93.25%	0.19%	4.21%

Table 7. Classification probabilities corresponding to different recognition methods (sub-image and original image).

Based on the obtained results, the computing time of GPU is much lower than CPU for the four experimental CNNs, whether in different running processes (such as validation and testing) or using a different model. Using the GPU processor instead of traditional CPU, Inception-ResNet-V2 exhibited the best performance over the other three CNNs.

In addition, the model trained by a large database can obtain the object features more comprehensively, leading to higher accuracy. Compared with the original image classification method, the sub-image method is closer to the reality considering both the accuracy and the perspective of error divergence.

As the first attempt to use CNNs for classification of rock mass structures captured from the under-construction tunnel face, this research made the following two contributions. First, it paves the way for other researchers to apply a higher accuracy and efficiency framework in order to classify the rock structure in the under-construction tunnel face. Secondly, it confirms that the proposed sub-image technique significantly improves the efficiency of conventional overall recognition. However, there are two research aspects remained that can be further improved: (1) establishing a real-time tunnel face image recognition system during the construction as the most urgent need in the field, and (2) handling the time imposed by the pretreatment and post-processing of the sub-image classification method, which is usually longer than the testing time. These issues can be investigated by the authors in future research for designing a more automatic recognition system.

Source: Deep learning based classification of rock structure of tunnel face

(ENGINEERING GEOLOGY, September 3, 2020,

https://geologyengineering.com/2020/09/classification-of-rock-structure-of-tunnel-face)

The February 2018 Mangapoike landslide, New Zealand: an intriguing failure mechanism?

Zealand: an intriguing failure mechanism?

On a morning in which the media is full of a landslide that fail to materialise, I can find solace in the real thing. On 24 February 2018 an 8 million cubic metre landslide dammed the Mangapoike River in a remote upland area of eastern North Island in New Zealand. I blogged about this landslide at the time – it is a rather beautiful example. The height of landslide dam was managed through blasting, although the landslide remains intact, leaving interesting questions about the cause of the failure. This is a Google Earth image of the landslide:-

Google Earth imagery of the 24 February 2018 Mangapoike landslide, New Zealand.

An interesting paper has been published in the journal *Landslides* about the Mangapoike landslide (McGovern *et al.* 2020). This is provides a detailed description and analysis of the feature, which was a wedge failure in weak rock sandstones and mudstones, with the slide surface being defined by a smoothed, northwest-dipping bedding plane. The elegant diagram below, which is an exemplar of how to use graphics to present landslide information, shows the source area of the slide:

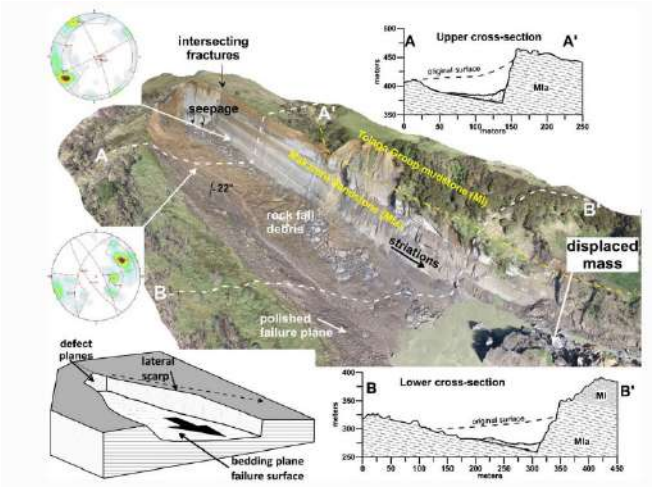

The source area of the February 2018 Mangapoike landslide, New Zealand. Diagram from McGovern *et al.* (2020).

The landslide mass itself partially disaggregated into blocks, which of course meant that the river was more effectively dammed.

The really interesting aspect of this paper though is its consideration of the causes and triggers of the Mangapoike landslide. The underlying causes are clear (and are well-explained), but what triggered the failure? McGovern *et al.* (2020) demonstrate clearly that there was no unusual rainfall event prior to the failure. Indeed, they are remarkably definitive about this:

"…it seems implausible that rainfall and elevated groundwater were important triggering factors".

Instead McGovern *et al.* (2020) propose that fluid overpressure might have played a role. As they put it:

"The Makaretu Sandstone is a known hydrocarbon reservoir formation within the Tolaga Group, with overlying mudstone units acting [as] seals".

There is geodetic evidence that prior to the landslide the region underwent approximately 15 mm of vertical movement, which may indicate that there was a fluid overpressurisation event occurring. The authors postulate that gas migrated vertically though the sandstones but was trapped by the mudstones at the base of the landslide, reducing the normal effective stress and triggering the failure.

This mechanism is a hypothesis, and indeed the authors state that:

"Whether fluid overpressure was a contributing factor to the Mangapoike landslide is equivocal."

There have been previous suggestions that gas overpressurisation might be a factor in certain landslide failures. The interesting thing about this one is that the data is so good that it invites detailed modelling to understand the potential mechanism, and its efficacy, better.

Reference

McGovern, S., Brook, M.S. & Cave, M. 2020. Geomorphology and triggering mechanism of a river-damming block slide: February 2018 Mangapoike landslide, New Zealand. *Landslides* (2020). https://doi.org/10.1007/s10346-020-01572-7

(Dave Petley / THE LANDSLIDE BLOG, 4 November 2020, https://blogs.agu.org/landslideblog/2020/11/04/mangapoike-landslide/)

Geomorphology and triggering mechanism of a river-damming block slide: February 2018 Mangapoike landslide, New Zealand

Sam McGovern, Martin S. Brook & Murry Cave

Abstract

Landslide dams can be very dangerous, with inundation occurring via rising waters upstream, and flooding downstream via dam breaching. Here, we report on a landslide that dammed the Mangapoike River in eastern North Island, New Zealand. The landslide is a low-angle wedge failure in the Miocene weak rock sandstones and mudstones of the Tolaga Group, forming a landslide dam (volume c. 8 million m^3) and a lake 50 m deep with a surface area of 0.35 km^2, before explosives were used to form a dam spillway to decrease lake level. The landslide formed along an escarpment in north-

west-dipping sandstones, and is characterised by a linear lateral scarp, a headscarp, and a bedding-plane rupture surface, which controlled the landslide block geometry. The headscarp and lateral scarp have developed along propagating vertical fractures. The slide surface is a smoothed, northwest-dipping bedding plane, and intersects the vertical fractures in the lateral scarp, forming a wedge. While the principal failure mechanism was sliding involving a single large wedge-shaped block, the rapid movement led to disintegration of most of the block. Part of the detached slide block remained intact, but most of the displaced mass forming the landslide dam is disaggregated blocks in a sandy-silty matrix. Rainfall and meteoric groundwater probably did not initiate failure. Instead, river incision of the dip slope toe, and overpressurisation of fluids that are known to accumulate in sandstones overlain by impermeable mudstones in the region, probably decreased the effective stress along the existing bedding plane, initiating failure.

https://link.springer.com/article/10.1007/s10346-020-01572-7

A systematic exploration of satellite radar coherence methods for rapid landslide detection

Katy Burrows, Richard J. Walters, David Milledge, and Alexander L. Densmore

Emergency responders require information on the distribution of triggered landslides within 2 weeks of an earthquake or storm. Useable satellite radar imagery is acquired within days of any such event worldwide.

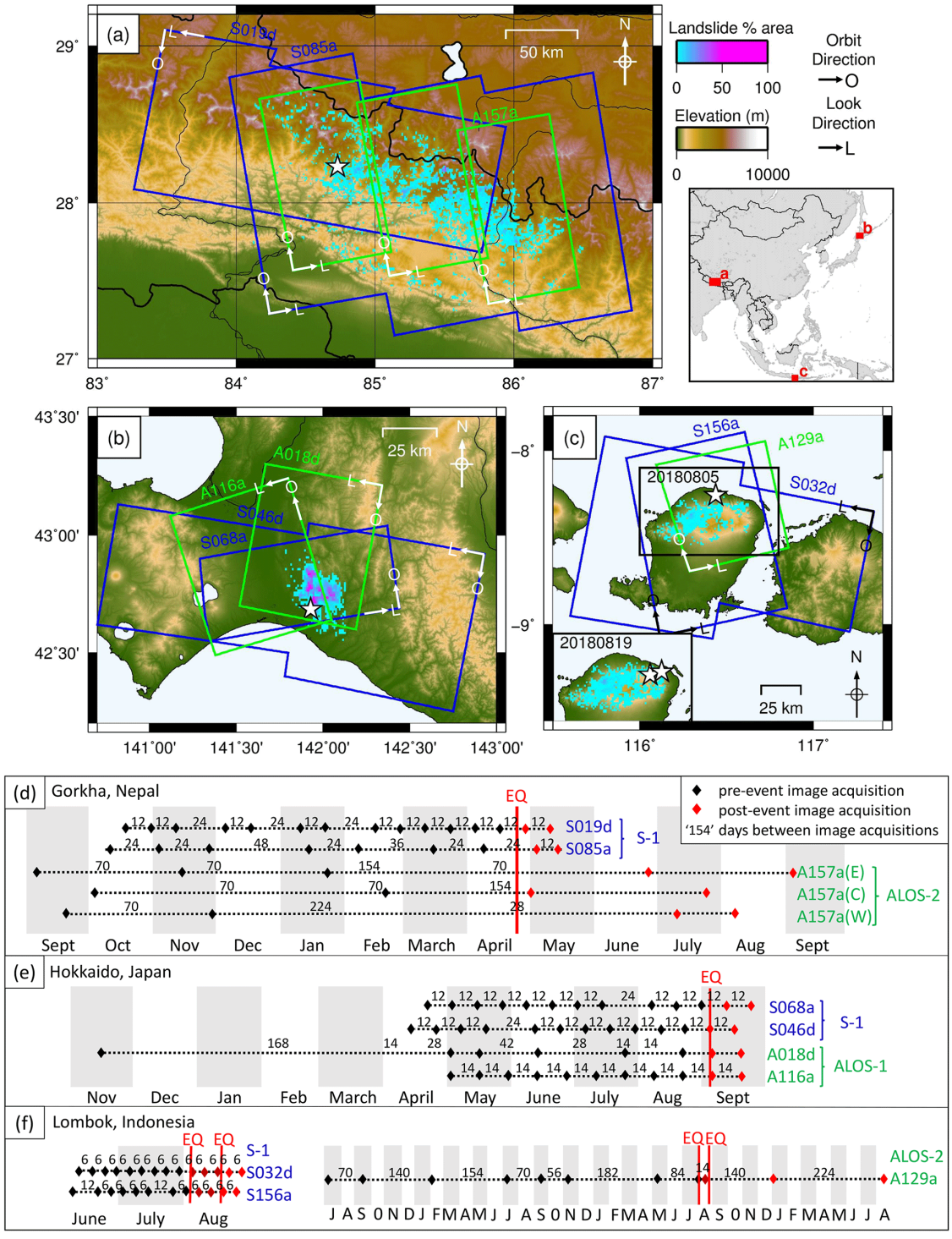

Figure 1(a–c) Landslides triggered, respectively, by the 2015 Gorkha, Nepal, earthquake; the 2018 Hokkaido, Japan, earthquake; and the 2018 Lombok, Indonesia, earthquakes (Roback et al., 2018; Zhang et al., 2019; Ferrario, 2019). The landslides are plotted as the areal density of landsliding based on 1 km^2 cells. ALOS-2 SAR acquisitions are shown in green and Sentinel-1 in blue. In **(c)**, a second earthquake, referred to as "Lombok-2", is inset. **(d–f)** Acquisition dates and track numbers of SAR imagery used in this study. Earthquakes are shown as vertical red lines, black symbols show pre-event image acquisition dates, and red symbols show post-event dates

Recently, several landslide detection methods that use these data have been developed, but testing of these methods has been limited in each case to a single event and satellite sensor. Here we systematically test five methods using ALOS-2 and Sentinel-1 data across four triggering earthquakes. The best-performing method was dependent on the satellite sensor. For three of our four case study events, an initial ALOS-2 image was acquired within 2 weeks, and with these data, co-event coherence loss (CECL) is the best-performing method. Using a single post-event Sentinel-1 image, the best-performing method was the boxcar–sibling (Bx–S) method. We also present three new methods which incorporate a second post-event image. While the waiting time for this second post-event image is disadvantageous for emergency response, these methods perform more consistently and on average 10 % better across event and sensor type than the boxcar–sibling and CECL methods. Thus, our results demonstrate that useful landslide density information can be generated on the timescale of emergency response and allow us to make recommendations on the best method based on the availability and latency of post-event radar data.

Nat. Hazards Earth Syst. Sci., 20, 3197–3214, 2020
https://doi.org/10.5194/nhess-20-3197-2020

(https://nhess.copernicus.org/articles/20/3197/2020)

The Mw = 5.6 Kanallaki Earthquake of 21 March 2020 in West Epirus, Greece: Reverse Fault Model from InSAR Data and Seismotectonic Implications for Apulia-Eurasia Collision

Sotiris Valkaniotis, Pierre Briole, Athanassios Ganas, Panagiotis Elias, Vassilis Kapetanidis, Varvara Tsironi, Anna Fokaefs, Helena Partheniou and Panagiotis Paschos

Abstract

We identify the source of the Mw = 5.6 earthquake that hit west-central Epirus on 21 March 2020 00:49:52 UTC. We use Sentinel-1 synthetic aperture radar interferograms tied to one permanent Global Navigation Satellite System (GNSS) station (GARD). We model the source by inverting the INSAR displacement data. The inversion model suggests a shallow source on a low-angle fault (39°) dipping towards east with a centroid depth of 8.5 km. The seismic moment deduced from our model agrees with those of the published seismic moment tensors. This geometry is compatible with reverse-slip motion along the west-verging Margariti thrust fault that accommodates part of the convergence within the collision zone between Apulia and Eurasia. We also processed new GNSS data and estimate a total convergence rate between Apulia and Eurasia of 8.9 mm yr^{-1}, of which the shortening of the crust between the Epirus coastal GNSS stations and station PAXO in the Ionian Sea (across the Ionian Thrust) is equivalent to ~50% of it or 4.6 mm yr^{-1}. By back-slip modelling we found that a 60-km wide deformation zone takes up nearly most of the convergence between Apulia-Eurasia, trending N318°E. Its central axis runs along the southwest coast of Corfu, along the northeast coast of Paxoi, heading toward the northern extremity of the Lefkada island. The island of Paxoi appears kinematically as part of the Apulian plate.

1. Introduction

The tectonics of Epirus is characterised by on-going compression due to the active collision between the Apulian continental block [1,2,3,4] and Eurasian (Aegean) plate. The Apulian continental lithosphere subducts beneath Epirus and was imaged at 70–80 km depth by [5]. Both seismological and geodetic data show that active deformation is occurring by crustal shortening directed in a NNE–SSW to NE–SW orientation [6,7,8,9,10,11] (Figure 1). The overall tectonic strain rate was estimated at 40–50 ns yr^{-1} of contraction by [11] for west-central Epirus. At least 50 km of horizontal shortening has been suggested for Epirus by geological data [12,13,14,15] accompanied by large scale clockwise rotations [12].

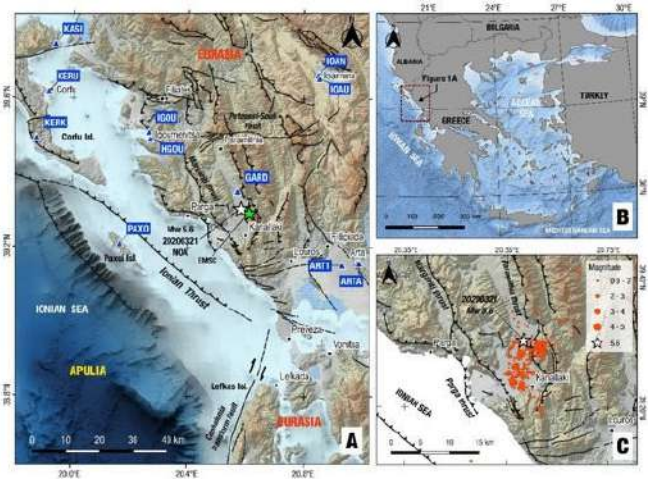

Figure 1. Map of Epirus (**A**) showing active fault traces (black lines with ticks on the overriding side), Global Navigation Satellite System (GNSS) stations (blue triangles) and epicentres determined for the 21 March 2020 Mw = 5.6 earthquake. Panel (**B**) shows the study area in the NW corner of Greece. Panel (**C**) shows the relocated epicentre of the mainshock (this study; white star) and its aftershocks (red circles; period 20 March 2020–23 May 2020). Fault traces modified after [16,17]. The black line between the Paxoi and Corfu islands indicates the trace of the Ionian thrust (ticks on the overriding side).

…

Geosciences **2020**, *10*(11), 454;
https://doi.org/10.3390/geosciences10110454

(https://www.mdpi.com/2076-3263/10/11/454/htm)

ΝΕΑ ΑΠΟ ΤΙΣ ΕΛΛΗΝΙΚΕΣ ΚΑΙ ΔΙΕΘΝΕΙΣ ΓΕΩΤΕΧΝΙΚΕΣ ΕΝΩΣΕΙΣ

Υλικό από τη διαδικτυακή ημερίδα του ΕΤΑΜ για τον σεισμό της Αλβανίας (26 Νοε 2019)

Διαδικτυακό σεμινάριο (webinar) της 5ης Οκτωβρίου 2020 με θέμα το σεισμό μεγέθους Μ6.4 της Αλβανίας (2019). Παρουσιάσθηκαν σεισμολογικά δεδομένα, δομικές και γεωτεχνικές βλάβες που παρατηρήθηκαν στο Δυρράχιο και στο Θουμάνι καθώς και τα αποτελέσματα του ταχέως οπτικού ελέγχου.

www.eltam.org/images/nltr/newsletters/20201117/etamreport_albania2019earthquake.pdf

https://www.youtube.com/watch?v=3YVhmkT36vc&feature=youtu.be


ΕΛΛΗΝΙΚΗ ΓΕΩΛΟΓΙΚΗ ΕΤΑΙΡΙΑ

Ετήσια Ομιλία «Γ. Μαρίνος - Ι. Παπασταματίου»

Πρόσκληση

Το Διοικητικό Συμβούλιο της Ελληνικής Γεωλογικής Εταιρίας έχει την τιμή να σας καλέσει στην καθιερωμένη Ετήσια Ομιλία «Γ. Μαρίνος - Ι. Παπασταματίου», για το έτος 2020.

Η ομιλία θα πραγματοποιηθεί από τον

Δρ. Δημήτρη Παπανικολάου

Ομ. Καθηγητή Γεωλογίας, Ε.Κ.Π.Α.

με θέμα:

«Οι φυσικές κλιματικές αλλαγές του παρελθόντος της Γης και η σημερινή ανθρωπογενής επίδραση»

Η ομιλία θα πραγματοποιηθεί διαδικτυακά την **Πέμπτη 10 Δεκεμβρίου 2020** και ώρα **19:00**

Σύνδεσμος: https://authgr.zoom.us/j/95398439294?pwd=cmlwWEpXWlVOMGF0cDZGaVVaZ1BwZz09

ΣΥΝΟΨΗ ΟΜΙΛΙΑΣ

Οι κλιματικές αλλαγές αποτελούν τον κανόνα στην ιστορία του πλανήτη μας από την δημιουργία του πριν 4,6 δις έτη έως σήμερα. Η σύσταση της γήινης ατμόσφαιρας άλλαξε δραματικά κατά την διάρκεια των πρώτων δύο δις ετών και από την κυριαρχία του διοξειδίου του άνθρακα και του μεθανίου πέρασε σε μία σταδιακή εμφάνιση και αύξηση του οξυγόνου, που έφθασε πριν από περίπου 500 εκ. έτη σε ποσοστό της τάξεως του 20%. Οι παλαιοθερμοκρασίες που έχουν υπολογισθεί δείχνουν ότι συνολικά επικρατούσε πολύ πιο θερμό κλίμα, με εξαίρεση το τέλος του ΠροΚαμβρίου, πριν 750-550 εκ. έτη, το τέλος του Άνω Παλαιοζωικού πριν 330-280 εκ. έτη και το Τεταρτογενές τα τελευταία 2,6 εκ. έτη. Επομένως, η σημερινή περίοδος που τη θεωρούμε κλιματικά «φυσιολογική» αποτελεί μία ακραία ψυχρή περίοδο της ιστορίας της Γης. Είναι χαρακτηριστικό ότι έχουν παρατηρηθεί τελείως ακραίες κλιματικές περίοδοι στο τέλος του Προκάμβριου όταν η Γη αποτελούσε μία χιονόμπαλα (Snowball Earth) και στο Ηώκαινο όταν υπήρχαν οργανισμοί της ισημερινής ζώνης σχεδόν σε όλα τα πλάτη, έως τον Καναδά. Το βασικό αίτιο των κλιματικών αλλαγών είναι η διαφοροποίηση της προσπίπτουσας ηλιακής ενέργειας ανάλογα με τις κινήσεις της Γης και τις τροχιακές παραμέτρους της κλόνησης, της μετάπτωσης των ισημεριών και της λόξωσης, οι οποίες επαναλαμβάνονται σε κύκλους 20, 40 και 100 χιλιάδων ετών, που είναι γνωστοί ως κύκλοι του Milankovich. Έτσι, οι παγετώδεις περίοδοι του Μέσου-Ανωτέρου Πλειστοκαίνου επαναλαμβάνονται ανά 100.000 έτη ενώ οι ενδιάμεσες μεσοπαγετώδεις περίοδοι διαρκούν περίπου 10.000 έτη. Μία άμεση επίδραση των κλιματικών αλλαγών είναι μεταβολή της θαλάσσιας στάθμης με χαμηλή και υψηλή στάθμη (Low stand, High stand) αντίστοιχα για παγετώδεις και μεσοπαγετώδεις περιόδους. Έτσι, στην Μεσόγειο είναι γνωστή η προηγούμενη παλαιοακτή του Ανωτέρου Πλειστοκαίνου πριν 18.000 έτη στα -123 μ. Έτσι, έχουμε σημαντικές παλαιογεωγραφικές αλλαγές κυρίως στις παράκτιες περιοχές και στα νησιά. Η ενεργός τεκτονική με τις σεισμικές μετατοπίσεις αλληλοεπηρεάζεται με τις ευστατικές κινήσεις της κλιματικής αλλαγής και δίνουν ιδιαίτερα τοπία- χαρακτηριστικά σεισμικά ανάγλυφα, όπως π.χ. οι ακτές της Βόρειας Πελοποννήσου στον Κορινθιακό Κόλπο, ο οποίος κατά τις παγετώδεις περιόδους ήταν λίμνη ενώ οι παλαιοακτές του εντοπίζονται σε υψόμετρα έως και 750μ. Με δεδομένο ότι ήδη έχουν περάσει 10.000 έτη κατά τη σημερινή μεσοπαγετώδη περίοδο, η φυσική αναμενόμενη εξέλιξη του κλίματος είναι η μετάβαση στην επόμενη παγετώδη περίοδο. Το κρίσιμο θέμα είναι εάν η ανθρωπογενής επίδραση μπορεί να καθυστερήσει ή και να αναστείλει την φυσική διαδικασία της κλιματικής αλλαγής. Η απάντηση στο ερώτημα προϋποθέτει την γνώση των διακυμάνσεων του κλίματος μέσα στην μεσοπαγετώδη περίοδο και τη σύγκριση των παρατηρούμενων κλιματικών μεταβολών με αυτές. Είναι γνωστό ότι στην Σαχάρα πριν περίπου 5.500 χιλιάδες έτη υπήρχαν τοπία πράσινης χλωρίδας και αντίστοιχης πανίδας που έχουν αποτυπωθεί σε βραχογραφίες σπηλαίων, που δείχνουν ένα πολύ πιο υγρό και ψυχρό κλίμα. Επίσης είναι γνωστό ότι στην κεντρική Ευρώπη παρατηρήθηκαν πολύ χαμηλότερες θερμοκρασίες τον 16ο έως τον 19ο αιώνα με παγωμένες λίμνες που έχουν απεικονιστεί σε πίνακες κυρίως Ολλανδών και Φλαμανδών ζωγράφων. Η περίοδος αυτή έχει χαρακτηρισθεί ως «Μικρή Παγετώδης Περίοδος» (Little Ice Age). Τα σημερινά κλιματικά στοιχεία δείχνουν μία σαφή απόκλιση από τις φυσικές διακυμάνσεις από τη δεκαετία του 1980. Εν τούτοις, η σύγκριση των στοιχείων της τελευταίας τριακονταετίας με τα σενάρια της κλιματικής αλλαγής του 1988 δείχνουν ότι βρισκόμαστε στο ηπιότερο από τα σενάρια που είχαν προταθεί. Τέλος, θα πρέπει να γίνει διάκριση ανάμεσα στην ανθρωπογενή επιβάρυνση του περιβάλλοντος και την κλιματική αλλαγή. Είναι βέβαιον ότι τα περισσότερα μέτρα που προτείνονται χρειάζονται για την αποκατάσταση και βελτίωση του περιβάλλοντος ανεξάρτητα από το ποσοστό της πιθανής ανθρωπογενούς προέλευσης της κλιματικής αλλαγής.

Ο **Δημήτρης Ι. Παπανικολάου** γεννήθηκε στην Αθήνα και σπούδασε στο Πανεπιστήμιο Αθηνών Φυσιογνωσία και Γεωγραφία (1971) και Γεωλογία (1976). Από το 1974 εργάστηκε ως Βοηθός του Εργαστηρίου Γεωλογίας στο Πανεπιστήμιο Αθηνών, όπου εκπόνησε διδακτορική διατριβή στη Γεωλογία της Νήσου Άνδρου (1978). Ακολούθησε όλες τις βαθμίδες ακαδημαϊκής εξέλιξης έως το 1993 όταν εξελέγη Καθηγητής στα αντικείμενα Δυναμική και Τεκτονική Γεωλογία, Γεωλογία της Ελλάδας και Θαλάσσια Γεωδυναμική. Κατά τη διάρκεια των ετών 2005-2016 ήταν διευθυντής των διατμηματικών μεταπτυχιακών προγραμμάτων «Ωκεανογραφία και Διαχείριση θαλασσίου Περιβάλλοντος» και «Μελέτη και Πρόληψη Φυσικών Καταστροφών». Κατά τα έτη 1979-1980 και 1981 εργάστηκε ως μεταδιδακτορικός ερευνητής στο Πανεπιστήμιο της Λωζάννης με έρευνα και δημοσιεύσεις στις Δυτικές Άλπεις. Το 1982-1983 δίδαξε ως Professeur associe Τεκτονική Γεωλογία στο Πανεπιστήμιο της Reims, Γαλλία. Το 2003 δίδαξε Γεωλογία και Τεκτονική Εξέλιξη της Μεσογείου στο MIT (Massachussets Institute of Technology) ΗΠΑ, όπου του απονεμήθηκε ο τίτλος του "Grosby Professor". Το 2008 έδωσε διαλέξεις στο "Jackson School of Geosciences" του Πανεπιστημίου του Τέξας στο Austin ως "Barnes Distinguished Lecturer". Διετέλεσε Πρόεδρος της Ελληνικής Γεωλογικής Εταιρίας (1988-1992, 1994-1996) και της Καρπαθο-Βαλκανικής Γεωλογικής Ένωσης (1993-1995). Διετέλεσε Διευθυντής του Προγράμματος IGCP No 276 Γεωλογικής Συσχέτισης της UNESCO/IUGS με θέμα «Paleozoic Geodynamic domains and their Alpidic evolution in the Tethys" (1987-1997) με συμμετοχή 24 χωρών. Εκλέχτηκε Διευθυντής/Πρόεδρος του Δ.Σ. του Εθνικού Κέντρου Θαλασσίων Ερευνών (1994-2000) και διετέλεσε Πρόεδρος του Οργανισμού Αντισεισμικού Σχεδιασμού και Προστασίας (ΟΑΣΠ)(1993-1998) καθώς και Γενικός Γραμματέας Πολιτικής Προστασίας του Υπουργείου Εσωτερικών (2000-2002). Είναι μέλος της Εκδοτικής Επιτροπής πολλών διεθνών επιστημονικών περιοδικών και έχει δημοσιεύσει πάνω από 320 εργασίες με πάνω από 4500 ετεροαναφορές. Το βιβλίο του «Γεωλογία της Ελλάδας» που εκδόθηκε από τις Εκδόσεις Πατάκης το 2015 βρίσκεται υπό εκτύπωση από τον Διεθνή Οίκο "Springer" στην αγγλική γλώσσα. Από το 2009 συμμετέχει στην Επιστημονική Επιτροπή Μελέτης των Επιπτώσεων της Κλιματικής Αλλαγής της Τράπεζας της Ελλάδας με ευθύνη στις Παλαιο-Κλιματικές Αλλαγές και τις μεταβολές της Θαλάσσιας στάθμης.

Οδηγίες σύνδεσης:

Για να παρακολουθήσετε την ομιλία, αρκεί να πατήσετε πάνω στην εικόνα της Πρόσκλησης, ή να ακολουθήσετε τον σύνδεσμο που περιλαμβάνεται σε αυτήν.

Τα πληρη στοιχεία της σύνδεσης έχουν ως εξής:

Topic: ΕΤΗΣΙΑ ΟΜΙΛΙΑ ΕΓΕ
Time: Dec 10, 2020 06:30 PM Athens
Join Zoom Meeting
https://au-thgr.zoom.us/j/95998439394?pwd=cmlwWEpXWHVOMGF0cDZGaVVaZ1BwZz09
Meeting ID: 959 9843 9394
Passcode: 076495
One tap mobile
+302111984488,,95998439394# Greece
+302311180599,,95998439394# Greece
Find your local number: https://au-thgr.zoom.us/u/ab9WSZilTu

SIMSG ISSMGE

International Society for Soil Mechanics and Geotechnical Engineering

ISSMGE News & Information Circular November 2020
https://www.issmge.org/news/issmge-news-and-information-circular-november-2020

1. 2021 TERZAGHI ORATION – News from the ISSMGE President Charles Ng

I am very pleased to announce that Professor Antonio Gens from the Universitat Politècnica de Catalunya in Spain has been selected as the 2021 Terzaghi Orator. Professor Gens was selected from a pool of 16 outstanding nominations including 5 former Rankine Lecturers. After reviewing the abstracts of proposed case histories including photographs submitted by 6 finalists and consultation among some distinguished peers in our Society, I had the privilege to select Professor Gens to be our next Orator although the decision was extremely difficult since we had so many outstanding candidates. I am absolutely confident that Professor Gens will deliver an excellent lecture in Sydney in 2021. Please join me in congratulating Professor Gens**.**

2. ISSMGE AWARDS – Deadline extended

Due to the COVID-19 Pandemic the Awards Committee in consultation with the President has decided to extend the submission deadline to 30 November 2020. Nominations should be submitted to the Secretary General.

3. TC - NOMINATIONS

These TCs are actively seeking nominations for members from the Member Societies. Please make sure that your Member Society representative is aware of your interest in joining either of these Committees.

TC107 – Tropical Residual Soils
TC214 - Foundation Engineering for Difficult Soft Soil Conditions.

4. WEBINARS

The following webinar was recently added to the ISSMGE educational resources available from the website: - Prof. Pijusch Samui: "Machine Learning in Geotechnical Engineering

5. ISFOG 2020 – Proceedings now available

The proceedings for ISFOG 2020 (a specialist conference on offshore geotechnics held under the auspices of TC209) have just been released. The conference itself has been postponed to late 2021, but the decision was taken to make the proceedings available this time - to ensure the material comes out in a timely fashion, and to honour the commitment of authors to the conference. The link to purchase the proceedings is at https://www.isfog2020.org/proceedings. The cost

is USD150.00 and will be deducted from the cost of your conference registration. Registration will open to the public in June 2021. Registrants will be contacted closer to that date and given instructions on how to obtain credit for the purchase of the proceedings.

6. BULLETIN

The latest edition of the ISSMGE Bulletin (Volume 14, Issue 5, October 2020) is available from the website https://www.issmge.org/publications/issmge-bulletin/vol-14-issue-5-october-2020

7. ISSMGE ONLINE LIBRARY – OPEN ACCESS

The ISSMGE Online library (https://www.issmge.org/publications/online-library) is in continuous development – please note the following additions:

- 1st (2007) and 7th (2019) International Symposium on Geotechnical Safety and Risk
- 10th International Symposium on Field Measurements in Geomechanics (FMGM2018)
- 25th European Young Geotechnical Engineers Conference

8. ISSMGE FOUNDATION

The next deadline for receipt of applications for awards from the ISSMGE Foundation is the 31st January 2021. Click **here** for further information on the ISSMGE Foundation.

9. CONFERENCES

For a listing of all ISSMGE and ISSMGE supported conferences, and full information on all events, including deadlines, please go to the Events page at https://www.issmge.org/events. However, for updated information concerning possible changes due to the coronavirus outbreak (i.e. postponements, cancellations, change of deadlines, etc.), please refer to that specific event's website.

As might be expected, many events have been rescheduled and we update the Events page whenever we are advised of changes.

The following are events that have been added since the previous Circular:

ISSMGE Events

GEOTECHNICAL ADVANCES AND CHALLENGES IN URBAN DEVELOPMENT - 13-11-2020 - 14-11-2020
Online, Sydney Australia, Sydney; Language: English; Organiser: Australian Geomechanics Society; Contact person: Ali Parsa; Address: 115 Wicks Road, Phone: +612 9888 5000, Email: aparsa@jkgeotechnics.com.au, Website: https://australiangeomechanics.org/meetings/geotechnical-advances-and-challenges-in-urban-development/.

All Proceedings from the Australian New Zealand Conferences on Geomechanics available in open access!

The Innovation and Development Committee of the ISSMGE is pleased to announce that through the initiative of the Australian Geomechanics Society (AGS) and the New Zealand Geotechnical Society (NZGS), 1850 papers from the Australia New Zealand Conferences on Geomechanics, are now available in the online library here:

https://www.issmge.org/publications/online-library

The database includes the proceedings from all 13 Australian New Zealand Conferences on Geomechanics, held from 1971 up to 2019, and can be searched by theme, title and authors! More specifically, it includes:

1st Australia New Zealand Conference on Geomechanics (Melbourne, 1971): 81 papers

2nd Australia New Zealand Conference on Geomechanics (Brisbane, 1975): 62 papers

3rd Australia New Zealand Conference on Geomechanics (Wellington, 1980): 110 papers

4th Australia New Zealand Conference on Geomechanics (Perth, 1984): 129 papers

5th Australia New Zealand Conference on Geomechanics (Sydney, 1988): 114 papers

6th Australia New Zealand Conference on Geomechanics (Christchurch, 1992): 104 papers

7th Australia New Zealand Conference on Geomechanics (Adelaide, 1996): 154 papers

8th Australia New Zealand Conference on Geomechanics (Hobart, 1999): 129 papers

9th Australia New Zealand Conference on Geomechanics (Auckland, 2004): 127 papers

10th Australia New Zealand Conference on Geomechanics (Brisbane, 2007): 203 papers

11th Australia New Zealand Conference on Geomechanics (Melbourne, 2012): 277 papers

12th Australia New Zealand Conference on Geomechanics (Wellington, 2015): 159 papers

13th Australia New Zealand Conference on Geomechanics (Perth, 2019): 201 papers

Detailed acknowledgements for all 13 Australian New Zealand Conferences on Geomechanics and bibliographical details for referencing can be found at the ISSMGE Online Library Acknowledgements section.

ISRM International Society for Rock Mechanics and Rock Engineering

News
www.isrm.net/noticias/?tipo=1&todas=1

2019 Müller lecture by Dr Peter Kaiser is now on the website

The 8th Müller Award Lecture (2019) "From common to best practices in underground rock engineering" by Prof. Peter Kaiser is now on the website.

New ISRM Young Rock Engineer Award

In October 2020, the ISRM Board decided to institute the ISRM Young Rock Engineer Award, to acknowledge excellence in the field of rock engineering by ISRM members who are in early stages of their career. The deadline for submission of nominations for the ISRM Young Rock Engineer Award 2021 is 20 March 2021.

32nd ISRM Online Lecture on December 17

The 32nd Online Lecture with the title "Empirical Design Methods in Underground Mining" by Professor Antonio Samaniego will broadcast on the 17th December at 10 A.M. GMT.

XIII ISL - International Symposium on Slides will be in virtual mode

XIII ISL - International Symposium on Slides will be in virtual mode. The Symposium will be held in Colombia from February 22 to 26, 2021.

The News Release of the 2020 Council meeting is available for download

The ISRM Council meeting took place as a videoconference on 28 October. It was preceded by the Board meeting on 20, 21 and 22 October.

Eurock 2020 Proceedings now on OnePetro

The proceedings of Eurock 2020 are now available on OnePetro.com. ISRM are entitled to download 100 papers for free every year.

New ISRM Suggested Method Video - triaxial compression tests

A video for the Suggested Method for Determining the Strength of Rock Materials in Triaxial Compression was published, in a cooperation between Prof. Seokwon Jeon from Seoul National University (South Korea) and the ISRM Commission on Testing Methods.

2022 ISRM International Symposium in Asuncion, Paraguay

The ISRM Council selected the IX Latin American Rock Mechanics Symposium - LARMS 2022, in Asunción, Paraguay, 15 to 18 May, as the venue for the 2022 ISRM International Symposium, where the ISRM Board, Council and Commissions will also hold their annual meetings.

Digital Inspections – A Better Way – Tomorrow!

Will Howlett and James Connell (Arup) presented on Digital Inspections. With an increasingly digital approach to asset management and design delivery in the construction industry, clients can realise huge benefits in both quality and safety when they employ digital techniques. Arup have opted a variety of innovations to inspect and assess existing tunnels from small linear to large diameter tunnels. This presentation will review some of the projects in more detail and the techniques used to create 3D models including enabling the development of digital twins. Health & Safety Executive (HSE) best practice and effectively working within the Confined Spaces Act will be discussed including examples of remote inspection which has become more traditional following COVID-19.

Thursday, 5th November

Streaming Link : https://youtu.be/nCnI9wEU8VI

BTS Harding Memorial Lecture 2020
Tunnelling in a Changing World

This year's Harding Memorial Lecture was delivered by Dr Keith Bowers (Cowi) on 12th November.

This lecture looked at changes affecting our industry and what we may need to do differently now and in the future.

Tunnels have been an essential part of our infrastructure for centuries and the tunnelling industry remains an essential participant in the development of the infrastructure of the modern world. As an industry we can still trace some of our practices back to the early days and we continue to learn the lessons from earlier projects. Our practices will always need to continue evolving to be fit for the future. Change is normal.

A thirty-year career in the industry is long enough to observe some of these changes happening. Some relate to technology – our methods and materials. Other changes are imposed on us by society and circumstance. A year ago we were contemplating Brexit as possibly the biggest business change we could foresee. We did not anticipate social distancing and the demise of urban commuting. Pandemics happened in movies.

What changes will be expected of us for future tunnelling projects? Certainly more than just new methods and materials, important as they are. We need to respond to our growing knowledge of the world about us and particularly how our work interacts with our, evidently fragile, environment. As a society our expectations of "work" are changing. Wellbeing matters. Through all this what will attract the next generation of tunnellers into our industry in a digitally enabled age?

Thursday, 12th November

Streaming Link : https://youtu.be/81g6wcQ1SJc

https://britishdams.org

BDS YouTube channel

The BDS has recently created a playlist on our 'YouTube' page of videos from around the web related to dam safety and history that we feel may be of interest to our members. From educational videos about dam engineering principles to fascinating history of some of the UKs most iconic dams, we have curated many nuggets of information that provide insights into the world of dam engineering. The playlist can be viewed here (https://www.youtube.com/playlist?list=PL5RIxlQU-zazVJP4k-JzAMyuQC-A6KdxSs). Whilst every care has been taken to check the links are appropriate, the BDS is not responsible for the content or comments on these 3rd party videos.

Meet some of this year's award winning authors

Each year, we award authors from both industry and academia who have produced work judged by their peers to be of exceptional quality and benefit to the civil engineering, construction and materials science community.

Usually, their success is acknowledged at the ICE Publishing Awards ceremony, held at One Great George Street in London, UK. This year the ceremony was held digitally and celebrated with a range of videos from the award winners.

Watch the highlights

The top three papers selected from across all our journal this year:

Telford Gold Medal

Best paper overall

Pore water pressure and total horizontal stress response to EPBM tunnelling in London Clay written by; Michael Wan, J. R. Standing, David. M. Potts and, John. B. Burland (Imperial College, London, UK); published in Volume 69 Issue 5 of the *Géotechnique* journal. Established in 1948, *Géotechnique* is the world's premier geotechnics journal, publishing research of the highest quality on all aspects of geotechnical engineering.

The authors had this to say about their win: 'It is a huge honour and we are absolutely delighted.'

Watch the video - Read the paper

George Stephenson Medal

Second best paper overall

Downwind flow behaviours of cuboid-shaped obstacles: modelling and experiments, written by Karl An, Julian C. R. Hunt, and Jimmy C. H. Fung (Hong Kong University of Science and Technology and Cambridge University); published in Volume 172 Issue 1 of *Engineering and Computational Mechanics*. The journal has previously won the George Stephenson medal, Grafsronningen and Jensen, 2015. It has also won the ICE's Telford Gold medal twice: for Vardy, 2008 and Hunt et al, 2013.

Watch the video - Read the paper

Baker Medal

Third best paper overall

Rehabilitation of Brougham Castle Bridge, written by engineers David Wiggins, Kiera Mudd, and Matthew Healey and published in Volume 172 Issue 1 of *Engineering History and Heritage*. The journal publishes papers on existing infrastructure, buildings and civil engineering structures around the world, and issues related to their conservation, restoration and adaptation to meet the challenges of the 21st century.

The authors said this on discovering their win: "This award was a complete surprise and is a very humbling recognition of a lot of hard work."

Watch the video - Read the paper

All winning papers are free to read, forever, as part of our commitment to furthering knowledge and best practice in civil engineering.

View all of this, and past year's award-winning papers

ΔΙΑΚΡΙΣΕΙΣ ΕΛΛΗΝΩΝ ΓΕΩΤΕΧΝΙΚΩΝ ΜΗΧΑΝΙΚΩΝ

Prof. Harry Poulos

A world expert in pile foundation design, whose work has underpinned many of the world's tallest buildings, has received Australia's most prestigious engineering prize.

Professor **Harry Poulos** AM was awarded the 2020 Peter Nicol Russell Career Achievement Memorial Medal at the Engineers Australia Pinnacles Awards Ceremony last night.

An academic and consultant, Poulos has applied his research to projects including Dubai's Burj Khalifa, as well as freeways, bridges, tunnels and mines.

Presenting Poulos with his award during the virtual event, Engineers Australia National President Chris Champion recognised his distinguished career, which spans almost six decades.

"Harry has transformed the geotechnical understanding of how structures interact with the ground and developed more reliable design approaches that have superseded previous procedures based on empirical experience," Champion said.

Named in memory of a Sydney industrialist from the latter half of the 19th century, the Peter Nicol Russell Medal recognises a person who has made a notable contribution to the science and/or practice of engineering within Australia.

Poulos described the honour as a "pinnacle" of his career.

"I have made a number of decisions in my lifetime that have proved to be beneficial, and doing engineering as a profession was one of the first and foremost," he said.

"But an award like this is not a solo award. It is based on interactions with many other people … One of my great decisions was to marry my wife Maria. She and my four children have been remarkably supportive."

(Create Digital, November 10, 2020, https://www.createdigital.org.au/2020-winners-of-australias-top-engineering-awards-revealed)

Δρ. Άντα Αθανασοπούλου – Ζέκκου

Η Δρ. **Άντα Αθανασοπούλου – Ζέκκου**, Assistant Professor, Department of Civil and Environmental Engineering, University of California, Berkeley και μέλος της ΕΕΕΕΓΜ παρουσίασε στις 11 Νοεμβρίου 2020 την 30th William H. Mueser and Philip C. Rutledge Memorial Lecture (webinar) με θέμα **Liquefaction of Gravelly Soils and the Impact on Critical Infrastructure**.

This lecture honors William H. Mueser (1900-1985) and Philip C. Rutledge (1906-1990), former partners of Mueser Rutledge Consulting Engineers (MRCE). MRCE has established an endowment to provide funding for this lecture series. The goal is to have nationally and internationally known speakers with construction experience in foundations to deliver interesting talks of practical significance in the design and construction of foundations. ASCE Metropolitan Section.

Adda Athanasopoulos-Zekkos elected President of USUCGER

Adda Athanasopoulos Zekkos was elected this year as President of the United States Universities Council on Geotechnical Education and Research (USUCGER). USUCGER was founded in 1985 to provide advocacy for the continued development and expansion of high quality geotechnical engineering research and education by US academic institutions. Adda will be serving a two year term as President.

You can access USUCGER here

Δρ. Κατερίνα Ζιωτοπούλου

Arthur Casagrande Professional Development Award

This award was established by the Geotechnical Engineering Division (now the Geo-Institute) of ASCE as a memorial to the outstanding contributions of Arthur Casagrande, Hon. M. ASCE, to the teaching, research, and practice of geotechnical engineering. The award is funded by gifts from the many students, colleagues, and friends of Arthur Casagrande. The

award was established to provide professional development opportunities for outstanding young practitioners, researchers, and teachers of geotechnical engineering. It is administered by the Geo-Institute through the Honors and Awards Program.

Γεώργιος Τζιάλλας

Η Tunnelling Association of India Young Members διωργάνωσε webinar στις 7 Νοεμβρίου 2020 με ομιλητή τον Γεώργιο Τζιάλλα, Head of Department, Underground works, Lombardi Engineering India Pvt. Ltd. και θέμα "RAILWAY TUNNELS - DESIGN AND OPERATIONS - BASICS AND GENERAL".

https://www.youtube.com/watch?v=ofzSrFQBCCE&feature=emb_logo

ΠΡΟΣΕΧΕΙΣ ΓΕΩΤΕΧΝΙΚΕΣ ΕΚΔΗΛΩΣΕΙΣ

Για τις παλαιότερες καταχωρήσεις περισσότερες πληροφορίες μπορούν να αναζητηθούν στα προηγούμενα τεύχη του «περιοδικού» και στις παρατιθέμενες ιστοσελίδες.

ASIA 2020 Eighth International Conference and Exhibition on Water Resources and Renewable Energy Development in Asia, 8-10 December 2020, Kuala Lumpur, Malaysia, www.hydropower-dams.com/asia-2020

International Webinar Series on Forensic Geotechnical Engineering, December 10, 2020 Bangalore, India, http://tc302-issmge.com

Postponed ISGPEG 2020 International Conference on Innovative Solutions for Geotechnical Problems in Honour of Prof. Erol Guler, 2021, Istanbul, Turkey, www.isgpeg2020.org/en

Online 14th Baltic Sea Geotechnical Conference 2020 Future Challenges for Geotechnical Engineering, 18-20 January 2021, Helsinki, Finland, www.ril.fi/en/events/bsgc-2020.html

Online Nordic Geotechnical Meeting Urban Geotechnics, 18-20 January 2021, Helsinki, Finland, www.ril.fi/en/events/ngm-2020.html

17th World Conference ACUUS2020 Deep Inspirations, 3-4 February 2021, www.ril.fi/en/events/acuus-2020.html

XIII International Symposium on Landslides - Landslides and Sustainable Development, 22-26 February 2021, Cartagena, Colombia, www.scg.org.co/xiii-isl

Sustainable Development of Dams and River Basins
24-27th February 2021, New Delhi, India
https://icold2020.org

The ICOLD Board has decided than INCOLD will organize the Symposium on "Sustainable Development of Dams and River Basins" which will take place as Hybrid event (Physical and virtual both) from 24-27th February 2021 at New Delhi. The papers received for the ICOLD Symposium and APG Symposium will be presented in the INCOLD Annual event. The perspective authors (Foreign and Indian) are invited to participate either physically or virtually and make presentation of their papers to share their experiences with Indian Dam Professionals as well as with international delegates participating in the event.

2021 GEOASIA7 - 7th Asian Regional Conference on International Geosynthetics Society, March 1-4, 2021, Taipei, Taiwan, www.geoasia7.org

This British Tunnelling Society "BTS 2020" Conference and Exhibition, March 2nd-3rd, 2021, London, United Kingdom, www.btsconference.com.

International Conference on Challenges and Achievements in Geotechnical Engineering, 31.03.2021 – 02.04.2021, Tirana, Albania, Erdi Myftaraga, emy@greengeotechnics.com

Second International Conference on Geotechnical Engineering - Iraq 2021
5-6 April 2021, Akre (Aqrah), Duhok, Iraq
http://ocs.uobaghdad.edu.iq/index.php/icge-otecheng/icgte

Second International Conference on Geotechnical Engineering-Iraq, 2021 (ICGE-2021) is going to be held on 5-6th April 2021 in Akre (Aqrah)/Duhok/Iraq. The conference is organized by the Iraqi Scientific Society of Soil Mechanics and Foundation Engineering (ISSSMFE) in collaboration with the College of Engineering/University of Baghdad and Technical Institute of Akre/Duhok Polytechnic University. The conference aims to provide a scientific platform to present and discuss the latest research and studies in geotechnical engineering and all related researches in different fields such as civil engineering, environmental engineering, and architectural engineering. This scientific event is a great chance for participants from both academics and industry to meet and exchange the development and experiences in these fields. This conference will be real opportunity to share new ideas and experiences face to face, establish business or research relations, and find global partners for future collaboration.

Themes of Conference

- Geotechnical Engineering

- Soil-Structure Interaction
- Structural Dynamics and Earthquakes
- Geoenvironmental Engineering and Sustainability
- Transportation Geotechnique and Materials
- Construction Management
- Remote Sensing and Surveying Engineering
- Environmental Engineering
- Architectural Engineering
- Water Resources Engineering

Conference Contact

Principal Contact Issmfe.conference@gmail.com
Support Contact Issmfe.conference@gmail.com

EUROENGEO 3RD EUROPEAN REGIONAL CONFERENCE OF IAEG, 8 - 12 April 2021, Athens, Greece, www.euroengeo2020.org

Rocscience International Conference on Numerical Modelling "The Evolution of Geotech: 25 Years of Innovation", April 20th - 21st, 2021, virtual www.rocscience.com/learning/rocscience-conference

2nd Vietnam Symposium on Advances in Offshore Engineering – Sustsainable Energy & Marine Planning, 22-24 April 2021, Ho Chi Minh City, Vietnam, https://vsoe2021.sciences-conf.org

16th International Conference of the International Association for Computer Methods and Advances in Geomechanics – IACMAG - CHALLENGES and INNOVATIONS in GEOMECHANICS, 03-05-2021, Torino, Italy, www.symposium.it/en/events/2020/16th-international-conference-of-iacmag?navbar=1

9th International Symposium on Geomechanics
3 - 6 May, 2021, Medellin, Colombia

Organizer: Sociedad Colombiana de Geotecnia and Universidad Nacional de Colombia

Telephone: + 57 4 425 5146

E-mail: gaalzate@unal.edu.co

ATS 2020 AUSTRALASIA TUNNELLING CONFERENCE, 10th – 13th May 2021, Melbourne, Australia, https://www.ats2020.com.au

EUROGEO WARSAW 2020 7th European Geosynthetics Congress, 16-19 May 2021, Warsaw, Poland, www.eurogeo7.org

TISOLS Tenth International Symposium on Land Subsidence, Living with Subsidence, 17-21 May 2021, Delft - Gouda, the Netherlands, www.tisols2020.org/tisols2020

7th International Conference on Industrial and Hazardous Waste Management 18 - 21 May, 2021, Chania, Crete, Greece, http://hwm-conferences.tuc.gr

2020 CHICAGO ICTG International Conference on Transportation Geotechnics, May 23 - 26, 2021, Chicago, Illinois, USA, http://conferences.illinois.edu/ICTG2020

Fifth International Conference on New Developments in Soil Mechanics and Geotechnical Engineering, 27 – 29 May 2021, Nicosia, Northern Cyprus https://zm2020.neu.edu.tr/

Joint meeting of ISSMGE TC201 and TC210, ICOLD TC E and TC LE "Dams and Levees: Particle Movements – Case Studies, Experiments, Theory", June, 2020, Budapest, Hungary, www.isc6-budapest.com

6th International Conference on Geotechnical and Geophysical Site Characterization "Toward synergy at site characterisation", June 2021, Budapest, Hungary, www.isc6-budapest.com

2021 ICOLD MARSEILLE - ICOLD 27th Congress - 89th Annual Meeting Sharing Water: Multipurpose of Reservoirs and Innovations, 4 - 11 June 2021, Marseille, France, https://cigb-icold2021.fr/en/

International Airfield and Highway Pavements Conference, June 6-9, 2021, Austin, Texas, USA, www.pavementsconference.org

MSL 2021 The 1st Mediterranean Symposium on Landslides SLOPE STABILITY PROBLEMS IN STIFF CLAYS AND FLYSCH FORMATIONS, 7-9 June 2021, Naples, Italy, https://medsymplandslides.wixsite.com/msl2021

9th International Conference on Computational Methods for Coupled Problems in Science and Engineering (COUPLED PROBLEMS 2021), 13-16 June 2021, Sardinia, Italy, coupledproblems_sec@cimne.upc.edu

Rapid Excavation and Tunneling Conference RETC2021, June 13-16, 2021, Las Vegas, Nevada, USA, www.retc.org

Cities on Volcanoes 11 - Volcanoes and Society: environment, health and hazards, 14-18 June 2021, Heraklion, Crete, https://pcoconvin.eventsair.com/volcanoes11

EGRWSE 2020 - 3rd International Conference on Environmental Geotechnology, Recycled Waste Materials and Sustainable Engineering, 17-19 June 2021, Izmir, Turkey, www.egrwse2020.com

2nd ICPE 2021 The Second International Conference on Pressin Engineering, 19-21 June 2021, Kochi, Japan, https://icpe-ipa.org/

3rd International Conference on Discrete Fracture Network Engineering (in conjunction with ARMA 2021)
June 23-25, Houston, Texas, USA
www.dfne2021.org

We are very excited to present the important advances that have occurred since the previous conference, as DFNE approaches are broadly applied in engineering, geology, and geophysics, providing practical solutions for rock mass characterization, geomechanics, and fluid flow and transport.

- DFN Fundamentals
- DFN Radioactive Waste Management
- DFN Civil / Infrastructure
- DFN Mining
- DFN Oil & Gas
- DFN Environmental
- DFN Geothermal
- DFN Induced Seismicity

1st International Conference on Sustainability in Geotechnical Engineering, ICSGE, 27-30 June 2021, Lisboa, Portugal, http://icsge.lnec.pt/#

IS-Cambridge 2020 10th International Symposium on Geotechnical Aspects of Underground Construction in Soft Ground, 28 June to 01 July 2021, Cambridge, United Kingdom, www.is-cambridge2020.eng.cam.ac.uk

ICONHIC2021: THE STEP FORWARD - 3rd International Conference on Natural Hazards & Infrastructure, 22 – 24 June 2021, Athens, GREECE, https://iconhic.com/2021

DFI Deep Mixing, 5-8 July 2020, TBD, Gdansk, Poland, www.dfi.org/DM2020

II International Seminar "Tailings and Waste Rock Disposal", July 12 – 14, 2021, Lima, Peru, www.geoingenieria.org.pe

7th ICRAGEE International Conference on Recent Advances in Geotechnical Earthquake Engineering and Soil Dynamics, 12-17 July 2021, Bengaluru, India, http://7icragee.org

AFRICA 2021 Water Storage and Hydropower Development for Africa, 13-15 July 2021, Lake Victoria, Uganda, www.hydropower-dams.com/africa-2021

GEOCHINA 2021 - 6th GeoChina International Conference Civil & Transportation Infrastructures: From Engineering to Smart & Green Life Cycle Solution, July 19 to 21, 2021, Nan-Chang, China, http://geochina2021.geoconf.org

PanAm Unsat 2021 3rd Pan-American Conference on Unsaturated Soils, 25-28 July 2021, Rio de Janeiro, Brazil, https://panamunsat2021.com

37th General Assembly of the European Seismological Commission, September 2021, Corfu, Greece, www.escgreece2020.eu

ACE 2020 14th International Congress on Advances in Civil Engineering, September 2021, Istanbul, Turkey, www.ace2020.org/en

XVIth International Congress AFTES 2021 Underground, a space for innovation, 6 to 8 September 2021, www.aftes2020.com

COMPLAS 2021 XVI International Conference on Computational Plasticity, Fundamentals and Applications, 7-10 September 2021, Barcelona, Spain, https://congress.cimne.com/complas2021/frontal/default.asp

RMEGV 2021 - 5th International Workshop on Rock Mechanics and Engineering Geology in Volcanic Fields, 9÷11 September 2021, Fukuoka, Japan, https://ec-convention.com/rmegv2021

SYDNEY 7iYGEC 2021 7th International Young Geotechnical Engineers Conference A Geotechnical Discovery Down Under, 10-12 September 2021, Sydney, Australia, http://icsmge2021.org/7iygec

SYDNEY ICSMGE 2021 20th International Conference on Soil Mechanics and Geotechnical Engineering, 12-17 September 2021, Sydney, Australia, www.icsgme2021.org

International Conference on Textile Composites and Inflatable Structures (MEMBRANES 2021), 13-15 September 2021, Munich, Germany, https://congress.cimne.com/membranes2021/frontal/default.asp

EUROCK TORINO 2021 - ISRM European Rock Mechanics Symposium Rock Mechanics and Rock Engineering from theory to practice, 20-25 September 2021, Torino, Italy, http://eurock2021.com

10th International Conference on Scour and Erosion (ICSE-10), October 17-20, 2021, Arlington, Virginia, USA, www.engr.psu.edu/xiao/ICSE-10 Call for abstract.pdf

3rd International Symposium on Coupled Phenomena in Environmental Geotechnics, 20-22 October 2021, Kyoto, Japan, https://cpeg2020.org

ARMS11 11th Asian Rock Mechanics Symposium, Challenges and Opportunities in Rock Mechanics, 21-25 October 2021, Beijing, China, www.arms11.com

EURO:TUN 2021 Computational Methods and Information Models in Tunneling, October 27th - 29th, 2021, Bochum, Germany, http://eurotun2021.rub.de

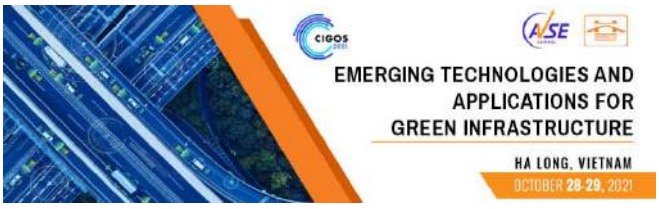

28-29 October 2021, Ha Long, Vietnam
https://cigos2021.sciencesconf.org

Since the first conference in 2010, the International Conference series on Geotechnics, Civil Engineering and Structures (CIGOS) has firmly established its international reputation as an important forum to attract a broad range of academics, researchers, designers and manufacturers, in order to promote professional and high-quality exchange of research knowledge and ideas.

The 6th edition, CIGOS 2021 co-organized by the Association of Vietnamese Scientists and Experts (AVSE Global) and the University of Transport Technology (UTT) in scientific collaboration with the National University of Civil Engineering (NUCE) will be held in Ha Long, Vietnam on October 28 to 29, 2021.

CIGOS 2021 welcomes the submission of quality papers from world-wide researchers, practitioners, policymakers and entrepreneurs with their recent advancements as well as knowledge and experiences on various topics related to the theme of "**Emerging Technologies and Applications for Green Infrastructure**". Moreover, CIGOS 2021 particularly aims at promoting beneficial economic partnership, technological transfers within enterprises as well as on developing the institutional cooperation on research and higher education.

The main topics of the conference include, but are not limited to:

- Advanced Modeling and Characterization of Structures (AMCS)
- Sustainable Construction Materials and Technologies (SCMT)
- Geotechnics for Environment and Energy Efficiency (GEEE)
- Smart Technologies for Big Construction Projects (STBCP)
- Architecture and Planning for Sustainable Community (APSC)
- Construction Economics and Management (CEM)
- Green Transport and Environment (GTE)
- BIGDATA and Data Mining (BDM)
- Digital Transformation and Internet of Things (DTIT)

For any query, please contact us at cigos@avseglobal.org.

5TH World Landslide Forum Implementation and Monitoring the USDR-ICL Sendai Partnerships 2015-2015, 2-6 November 2021, Kyoto, Japan, http://wlf5.iplhq.org

ISFOG 2020 4th International Symposium on Frontiers in Offshore Geotechnics, 8 – 11 November 2021, Austin, United States, www.isfog2020.org

2021 GEOASIA7 - 7th Asian Regional Conference on International Geosynthetics Society, November 22-26, 2021, Taipei, Taiwan, www.geoasia7.org

ICGE – Colombo – 2020 3rd International Conference in Geotechnical Engineering, 6-7 December 2021, Colombo, Sri Lanka, http://icgecolombo.org/2020/index.php

GeoAfrica 2021 - 4th African Regional Conference on Geosynthetics Geosynthetics in Sustainable Infrastructures and Mega Projects, 21-24 February 2022, Cairo, Egypt, https://geoafrica2021.org

ICEGT-2020 2nd International Conference on Energy Geotechnics, 10-13 April 2022, La Jolla, California, USA, https://icegt-2020.eng.ucsd.edu/home

WTC 2021 World Tunnel Congress 2021 - Underground solutions for a world in change, 22-28 April 2022, Copenhagen, Denmark, www.wtc2021.dk

LARMS 2021 – IX Latin American Rock Mechanics Symposium Challenges in rock mechanics: towards a sustainable development of infrastructure, 15 – 18 May 2022, Asuncion, Paraguay, https://larms2021.com

CPT'22

5th International Symposium on Cone Penetration Testing
8-10 June 2022, Bologna, Italy

The Italian Geotechnical Society (AGI) and the University of Bologna are pleased to announce the 5th International Symposium on Cone Penetration Testing, CPT'22, to be held in Bologna, Italy, on June 8-10, 2022. CPT'22, organized under the auspices of the ISSMGE Technical Committee TC102, follows the successful symposia held in Delft, The Netherlands (2018), Las Vegas, Nevada USA (2014), Huntington Beach, California USA (2010) and Linköping, Sweden (1995).

As tradition of the CPT events, which foster a lively debate on recent advancements on cone penetration testing, the Symposium aims at providing Researchers, Practitioners and Contractors with a unique opportunity of sharing up-to-date knowledge in equipment, testing procedures, data interpretation and related applications, as well as discussing emerging solutions and new ideas with the largest gathering of world's experts, academics and non-academics, working in the broad and dynamic area of CPTs.

Organizer

Italian Geotechnical Society (AGI) and University of Bologna (endorsed by TC102)

Contact Information

Contact person: Susanna Antonielli (AGI),
Prof. Guido Gottardi (University of Bologna)

Email: guido.gottardi2@unibo.it,
Email: agi@associazionegeotecnica.it

Eurock 2022

Rock and Fracture Mechanics in Rock Engineering and Mining
12÷15 September 2022, Helsinki, Finland

Themes

- Rock mass Characterization
- Geophysics in rock mechanics
- Mechanics of rock joints
- Jointed rock mass behaviour
- Rock support, probability based design
- Rock stress measurements
- Constitutive modelling of rock
- Rock drilling
- Blast induced fractures
- Rock engineering and mining education
- Geological disposal of spent nuclear fuel
- Recent advances in rock mechanics research
- Field and laboratory investigations
- Case studies

Contact Person: Lauri Uotinen
E-mail: lauri.uotinen@aalto.fi

3rd European Conference on Earthquake Engineering and Seismology (3ECEES), 19-24 June 2022, Bucharest, Romania, https://3ecees.ro

9th International Congress on Environmental Geotechnics
Highlighting the role of Environmental Geotechnics in Addressing Global Grand Challenges
26-29 June 2022, Chania, Crete island, Greece
www.iceg2022.org

The 9th International Congress on Environmental Geotechnics is part of the well established series of ICEG. This conference will be held on an outstanding resort in the town of Chania of the island of Crete in Greece. The theme of the conference is "Highlighting the role of Environmental Geotechnics in Addressing Global Grand Challenges" and will highlight the leadership role of Geoenvironmental Engineers play on tackling our society's grand challenges.

Contact Information

- Contact person: Dr. Rallis Kourkoulis
- Email: rallisko@grid-engineers.com

UNSAT2022
8th International Conference on Unsaturated Soils
June or September 2022, Milos island, Greece

6th Australasian Ground Control in Mining Conference – AusRock 2022
17 – 19 September 2022, Melbourne, Australia

Organizer: UNSW Sydney, AusIMM
Contact Person: Ismet Cambulat
E-mail: icambulat@unsw.edu.au

XII ICG - 12th International Conference on Geosynthetics, September 18 – 22, 2022, Rome, Italy, www.12icg-roma.org

28th European Young Geotechnical Engineers Conference and Geogames, 17 – 19 September 2022, Moscow, Russia https://t.me/EYGEC2020

11th International Conference on Stress Wave Theory and Design and Testing Methods for Deep Foundations
20 - 23 september 2022, De Doelen, Rotterdam, The Netherlands
https://www.kivi.nl/afdelingen/geotechniek/stress-wave-conference-2022

The conference will cover the application of static and dynamic test methods to deep foundations, both driven and cast-in-place, offshore as well as onshore. Subject matters that will be covered include wave mechanics applications to foundations, high strain dynamic testing, low strain integrity testing, rapid load testing, static load testing (compression, tension as well as bi-directional), soil-structure interaction from dynamic, rapid and static testing, lateral testing, vibratory analysis and monitoring of piles and sheet piles, and pile

installation effects and drivability in relation to soil investigation methods.

Today's energy transition has changed our view on deep foundations. The drive to lower the cost of renewable energies has resulted in upscaling in volume and size. As an example in the wind industry the turbine size has grown from 2 MW in 2000 up to 12 MW in 2020. This increase in size, in combination with increasing water and installation depths, is also reflected in the size of the used foundations, wich in turn provides challenges to the installation methods.

The current diameter of the monopile foundation already reaches 9 meter, and diameters up to 12 meter shall be common in the very near future.

Maybe even more important now than ever before is that we strive to limit our impact on the world's eco-system and environment. To protect the environment the industry is pushed to come up with foundation technologies that have a low environmental impact on emissions (CO2, NOx), and also generate low (underwater) noise levels. But as cities and urbanized areas around the world become more densely built and populated, not only emissions should be lowered but hindrance should be minimized as well to keep them livable. Therefore buildings in urbanized environment require foundation technologies that have a smaller footprint, and can be installed with lower displacements, noise and vibrations in the subsoil.

The conference shall cover the effects of the above mentioned global trends on the deep foundations and the applied installation technologies. The conference therefore shall discuss and demonstrate new installation technologies, soil investigation methods and other developments, and their effects (relation) on static and dynamic testing.

Themes

This conference aims to bring together engineers, educators, researchers and practitioners to create a better understanding and management of the stress wave theory as well as design, installation and testing methods for deep foundations. The following 8 themes are applicable:

- Load Testing including; High strain dynamic testing, Rapid load testing, Axial compression, tension, and bidirectional load testings, Lateral testing for conventional installation, vibration and other methods.
- Quality assurance testing for driven and drilled deep foundations, Low strain integrity testing, crosshole sonic logging, thermal profiling, etc.
- Wave mechanics applications
- Soil-structure interaction for dynamic, rapid and static testing, pile installation including novel installation techniques, static resistance to driving and dynamics.
- Vibration monitoring due to dynamic effects – theory and measurements
- Design codes and test standards for testing of deep foundations
- Case studies of driven and drilled deep foundation testing
- Environmental implications

Organisation

The conference will be organized by the Dutch department KIVI of the ISSMGE. The following contact details are applicable:

Stress Wave 2022 Organizing Committee
Attn. Angelique van Tongeren
Royal Society of Engineers (KIVI)
Phone: +31 (0)70-3919890
E-mail: SW2022@kivi.nl

88th ICOLD Annual Meeting & Symposium on Sustainable Development of Dams and River Basins, April 2023, New Delhi, India, https://www.icold2020.org

15th ISRM

International Congress in Rock Mechanics
9÷14 October 2023, Salzburg, Austria

Contact Person: Prof. Wulf Schubert
E-mail: salzburg@oegg.at

ΕΝΔΙΑΦΕΡΟΝΤΑ ΓΕΩΤΕΧΝΙΚΑ ΝΕΑ

Αυτά είναι τα «κόκκινα» σημεία στην Αττική που... δίνουν κατολισθήσεις

Κακιά Σκάλα, τρύπες του Καραμανλή και Μαλακάσα, είναι μόνο μερικά από τα... «κόκκινα» σημεία της Αττικής που θα μπορούσαν να εκδηλωθούν εκ νέου φαινόμενα κατολισθήσεων, έπειτα από έντονες φυσικές ή καιρικές συνθήκες.

Την ανάγκη να υπάρχει σαφής πληροφορία σε πραγματικό χρόνο ώστε φορείς και πολίτες να βρίσκονται σε ετοιμότητα ανά πάσα στιγμή, κάνει πράξη η ερευνητική ομάδα του Δημοκρίτειου Πανεπιστημίου Θράκης μέσω της ερευνητικής πρότασης, η οποία αφορά στην δημιουργία χαρτών κατολισθητικού κινδύνου.

Οπως εξηγεί στον Ελεύθερο Τύπο ο επικ. Καθηγητής ΔΠΘ Γιώργος Παπαθανασίου και μέλος της ερευνητικής ομάδας, «ο κυριότερος σκοπός της έρευνας είναι να συνδράμει τις δημόσιες αρχές και ειδικότερα αυτές της Περιφέρειας Αττικής με μια μεθοδολογία εκτίμησης και ποσοτικοποίησης του κατολισθητικού κινδύνου που μπορεί δυνητικά να προκύψει σε διάφορες θέσεις στα γεωγραφικά και διοικητικά όρια στην Περιφέρεια Αττικής».

Οπως σημειώνει ο κ. Παπαθανασίου, με δεδομένο ότι στην Αττική ζει σχεδόν ο μισός πληθυσμός της χώρας, αυτό την καθιστά πρώτη προκειμένου να εφαρμοστεί το μοντέλο της ερευνητικής πρότασης.

Ποιες περιοχές όμως έχουν εκδηλώσει κατά το παρελθόν φαινόμενα κατολισθήσεων;

– Διαχρονικά παρατηρούμενες αστοχίες πρανών στα παράλια της ΒΔ Αττικής (Αλεποχώρι, Ψάθα)

– Οι καταστροφικές πλημμύρες στη Δυτική Αττική, τον Νοέμβριο του 2017 (περιοχές Μάνδρας, Ν. Περάμου και Μεγάρων) διέβρωσαν τμήματα πρανών οδών και ρεμάτων με τέτοιο τρόπο, ώστε είναι πολύ πιθανό μεσομακροπρόθεσμα οι διαβρώσεις αυτές να οδηγήσουν σε αστοχίες πρανών.

– Η μεγάλη καταστροφή στην περιοχή Μάτι της Ανατολικής Αττικής υποχρεώνει τις αρμόδιες υπηρεσίες σε μέτρα άμεσης αντιμετώπισης εν όψει μάλιστα κινδύνου κατολισθήσεων, εδαφικών ροών, βραχοκαταπτώσεων σε περίπτωση παρατεταμένων και έντονων βροχοπτώσεων.

– Εντός του κύριου αστικού ιστού της Αθήνας και συγκεκριμένα στην Περιφερειακή Οδό του Αττικού Αλσους (Τουρκοβούνια) και Πανοράματος (Γαλάτσι), διαχρονικά παρατηρούνται καταπτώσεις βράχων με άμεσο κίνδυνο στους διερχόμενους οδηγούς, πεζούς και κατοίκους κατάντη των επισφαλών πρανών.

– Στην Πεντέλη (π.χ. Ντράφι). παρατηρούνται κατά περιόδους αστοχίες πρανών.

– Στον αυτοκινητόδρομο Αθήνας – Θεσσαλονίκης, στο ύψος της Μαλακάσας, έχει συμβεί στο παρελθόν (1995) μια από τις σημαντικότερες κατολισθήσεις σε όλη τη χώρα.

– Επίσης, σε πολλά ρέματα που διατρέχουν την Αττική, παρατηρούνται διαβρώσεις του μετώπου ή και υποσκαφές στο πόδι των πρανών τους, με αποτέλεσμα να κινδυνεύουν άμεσα γειτνιάζοντες δρόμοι, εγκαταστάσεις και κατοικίες.

Σε κάθε περίπτωση, όπως τονίζει ο καθηγητής, τόσο οι δημόσιες αρχές, όσο και τα άτομα που λαμβάνουν αποφάσεις ως προς την αντιμετώπιση του κατολισθητικού κινδύνου, χρειάζονται χάρτες που να απεικονίζουν τις περιοχές που μπορεί να επηρεασθούν από αστοχίες πρανών, ώστε όχι μόνο να ληφθούν υπόψη σε σχέδια αστικής ανάπτυξης και οικιστικής επέκτασης αλλά και για να χρησιμοποιηθούν για τον σχεδιασμό εκ των προτέρων των απαραίτητων μέτρων αντιμετώπισης σε περιπτώσεις δυνητικών καταστροφών από επικείμενες κατολισθήσεις.

Μελλοντικός στόχος των ερευνητών είναι η δημιουργία ενός συστήματος κατολισθητικών φαινομένων στα πλαίσια ενός επόμενου ερευνητικού προγράμματος.

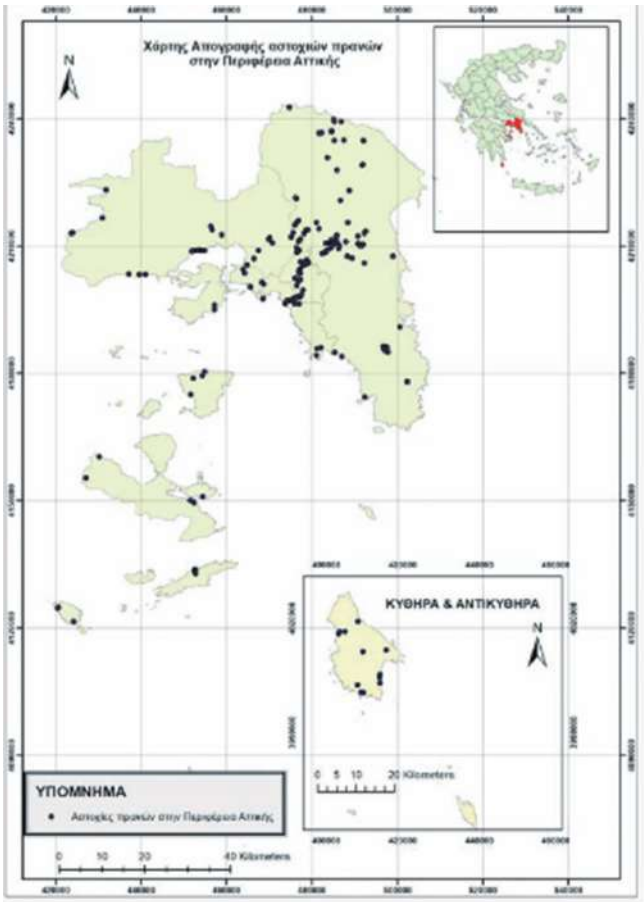

Τα δεδομένα που λαμβάνει υπόψη η ερευνητική ομάδα είναι:

(Α) Τοπογραφία (υψόμετρο, κλίση, προσανατολισμός πρανών).

(Β) Γεωλογία (τύποι πετρωμάτων, μανδύας αποσάθρωσης, ρήγματα και ειδικότερα απόσταση από ενεργά ρήγματα ή πλά-

τος-έκταση διαρρήξεων).

(Γ) Υδρογεωλογία (υδροπερατότητα, απόσταση από ποτάμια).

(Δ) Γεωμορφολογία (παλαιές κατολισθήσεις, ιστορικό κατολισθήσεων το οποίο είναι σημαντική πληροφορία για τον προσδιορισμό της κατολισθητικής επικινδυνότητας και της διακινδύνευσης).

(Ε) Χρήσεις Γης και παράγοντες ανθρωπογενούς προέλευσης (αλλαγές χρήσεων γης, απόσταση από δρόμους που γειτνιάζουν με πρανή και ορύγματα, πρανή για κατασκευές κτιρίων, δίκτυα ύδρευσης στα οποία η διαρροή μπορεί να προκαλέσει αστοχία, λατομεία όπου οι δονήσεις που λαμβάνουν χώρα δύναται να προκαλέσουν κατολισθήσεις, φράγματα και ταμιευτήρες όπου επηρεάζουν τις υδρολογικές συνθήκες και πιθανόν να επιφέρουν την αστοχία πρανών της λεκάνης κατάκλυσης).

(ΣΤ) Σεισμικότητα (συσχέτιση μεγέθους – συχνότητας, ιστορικότητα χαρτών έντασης που συνδέονται με κατολισθήσεις).

(Ζ) Κλιματολογία (βροχόπτωση, θερμοκρασία).

Η ερευνητική ομάδα απαρτίζεται από τους: Παπαθανασίου Γιώργος επικ. καθηγητής ΔΠΘ, Γκανάς Θανάσης διευθυντής ερευνών Γεωδυναμικού Ινστιτούτου ΕΑΑ, Ταβουλάρης Νίκος δρ. τεχνικός γεωλόγος ΕΜΠ και τον Αργυράκη Παναγιώτη υποψ. διδάκτωρ.

Σημειώνεται ότι η έρευνα (Διαχείριση της κατολισθητικής διακινδύνευσης στην Περιφέρεια Αττικής) συγχρηματοδοτείται από την Ελλάδα (υπουργείο Οικονομίας και Ανάπτυξης) και την Ευρωπαϊκή Ενωση (Ευρωπαϊκό Κοινωνικό Ταμείο), μέσω του Επιχειρησιακού Προγράμματος ΑΝΑΠΤΥΞΗ ΑΝΘΡΩΠΙΝΟΥ ΔΥΝΑΜΙΚΟΥ, ΕΚΠΑΙΔΕΥΣΗ & ΔΙΑ ΒΙΟΥ ΜΑΘΗΣΗ για την Πράξη με τίτλο «Υποστήριξη ερευνητών με έμφαση στους νέους ερευνητές-κύκλος Β'» (Μ.Ι.S. 5050327).

(Μαρίνα Ξυπνητού / B2G, 19/11/2020,
https://www.b2green.gr/el/post/85579)

ΕΝΔΙΑΦΕΡΟΝΤΑ - ΣΕΙΣΜΟΙ

Aftershocks are fluid-driven and decay rates controlled by permeability dynamics

Stephen A. Miller

Abstract

One aspect of earthquake physics not adequately addressed is why some earthquakes generate thousands of aftershocks while other earthquakes generate few, if any, aftershocks. It also remains unknown why aftershock rates decay as ~1/time. Here, I show that these two are linked, with a dearth of aftershocks reflecting the absence of high-pressure fluid sources at depth, while rich and long-lasting aftershock sequences reflect tapping high-pressure fluid reservoirs that drive aftershock sequences. Using a physical model that captures the dominant aspects of permeability dynamics in the crust, I show that the model generates superior fits to observations than widely used empirical fits such as the Omori-Utsu Law, and find a functional relationship between aftershock decay rates and the tectonic ability to heal the co- and post-seismically generated fracture networks. These results have far-reaching implications, and can help interpret other observations such as seismic velocity recovery, attenuation, and migration.

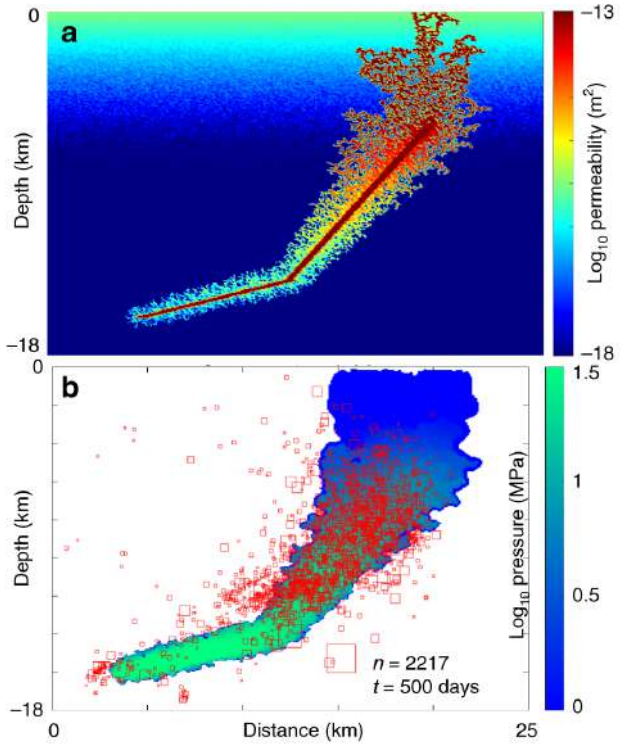

Citation: Miller, S.A. Aftershocks are fluid-driven and decay rates controlled by permeability dynamics. *Nat Commun* **11,** 5787 (2020). https://doi.org/10.1038/s41467-020-19590-3.

(Nature / Nature Communications, **Volume 11**, Article number: 5787 (2020), 13 November 2020, https://www.nature.com/articles/s41467-020-19590-3#citeas)

Devonian, Silurian and Cambro-Ordovician Layers

Satellite image of a part of the Piqiang Fault (China), a northwest trending strike-slip fault that runs roughly perpendicular to the thrust faults for more than 70 kilometers. The reddish, greenish and brownish bands are continental Devonian sandstones, Silurian deeper marine sediments and Cambro-Ordovician limestones, respectively. They form one of several parallel ridges (up to 1200 m high) which all are composed of the same stack of rocks and belong to the Keping Shan thrust belt immediately south of the Southern Tien Shan Mountains. (Photo: NASA Earth Observatory)

Here's What'll Happen When Plate Tectonics Grinds to a Halt

A new study says we may only have another 1.45 billion years to enjoy the dynamic action of Earth's geologic engine.

The Pu'u o Maui cinder cone is part of a dormant volcano in Haleakala National Park on Maui, Hawai.

There's no geological artist quite like Earth's plate tectonics.

Thanks to this ongoing operation, we have mountains and oceans, terrifying earthquakes, incandescent volcanic eruptions, and new land being born every single second.

But nothing lasts forever.

Eventually, the mantle will cool to such an extent that this planetwide conveyor belt will grind to a halt. At that point, you can say farewell to the carbon cycle, as well as the constant reshaping and reshuffling of landmasses that have been big drivers of evolution over eons.

Quiming Cheng, a mathematical geoscientist and president of the International Union of Geological Sciences, is the latest to take on the prophetic role of predicting when this bleak day may arrive. He calculates that the shutdown will arrive in about 1.45 billion years. That's well before the sun is expected to swell into a red giant and consume us in its death throes roughly 5.4 billion years from now.

The study, published this month in *Gondwana Research*, has provoked controversy, and some experts argue that we can never accurately predict the end of plate tectonics. But scientists largely agree that such an end will arrive one day, putting Earth on a path to a geologic standstill.

So, what will our home world be like when those major planetary processes give up the ghost?

Tectonic Jigsaw

Figuring that out means first understanding how plate tectonics work. Earth was born 4.54 billion years ago in the pyres of the early solar system. Once entirely molten, the heat generated by its formation and radioactive materials in the rock began to escape. As the planet cooled, Earth settled into its current layered structure, with a dense inner iron core, a liquid outer core, and a brittle upper mantle and crust sandwiching the hot, plastic-like rock of the lower mantle.

Anywhere between 600 million and 3.5 billion years ago, slabs made of the crust and upper mantle–collectively known as the lithosphere–became cold and dense enough to be able to sink into the lower mantle, kicking off the era of plate tectonics. The lithosphere became divided into a jigsaw puzzle of plates that are constantly jostling across the planet's surface, driving geological action above and below the oceans.

At mid-ocean ridges, mantle material rises, decompresses, and triggers profuse melting, creating oceanic lithosphere. The colder and denser edges of the slabs help pull this lithospheric plate away from these ridges and down into the depths. They usually dive beneath a less dense oceanic or continental plate in a process known as subduction. This activity generates explosive volcanoes and fresh crust at the surface.

When two continental slabs collide, they buckle, and mountain ranges like the Alps or the Himalaya form. Upwelling mantle plumes can sometimes appear beneath continental or oceanic slabs, and this ever-moving center of melting creates chains of volcanoes.

At some point, though, the mantle will cool to such an extent that the slabs can no longer sink into it, and several studies have attempted to predict when this will transpire.

Cheng's new paper uses mathematical models to estimate how fast the mantle is cooling, based on what we know about the intensity of the planet's magmatic activity from three billion years ago to now. That, he says, gives us a first-order estimate of when plate tectonics will end.

On the Path to Stillness

Regardless of the precision of this figure, plate tectonics will inevitably perish, says Ken Hudnut, a research geophysicist working with the United States Geological Survey. When that day arrives, it "may well be the end of the world as we know it."

Earth would likely enter a single lid regime, a completed jigsaw of titanic slabs that will no longer drift or sink. Mountain building will stop, but Earth will still have an atmosphere, so erosion by wind and waves will shave down the mighty peaks to hilly plateaus. Eventually, much of the flattened continents will be underwater.

Subduction zones will no longer exist, so while earthquakes will still happen every now and then, truly earthshattering events above magnitude 7 or so will be consigned to history. At the same time, much of the world's explosive volcanism would be extinguished—although volcanoes would not be entirely snuffed out.

Mars, a world of failed plate tectonics, did manage to forge some impressive volcanic features, including Olympus Mons, the largest volcano in the solar system. Without moving plates, a long-lived upwelling mantle plume focused plenty of crustal melting on that one single spot.

While the mantle of future Earth remains warm enough to convect and partially melt, we would get similar but scattered stationary hot spots of plume-driven volcanism. We would never get anything as large as Olympus Mons on Earth, as our gravitational field is too strong, and anything that massive and tall would simply sink into the crust. Instead, our voluminous volcanoes would be flatter and far more spread out.

And as happens today, parts of the lower lithosphere would continue to peel off and fall into particularly hot parts of the mantle. This would cause mantle material to rise in its place, pushing up the crust and forming isolated mountain ranges and associated basins. This activity would cause minor earthquakes and maybe even additional pockets of volcanism.

"These are the processes that shape Venus' surface," says Robert Stern, a plate tectonics expert at the University of Texas at Dallas, referring to another world without fully-functioning plate tectonics. But eventually, as cooling continues, those mechanisms will also cease to be, and the planet's final volcanic lights will be snuffed out. The mantle will be relatively frigid, and Earth will "become a dead planet, like Mercury," he says.

Perhaps just before it does, Earth's liquid core will cool enough to end convection, causing the planet's protective magnetic field to fail. The sun's stream of energetic particles will strip away our atmosphere, and its expansion will boil away the oceans.

"There is not a lot to look forward to after plate tectonics' demise," Hudnut says. The planet will just keep getting flatter and more boring, he predicts, until "Earth splashes into what's left of the sun."

Prophets of Plate Tectonics

Other researchers have come up with different plate tectonic death dates. One 2016 study used extremely detailed but simplified computer simulations to put the end date at five billion years, roughly around the time of the sun's demise.

Another 2008 paper used evidence of past plate tectonic activity to suggest that plate tectonics are intermittent. Its authors predict that the next major pause will take place 350 million years from now, when the Pacific Ocean closes and its many subduction zones deactivate.

"The question is a good one, and yes, it will end eventually," says Stern. However, he fundamentally disagrees with the new study's reasoning. "I don't believe any estimated time of death for plate tectonics," he says.

Christopher Scotese, an emeritus plate tectonics specialist at the University of Texas at Arlington, suggests that the paper shouldn't have focused on mantle cooling. Instead, it should have based its efforts on the slab pull mechanism, because "slab pull rules."

Instead of a gradual slowdown, Scotese predicts that plate tectonics will be invigorated during the next one to two billion years, before the conveyor belt ends. He reasons that as the mantle heat flow diminishes, the slabs will become extremely cool and dense, allowing them to subduct faster.

Hudnut notes that predicting any future geophysical events is, even in the short term, "challenging beyond current human capabilities." Despite this, he emphasizes that it's good to think ahead. And while none of the predictive papers are perfect, they do highlight the complexity of the subject matter and where there are intriguing gaps in our knowledge of how our own home planet operates.

The wildly differing models "help clarify our ideas about why plate tectonics happen in the first place," Scotese says. "There may be things we figure out about the future that can be applied to the past."

(Robin George Andrews / NATIONAL GEOGRAPHIC, August 29, 2018, https://www.nationalgeographic.com/science/2018/08/news-happens-plate-tectonics-end-earth-mountains-volcanoes-geology/)

Ancient fragment of the Pacific Ocean found buried 400 miles below China

Scientists have identified an old piece of the Pacific Ocean – the ancient remains of its long-ago seabed – extending hundreds of miles underneath China, as it is pulled downward into Earth's mantle transition zone.

This rocky slab that used to line the bottom of the Pacific is a relic of the oceanic lithosphere, the outermost layer of Earth's surface, composed of the crust and the solid outermost parts of the upper mantle.

The lithosphere isn't always destined to enjoy the views up top, however. The upper surface layer is composed of several fragmented tectonic plates, which slowly move and shift around at the surface, occasionally running into each other.

During these collisions, a geological process called subduction can occur, where one plate gets forced under the other at subduction zones, and ends up being driven ever deeper into the planet.

In a new study, scientists from China and the US have now witnessed this epic phenomenon taking place at greater depths than ever before observed.

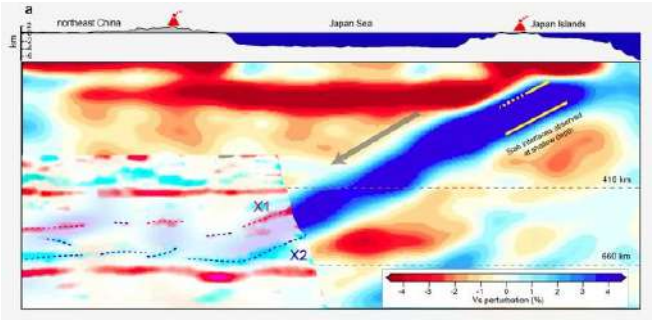

The scientists discovered the ancient remains of a long-ago seabed – extending hundreds of miles underneath China in Earth's mantle transition zone. (Image credit: CHEN Qifu's group)

Prior to this, scientists had recorded subducting slabs probing the boundaries at depths of about 200 kilometers (roughly 125 miles).

Now, thanks to giant network of over 300 seismic stations spread around northeastern China, researchers were able to see the event at a much lower point, imaging parts of the tectonic plate that used to lie under the Pacific Ocean being pushed into the mantle's mid-level transition zone, at depths ranging between 410–660 kilometers (254–410 miles) below Earth's surface.

To interpret the sinking slab, the team identified two seismic velocity discontinuities, regions far underground where seismic waves encounter anomalies. In this case, two anomalies were encountered, which the team says related to both the top and bottom sides of the plunging plate.

"Based on detail seismological analyses, the upper discontinuity was interpreted to be the Moho discontinuity of the subducted slab," says geophysicist Qi-Fu Chen from the Chinese Academy of Sciences.

"The lower discontinuity is likely caused by partial melting of sub-slab asthenosphere under hydrous conditions in the seaward portion of the slab."

While the plate's subduction can be seen in process below China, the subduction zone itself lies far to the east, with the slab being angled at a relatively shallow 25-degree angle downwards.

"Japan is located about where the Pacific plate reaches around 100-kilometre depths," says seismologist Fenglin Niu from Rice University.

Thanks to the new imaging, scientists are getting a better idea of what happens to a subducted slab when it reaches this part of the transition zone, including how deformed it gets, and how much water content it loses from its oceanic crust.

"A lot of studies suggest that the slab actually deforms a lot in the mantle transition zone, that it becomes soft, so it's easily deformed," Niu says.

"We are still debating whether this water is totally released in that depth. There is increasing evidence that a portion of the water stays inside the plate to go much, much deeper."

The findings are reported in *Nature Geoscience*.

This article was originally published by ScienceAlert. Read the original article here.

(Peter Dockrill - ScienceAlert, 18.11.2020, https://www.livescience.com/ancient-fragment-of-pacific-ocean-under-china.html)

Distinct slab interfaces imaged within the mantle transition zone

Xin Wang, Qi-Fu Chen, Fenglin Niu, Shengji Wei, Jieyuan Ning, Juan Li, Weijun Wang, Johannes Buchen and Lijun Liu

Oceanic lithosphere descends into Earth's mantle at subduction zones and drives material exchange between Earth's surface and its deep interior. The subduction process creates chemical and thermal heterogeneities in the mantle, with the strongest gradients located at the interfaces between subducted slabs and the surrounding mantle. Seismic imaging of slab interfaces is key to understanding slab compositional layering, deep-water cycling and melting, yet the existence of slab interfaces below 200□km remains unconfirmed. Here, we observe two sharp and slightly dipping seismic discontinuities within the mantle transition zone beneath the western Pacific subduction zone that coincide spatially with the upper and lower bounds of the high-velocity slab. Based on a multi-frequency receiver function waveform modelling, we found the upper discontinuity to be consistent with the Mohorovičić discontinuity of the subducted oceanic lithosphere in the mantle transition zone. The lower discontinuity could be caused by partial melting of sub-slab asthenosphere under hydrous conditions in the seaward portion of the slab. Our observations show distinct slab–mantle boundaries at depths between 410 and 660□km, deeper than previously observed, suggesting a compositionally layered slab and high water contents beneath the slab.

(*Nature Geoscience* (2020), 09 November 2020, https://www.nature.com/articles/s41561-020-00653-5)

Τεκτονικές δυνάμεις διαλύουν το νησί της Μαδαγασκάρης

Το εξωτικό νησί βρίσκεται στα όρια τεκτονικών πλακών που απομακρύνονται η μία από την άλλη

Ήταν πριν από περίπου 200 εκατομμύρια χρόνια όταν η υπερήπειρος της Παγγαίας άρχισε να σπάει σε κομμάτια και να δίνει τη θέση της στις ηπείρους που γνωρίζουμε σήμερα. Η ίδια διαδικασία συνεχίζεται όμως μέχρι σήμερα στην ανατολική Αφρική.

Σύμφωνα μάλιστα με την τελευταία μελέτη για το θέμα, η τεκτονική αναδιάταξη φτάνει μέχρι το νησί της Μαδαγασκάρης στον Ινδικό Ωκεανό, το οποίο μια μέρα θα χωριστεί σε τουλάχιστον τρία κομμάτια.

Το μεγαλύτερο μέρος της σημερινής Αφρικής εδράζεται στην αφρικανική τεκτονική πλάκα, η οποία όμως βρίσκεται σε διαδικασία διάσπασης: το ανατολικό κομμάτι της, γνωστό ως πλάκα της Σομαλίας, έχει αρχίσει να κινείται προς τα ανατολικά, μια μετατόπιση που τελικά θα χωρίσει τα κράτη της ανατολικής Αφρικής από την υπόλοιπη ήπειρο.

Πέρα όμως από την κεντρική αφρικανική πλάκα (ή πλάκα της Νουβίας) και την πλάκα της Σομαλίας, μια πληθώρα μικρότερων λιθοσφαιρικών πλακών εμπλέκεται στις τεκτονικές αλλαγές της ανατολικής Αφρικής.

«Οι περισσότερες προηγούμενες μελέτες υπεδείκνυαν ότι η επέκταση εντοπίζεται μόνοι σε στενές ζώνες γύρω από τεκτονικές μικροπλάκες οι οποίες κινούνται ανεξάρτητα από τις μεγάλες πλάκες» αναφέρει η Σάρα Σταμπς του Τεχνολογικού Ινστιτούτου της Βιρτζίνια, περισσότερο γνωστού ως Virginia Tech.

Η Σταμπς και οι συνεργάτες της ανατρέπουν τώρα αυτή την εικόνα με μελέτη τους που δημοσιεύεται στην έγκριτη επιθεώρηση **Geology**.

Η ομάδα της Σταμπς, στην οποία συμμετείχαν συνάδελφοί της στην Πορτογαλία αλλά και στο Αντανανάριβο, πρωτεύουσα της Μαδαγασκάρης, βασίστηκε σε μετρήσεις από πομπούς GPS που λειτουργούν στην ανατολική Αφρική, τη Μαδαγασκάρη και διάφορα άλλα νησιά του Ινδικού.

Η ανάλυση των μετρήσεων και τα υπολογιστικά μοντέλα που χρησιμοποίησαν οι ερευνητές έδειξαν ότι η διαδικασία διάσπασης είναι πιο περίπλοκη και καλύπτει μεγαλύτερη έκταση από ό,τι είχε εκτιμηθεί ως σήμερα.

Η εξωτική Μαδαγασκάρη, αναφέρουν οι ερευνητές, βρίσκεται στο ανατολικό άκρο μιας τεκτονικά ενεργής περιοχής που έχει πλάτος 600 χιλιόμετρα και φτάνει δυτικά μέχρι το εσωτερικό της Αφρικής.

Ολόκληρο το νησί έχει αρχίσει να διασπάται, καθώς το νότιο τμήμα κινείται μαζί με την μικροπλάκα του Λουάντλ, ενώ το κεντρικό τμήμα ακολουθεί την πλάκα της Σομαλίας. Το υπόλοιπο του νησιού παραμορφώνεται καθώς αυτά τα δύο τμήματα απομακρύνονται το ένα από το άλλο,

Η μελέτη ουσιαστικά θέτει νέα όρια για την μικροπλάκα του Λουάντλ και την πλάκα της Σομαλίας, κάτι που σύμφωνα με τους ερευνητές έχει κρίσιμη σημασία για την κατανόηση της συμπεριφοράς των λιθοσφαιρικών πλακών.

Η Μαδαγασκάρη, πάντως, δεν πρόκειται να σπάσει σε κομμάτια σύντομα.

Όπως λέει η Σταμπς, «ο ρυθμός της διάσπασης δεν υπερβαίνει τα μερικά χιλιοστά τον χρόνο, οπότε θα περάσουν εκατομμύρια χρόνια πριν σχηματιστούν νέοι ωκεανοί».

Όταν αυτό συμβεί, όμως, η Μαδαγασκάρη θα πάψει να υπάρχει, όπως συνέβη και με ολόκληρη την υπερήπειρο της Παγγαίας.

Σε αυτόν τον πλανήτη, τίποτα δεν μένει για πάντα.

(Βαγγέλης Πρατικάκης / in.gr, 16 Νοεμβρίου 2020, https://www.in.gr/2020/11/16/b-science/episthmes/tektonikes-dynameis-dialyoun-nisi-tis-madagaskaris/)

Redefining East African Rift System kinematics

D.S. Stamps, C. Kreemer, R. Fernandes, T.A. Rajaonarison, G. Rambolamanana

East African Rift System plate geometries and surface motions are some of the least constrained in the context of global plate motion models. In this study, we used GPS data to constrain Somalian plate rotation and to suggest a new tectonic plate geometry for the region. In addition, we tested geologic data from the Southwest Indian Ridge and new GPS data on Madagascar to determine refined kinematics of the Lwandle microplate. A zone of broad deformation was discovered, extending from the eastern boundary of the Rovuma microplate, across the Comoros Islands, and including parts of central and northern Madagascar. Madagascar is fragmenting, with southern Madagascar rotating with the Lwandle microplate and a piece of eastern and south-central Madagascar moving with the Somalian plate. Divergence of the Nubian-Somalian plate system across the East African Rift System involves both diffuse deformation and strain accommodation along narrow rift segments that bound rigid blocks.

https://doi.org/10.1130/G47985.1

(GeoScienceWorld / Geology (2020) / RESEARCH ARTICLE| SEPTEMBER 23, 2020, https://pubs.geoscienceworld.org/gsa/geology/article-abstract/doi/10.1130/G47985.1/591119/Redefining-East-African-Rift-System-kinematics?redirectedFrom=fulltext)

ΕΝΔΙΑΦΕΡΟΝΤΑ - ΓΕΩΛΟΓΙΑ

Santorini Volcano History

https://vimeo.com/113042536

Based on researches from several scientists, institutes and universities. Made by Nikos Korakakis. Music by Ross Bugden (youtube). After Effects, Photoshop, Illustrator

Συγκλονιστικές εικόνες στη Χαβάη

https://www.facebook.com/ubitravels/videos/2044145775922641

Offshore submarine freshwater discovery raises hopes for islands worldwide

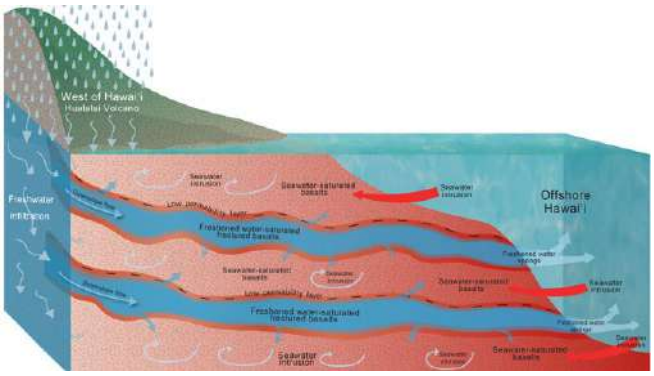

Fresh groundwater onshore-to-offshore transport mechanism.

Twice as much freshwater is stored offshore of Hawai'i Island than was previously thought, according to a University of Hawai'i study with important implications for volcanic islands around the world. An extensive reservoir of freshwater within the submarine southern flank of the Hualālai aquifer has been mapped by UH researchers with the Hawai'i EPSCoR 'Ike Wai project. The groundbreaking findings, published in *Science Advances*, reveal a novel way in which substantial volumes of freshwater are transported from onshore to offshore submarine aquifers along the coast of Hawai'i Island.

This mechanism may provide alternative renewable resources of freshwater to volcanic islands worldwide. "Their evidence for separate freshwater lenses, stacked one above the other, near the Kona coast of Hawai'i, profoundly improves the prospects for sustainable development on volcanic islands," said UH Manoa School of Ocean and Earth Science and Technology (SOEST) Dean Brian Taylor.

Paradigm shift

Through the use of marine controlled-source electromagnetic imaging, the study revealed the onshore-to-offshore movement of freshwater through a multilayer formation of basalts embedded between layers of ash and soil, diverging from previous groundwater models of this area. Conducted as a part of the National Science Foundation-supported 'Ike Wai project, research affiliate faculty Eric Attias led the marine geophysics campaign.

"Our findings provide a paradigm shift from the conventional hydrologic conceptual models that have been vastly used by multiple studies and water organizations in Hawai'i and other volcanic islands to calculate sustainable yields and aquifer storage for the past 30 years," said Attias. "We hope that our discovery will enhance future hydrologic models, and consequently, the availability of clean freshwater in volcanic islands."

Co-author Steven Constable, a professor of geophysics at the Scripps Institution of Oceanography, who developed the controlled source electromagnetic system used in the project, said, "I have spent my entire career developing marine electromagnetic methods such as the one used here. It is really gratifying to see the equipment being used for such an impactful and important application. Electrical methods have long been used to study groundwater on land, and so it makes sense to extend the application offshore."

Kerry Key, an associate professor at Columbia University who employs electromagnetic methods to image various oceanic Earth structures, who not involved in this study, said, "This

new electromagnetic technique is a game changing tool for cost-effective reconnaissance surveys to identify regions containing freshwater aquifers, prior to more expensive drilling efforts to directly sample the pore waters. It can also be used to map the lateral extent of any aquifers already identified in isolated boreholes."

Two-times more water

Donald Thomas, a geochemist with the Hawai'i Institute of Geophysics and Planetology in SOEST who also worked on the study, said the findings confirm two-times the presence of much larger quantities of stored groundwater than previously thought.

"Understanding this new mechanism for groundwater...is important to better manage groundwater resources in Hawai'i," said Thomas, who leads the Humu'ula Groundwater Research project, which found another large freshwater supply on Hawai'i Island several years ago.

Offshore freshwater systems similar to those flanking the Hualālai aquifer are suggested to be present for the island of O'ahu, where the electromagnetic imaging technique has not yet been applied, but, if demonstrated, could provide an overall new concept to manage freshwater resources.

The study proposes that this newly discovered transport mechanism may be the governing mechanism in other volcanic islands. With offshore reservoirs considered more resilient to climate change-driven droughts, volcanic islands worldwide can potentially consider these resources in their water management strategies.

This project is supported by the National Science Foundation EPSCoR Program Award OIA #1557349.

Story Source:

Materials provided by University of Hawaii at Manoa.

Journal Reference:

Eric Attias, Donald Thomas, Dallas Sherman, Khaira Ismail and Steven Constable. **Marine electrical imaging reveals novel freshwater transport mechanism in Hawai'i**. *Science Advances*, 2020 DOI: 10.1126/sciadv.abd4866

(Science Daily, November 25, 2020, https://www.sciencedaily.com/releases/2020/11/201125154829.htm)

Marine electrical imaging reveals novel freshwater transport mechanism in Hawai`i

Eric Attias, Donald Thomas, Dallas Sherman, Khaira Ismail and Steven Constable

Abstract

Conventional hydrogeologic framework models used to compute ocean island sustainable yields and aquifer storage neglect the complexity of the nearshore and offshore submarine environment. However, the onshore aquifer at the island of Hawai`i exhibits a notable volumetric discrepancy between high-elevation freshwater recharge and coastal discharge. In this study, we present a novel transport mechanism of freshwater moving from onshore to offshore through a multilayer formation of water-saturated layered basalts with interbedded low-permeability layers of ash/soil. Marine electromagnetic imaging reveals ~35 km of laterally continuous resistive layers that extend to at least 4 km from west of Hawai`i's coastline, containing about 3.5 km3 of freshened water. We propose that this newly found transport mechanism of fresh groundwater may be the governing mechanism in other volcanic islands. In such a scenario, volcanic islands worldwide can use these renewable offshore reservoirs, considered more resilient to climate change-driven droughts, as new water resources.

Science Advances 25 Nov 2020: Vol. 6, no. 48, eabd4866
DOI: 10.1126/sciadv.abd4866

(https://advances.sciencemag.org/content/6/48/eabd4866)

Geologists assess debris flow risk in Santa Cruz Mountains

History could tell story of future disasters

California Geological Survey Geologist David Longstreth stands in a historic debris flow, pondering the conditions that triggered the mass of soil, boulders and water to move.

Past dozens of burned playsets, cars and properties where all that remains is a single chimney, lies a geologic relic. Where most would see a mishmash of jumbled boulders, California Geological Survey scientists spot a debris flow.

"Geology tends to repeat itself," David Longstreth said, an engineering geologist with the California Geological Survey.

This Boulder Creek debris flow occurred around 40 years ago, according to Longstreth. Measuring by geologic time, which spans more than 4.9 billion years, the historic flow is mere seconds in time.

"Debris flows tend to occur in the same location over and over, so we're thinking another one could come here," Longstreth said.

Investigating historic debris flows is paramount to get insight on which areas of Santa Cruz County could be at risk this coming winter and beyond. California Geological Survey scientists working with Santa Cruz County, and the U.S. Geological Survey, are tracking what triggers debris flows using drones, rain gauges and cameras.

'They're everywhere'

Past a "DEBRIS FLOW HAZARD" sign on Highway 9 where work crews are clearing culverts in preparation for the rainy season, Longstreth spots another.

"Once your eyes get tuned in and you're driving around here, you start seeing debris flows everywhere," Longstreth said.

Historic debris flows underlie Boulder Creek, Brookdale and Ben Lomond roads, homes and businesses. It takes a trained eye to "see" these hidden deposits. To find them, Longstreth and other scientists scan satellite maps.

Longstreth estimates that the most ancient debris flows along the Highway 9 corridor could be more than 2 million years old.

That flow history, combined with relatively high rainfall rates, as well as steep slopes that drain into creeks and rivers near densely populated areas, are some of the factors that make the Santa Cruz Mountains vulnerable, Longstreth said.

"There is a huge risk for debris flows here," Longstreth said.

The CZU August Lighting Complex fire also stripped many of those slopes of trees, shrubs and root systems that armor landscapes from debris flows and floods. During a storm, that means more water will runoff and quickly accumulate in streams.

California Geological Survey scientists David Longstreth and Alex Morelan walk up Big Creek, searching for ancient debris flows.

The CZU Complex fire, ignited by lightning on Aug. 16, burned more than 86,500 acres in Santa Cruz and San Mateo counties. In Santa Cruz County alone, 911 homes were destroyed in the blaze.

For the last month, the California Geological Survey has been on the ground examining ancestral debris flows and setting up monitoring gear. It's been a seven-day-a-week job, Longstreth said.

"We're exhausted, everyone in our department, has been working at breakneck speed to try to get everything implemented," Longstreth said.

Desperate for data

Debris flows are fast-moving slurries of rock, soil and sediment carried in water, according to Amy East, a U.S. Geological Survey researcher collaborating with Longstreth.

"They're so powerful, large debris flows pick up boulders, cars and can absolutely destroy a house very quickly," East said.

While some debris flow monitoring sites are near residential areas, in Swanton, or off of Highway 9, others are in more remote places. Debris flows that are smaller in size, or happen in rugged areas, often don't cause such destruction and aren't recorded. Those flows can also be more challenging to track, but are equally important to investigate, East said.

Near the merging of Berry Creek and Big Creek, lie historic debris flows. This area was badly burned in the CZU August Lighting Complex fire.

Monitoring and studying debris flows at large in Northern California is a relatively new science. Most post-fire debris flow studies have been done in the southern part of the state.

East and other geologists want to understand what level of rainfall triggers debris flows in different regions of Santa Cruz County. Tracking the level of rainfall that triggers a flow is crucial for emergency planning efforts.

"Having the timing, and knowing what rain conditions were going on when the debris flow happened, will eventually guide evacuation protocols for this area," East said.

East and Longstreth with the California Geological Survey have set up rain gauges and cameras at more than a dozen sites around the CZU Complex burn scar.

"We're desperate to get data from Northern California," Longstreth said.

Drones take flight

On the western side of the CZU Complex burn scar, California Geological Survey scientists are investigating a severely burned area near Swanton. Longstreth and colleague Alex Morelan walk along Big Creek, past charred redwoods and downed pines. Longstreth points out loose sandy soil and broken up rock that litters the hillslopes.

"That mud, sand and silt is what's providing the mass in a debris flow," Longstreth said. "It's like a locomotive coming down and pushing the boulders in front of it."

Those boulders are what pummel houses, destroy infrastructure and kill people. They can range from a couple of feet in diameter, to the size of a car, weighing up to a couple of tons. In the 1982 Love Creek landslide and mudflow, 22 residents were killed and nine homes were destroyed. The natural disaster remains the deadliest in modern Santa Cruz County history.

The geologists are once again searching for a symptomatic jumble of boulders, sand and soil. At the confluence of Berry Creek and Big Creek, they find multiple ancestral debris flows.

Part of the team's monitoring work includes taking drone surveys.

"These surveys will help us make a more quantitative check on whether a debris flow did or didn't happen," Morelan, a geologist with the California Geological Survey, explained. Morelan also has a Federal Aviation Administration commercial drone pilot's license.

It's crucial to finish these surveys prior to the rainy season. Historically that wet season runs from November to May. During that time, the Santa Cruz County area might see anywhere from 23 inches to more than 30 inches of rain.

Alex Morelan, a geologist with the California Geological Survey, flies a drone on top of an ancient debris flow.

Between thin trunked patches of doug firs, and tan oaks Morelan has a narrow path — it's tricky flying here, he said.

The flight lasts about 30 minutes, and Morelan takes hundreds of photos that will be transformed into a 3D model of the debris flow.

The team is training Colleen Murphy, a UC Santa Cruz geology graduate student researcher, who's also a drone pilot. After storm events, Murphy will fly at these same monitoring sites and take images.

That post-storm flight will be compared to the baseline drone surveys Morelan's completed – using that data the scientists will be able to quantify the volume of boulders, sediment and woody debris that moved in a flow.

Murphy says she and the other scientists will track boulder and water level movement at these observation sites, as well as watch if a stream becomes cloudy, or muddy looking. They'll also be monitoring nearby culverts and bridges.

"A lot of what we know about debris flows has come from Southern California," Murphy said. "Because of different topography, vegetation, climate, the threshold that triggers a catastrophic debris flow down there, might be different than thresholds in Santa Cruz."

Tracking any changes at these historic debris-flow sites during the winter will help Murphy and other geologists understand what conditions create flows across Santa Cruz County.

In the long term, this data could also aid officials in making more precise evacuation decisions.

"You can't cry wolf," said the U.S. Geological Survey's East.

"Evacuations are costly, they're risky for people that have a hard time moving, like in a nursing home," East said. The COVID-19 pandemic further complicates evacuations.

Emergency planners must tow a challenging line, East said. If orders are issued often, residents could tire of heeding notices and get evacuation fatigue.

"You also don't want to go the other way and tell people you probably don't need to evacuate, and then there's a January 2018 Montecito situation," East said, referencing the Santa Barbara County debris flows that killed 20 people.

If the USGS or California Geological Survey scientists confirm a debris flow happens, first they'll immediately alert Santa Cruz County officials. While this information won't be used in the short-term for evacuation orders, Longstreth said he hopes that by notifying the county if a culvert or bridge is clogged, emergency responders could remove that choke-point before the next storm.

"Then the second priority is gathering the data over the long term, so that we can better predict when debris flows happen," Longstreth said.

Longstreth said he and his colleagues hope to launch additional debris flow monitoring sites to get more data.

But for the USGS and California Geological Survey scientists to expand their research, the monitoring would have to sustain into the future. Both government agencies are paying for this research using their own limited budgets, in an as-needed manner.

That means it's not clear how long the science can continue, Longstreth said. For the work to be consistent, the California Geological survey would need a funded program.

"I've worked on a lot of these debris flow projects and I've seen a lot of people killed in similar circumstances," Longstreth said.

"It's a really bad feeling when that happens," he said, "and so as much as it's in my power to use my skills to help more people, I want to do that."

(Hannah Hagemann / Monterey Herald, November 29, 2020, https://www.mercurynews.com/2020/11/29/geologists-assess-debris-flow-risk-in-santa-cruz-mountains)

ΕΝΔΙΑΦΕΡΟΝΤΑ - ΠΕΡΙΒΑΛΛΟΝ

The Arctic Ocean photographed in the same place 105 years ago vs today

ΕΝΔΙΑΦΕΡΟΝΤΑ - ΛΟΙΠΑ

Επινοήσεις υδραυλικών και ηλεκτρολόγων

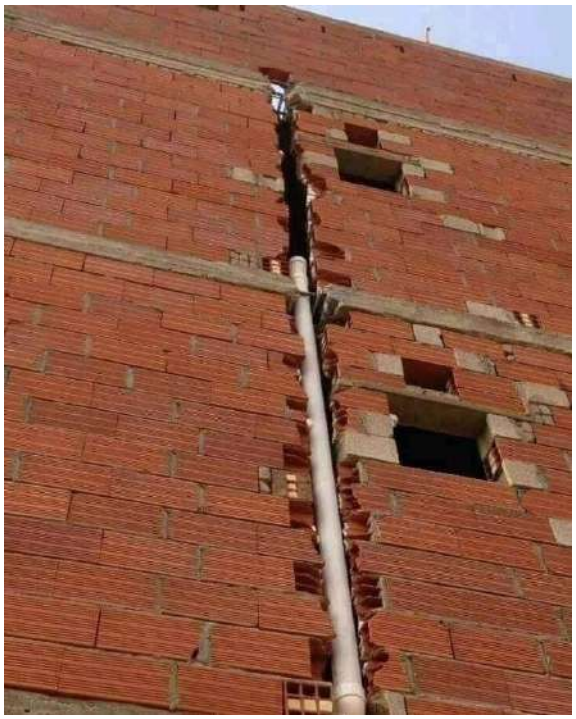

Rising Iceberg

When an iceberg falls off the cliff, it sinks due to momentum, but because the density of iceberg is less and the seawater is heavier, the iceberg instantly resurfaces, floats to the surface and continues to rise upward, forming a pillar!

Extremely rare capture.

https://www.facebook.com/kurdistangeology/videos/2718756408230576

Η αρχαία Εγνατία Οδός συντηρείται και αποκαλύπτει την ιστορία της

Η πόλη της Καβάλας έχει την τύχη -και ταυτόχρονα το προνόμιο- να διατηρεί στις παρυφές της, σε αρκετά καλή κατάσταση, ένα μεγάλο τμήμα της αρχαίας Εγνατίας Οδού, του μεγάλου αυτού δρόμου που ένωνε την Ανατολή με τη Δύση και που μέχρι και τις αρχές του 20ού αιώνα αποτελούσε μια από τις κυριότερες οδικές αρτηρίες της νότιας Βαλκανικής.

Είναι αυτός ο δρόμος που διέσχισε ο Απόστολος Παύλος μαζί με τους μαθητές του Σίλα, Τιμόθεο και Λουκά για να φτάσουν από το λιμάνι της αρχαίας Νεάπολης (σημερινή Καβάλα), στη φημισμένη πόλη των Φιλίππων και να διδάξουν το Ευαγγέλιο, ιδρύοντας έτσι την πρώτη ευρωπαϊκή και ελληνική εκκλησία. Είναι ο δρόμος τον οποίο διέσχισαν χιλιάδες Ρωμαίοι στρατιώτες για να πολεμήσουν στην ξακουστή μάχη των Φιλίππων που έμελλε να αλλάξει την ιστορία τής τότε ρωμαϊκής αυτοκρατορίας.

Αυτό το κομμάτι του λιθόστρωτου δρόμου, που δεν ξεπερνάει σε μήκος το περίπου ενάμισι χιλιόμετρο, θα επιδιώξει να συντηρήσει και να αναδείξει η Εφορεία Αρχαιοτήτων Καβάλας - Θάσου με χρηματοδότηση ύψους 350.000 ευρώ στο πλαίσιο της ΟΧΕ Πολιτιστικής Διαδρομής της Εγνατίας Οδού της Περιφέρειας Ανατολικής Μακεδονίας και Θράκης.

Πριν από περίπου είκοσι χρόνια, ο Δήμος Καβάλας είχε εκπονήσει ένα πρόγραμμα ανάδειξης του λιθόστρωτου μονοπατιού της αρχαίας Εγνατίας, καθώς μέχρι τότε μόνο μια μεγάλη σύγχρονη ταμπέλα πάνω στην εθνική οδό Καβάλας - Δράμας θύμιζε στους διερχόμενους οδηγούς την ύπαρξη του δρόμου. Με τη νέα μελέτη της Εφορείας Αρχαιοτήτων γίνεται εκ νέου μια προσπάθεια για τη συντήρηση και την ανάδειξη της αρχαία οδικής αρτηρίας ώστε να λειτουργήσει ως πόλος έλξης επισκεπτών από την Ελλάδα και το εξωτερικό.

Οι εργασίες συντήρησης και ανάδειξης αναμένεται να ξεκινήσουν την Άνοιξη, εφόσον δεν υπάρξουν καθυστερήσεις λόγω της πανδημίας του κορωνοϊού.

Η αρχαία Εγνατία Οδός σήμερα

Η αρχαία Εγνατία Οδός είναι σήμερα χωρισμένη σε δύο τμήματα, εξαιτίας των αυτοκινητόδρομων που έχουν διανοιχθεί στο ύψωμα του Αγίου Σίλα (σύμφωνα με την παράδοση εδώ κά-

θισε να ξεκουραστεί ο Απόστολος Παύλος μετά τον ανηφορικό δρόμο από το λιμάνι της Νεάπολης, προτού συνεχίσει τη διαδρομή του προς τους Φιλίππους).

Το ένα τμήμα κατηφορίζει από τον Άγιο Σίλα προς τον συνοικισμό του Σταυρού και βλέπει προς την εύφορη πεδιάδα των Φιλίππων. Το δεύτερο και πιο ενδιαφέρον τμήμα της παλιάς Εγνατίας, με μήκος 1.100 μέτρα, ξεκινά και τελειώνει στην περιοχή κάτω από το σημερινό γενικό νοσοκομείο της πόλης. Ο επισκέπτης μπορεί εύκολα να περπατήσει στο διατηρημένο πέτρινο οδόστρωμα που ανηφορίζει δίπλα στο ρέμα ή ακόμα καλύτερα να το κατηφορίσει, έχοντας μπροστά του την όμορφη θέα της πόλης και του κάστρου στη χερσόνησο της Παναγίας, παίρνοντας ταυτόχρονα και μια ιδέα για την εικόνα που αντίκριζαν τα παλιά χρόνια οι επισκέπτες της Καβάλας.

(naftemporiki.gr, Πέμπτη, 12 Νοεμβρίου 2020, https://www.naftemporiki.gr/story/1656778/i-arxaia-egnatia-odos-suntireitai-kai-apokaluptei-tin-istoria-tis)

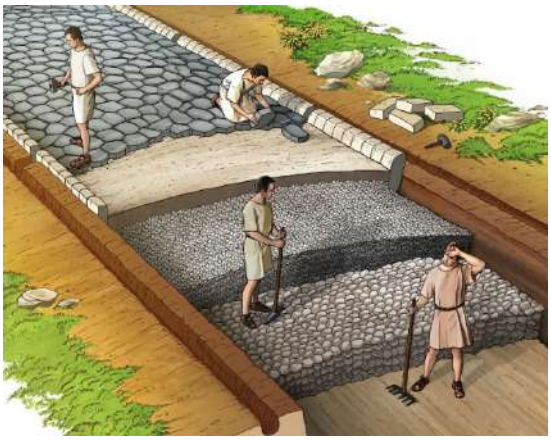

'All roads lead to Rome!' (Omnes viae Romam ducunt!)

Romans were famous for their roads (Latin singular: via) which allowed military, people and goods to travel quickly across their huge empire. They used stones, sometimes mixed with cement, sand, broken tiles and curving stones in order for the water to drain.

ΝΕΕΣ ΕΚΔΟΣΕΙΣ ΣΤΙΣ ΓΕΩΤΕΧΝΙΚΕΣ ΕΠΙΣΤΗΜΕΣ

ΚΑΤΟΛΙΣΘΗΣΕΙΣ ΣΤΗΝ ΕΛΛΑΔΑ
Εδαφομηχανική στην Πράξη

Σπύρος Καβουνίδης

Το βιβλίο παρουσιάζει 11 επιλεγμένες κατολισθήσεις στην Ελλάδα, με τη σημασία τους και τις ιδιαιτερότητες τους, την έρευνα και μελέτη τους και τα μέτρα αποκατάστασής τους, επιδεικνύοντας την πρακτική εφαρμογή της θεωρίας της εδαφομηχανικής σε πραγματικές συνθήκες.

Ιδιαίτερη αναφορά γίνεται σε κατολισθήσεις σε «ημιβραχώδεις» σχηματισμούς που αφθονούν στην Ελλάδα.

Επίσης γίνεται ειδική αναφορά στις αναλύσεις ευστάθειας σε τρεις διαστάσεις και την πιθανή χρησιμότητά τους στην ανάλυση κατολισθήσεων.

«Πολλές κατολισθήσεις συμβαίνουν σε "ημιβραχώδεις" σχηματισμούς. Ιδιαίτερα συμβαίνει αυτό σε μάργες και σχιστόλιθους που αφθονούν στην Ελλάδα. Το πρόβλημα εδώ είναι ότι αυτοί οι σχηματισμοί μπορεί να "εξαπατήσουν" τον μελετητή καθ' ότι (στην άθικτη μορφή τους εμφανίζουν υψηλή αντοχή. Όμως, συχνά, εμπεριέχουν ασυνέχειες με πολύ μικρότερη αντοχή, που αν αποτελέσουν μέρος της επιφάνειας ολίσθησης μπορεί να οδηγήσουν σε πολύ μικρότερη αντοχή από την υπολογιζόμενη βάσει του άθικτου υλικού».

Ο Σπύρος Καβουνίδης γεννήθηκε στην Αθήνα τον Δεκέμβριο του 1944. Πολιτικός Μηχανικός Ε.Μ.Π. – M.Sc., Ph.D. Stanford University. Δίδαξε ως Lecturer στο Imperial College του Λονδίνου (1978-80). Πρόεδρος της Ελληνικής Επιστημονικής Εταιρείας Εδαφομηχανικής και Γεωτεχνικής Μηχανικής (1998-2005). Πρόεδρος και Διευθύνων Σύμβουλος της εταιρείας «ΕΔΑΦΟΣ Σύμβουλοι Μηχανικοί Α.Ε.»

(Εκδόσεις ΠΑΠΑΣΩΤΗΡΙΟΥ, Νοέμβριοε 2020)

BIM for Project Managers: Digital construction management

Peter Barnes

BIM for Project Managers is a concise practical guide which shows how cutting-edge BIM related technologies can facilitate the successful management of construction and infrastructure projects. Focused specifically on core project management topic areas, the book shows how BIM can act as a catalyst for key project management functions in construction and lead to improved collaboration, communication and co-ordination. It also describes new skills and competencies which project managers need to acquire to work effectively on BIM projects, and important legal and contractual issues including dispute avoidance, copyright, liability and insurance. Covering the full project lifecycle from briefing, inception and pre-construction through to project closure or disposal, the book enables project managers to facilitate the use of BIM across the entire lifecycle.

BIM for Project Managers is a core reference that empowers project managers to play a more proactive role in BIM implementation at both project and organisational levels. Students seeking to understand how to integrate the new technology and methodologies of BIM with established principles of planning and project management also find this an indispensable reference.

(ICE Publishing, 30 November 2020)

ΗΛΕΚΤΡΟΝΙΚΑ ΠΕΡΙΟΔΙΚΑ

An official journal of the International Society for Soil Mechanics and Geotechnical Engineering
www.geocasehistoriesjournal.org/pub/issue/view/45

Ολοκληρώθηκε η έκδοση του Τεύχους 3 του Τόμου 5 του του International Journal of Geoengineering Case Histories με τα παρακάτω περιεχόμενα:

Application of Hybrid Drained-Undrained Model for Analyzing the Stability of Reinforced Soil Structures Over Soft Foundations with Prefabricated Vertical Drains, David Espinoza, Chunling Li, Lucas de Melo, Ranjiv Gupta

Pressuremeter Testing Along Interstate 10 in Tucson, Arizona, Naresh C. Samtani

Analysis of a Static Loading Test on an Instrumented Cased CFA Pile in Silt and Sand, Jakub Gabriel Kania, Kenny Kataoka Sørensen, Bengt Fellenius

Evaluation of Constitutive Models in Prediction of Surface Settlements in Cohesive Soils – A Case Study: Mashhad Metro Line 2, Behnam Eslami, Aliakbar Golshani, Sina Arefizadeh

Geo-Trends Review
A Crowdsourcing Magazine for the Geotechnical Engineering Community - Issue #13 - November 2020
https://www.mygeoworld.com/geotrends/issues/13-november-2020

International Geosynthetics Society

Κυκλοφόρησε το IGS Newsletter της International Geosynthetics Society με τα παρακάτω περιεχόμενα:

IGS NEWSLETTER – November 2020

Helping the world understand the appropriate value and use of geosynthetics

https://www.geosyntheticssociety.org/newsletters/

- Watch: The Launch Of The IGS Foundation READ MORE
- The GeoAmericas 2020 Corporate Case Study Competition Winners READ MORE
- Speakers Announced For ISGPEG 2021 READ MORE
- Free Access to Giroud Lectures READ MORE
- Results of the 4th Chinese National GeoWall Competition READ MORE
- XXX Italian National Conference on Geosynthetics READ MORE
- IGSE Webinar Report: Sustainable Soil Reinforcement READ MORE
- Online International Forum on Geosynthetics, Chengdu, China READ MORE
- IGS Chapter Focus: Portugal READ MORE
- Sustainability eBook Now In: Spanish! Turkish! Japanese!
- Calendar of Events

READ MORE AT GEOSYNTHETICSSOCIETY.ORG

ΕΚΤΕΛΕΣΤΙΚΗ ΕΠΙΤΡΟΠΗ ΕΕΕΕΓΜ (2019 – 2022)

Πρόεδρος	:	Μιχάλης ΜΠΑΡΔΑΝΗΣ, Δρ. Πολιτικός Μηχανικός, ΕΔΑΦΟΣ ΣΥΜΒΟΥΛΟΙ ΜΗΧΑΝΙΚΟΙ Α.Ε. mbardanis@edafos.gr, lab@edafos.gr
Α' Αντιπρόεδρος	:	Χρήστος ΤΣΑΤΣΑΝΙΦΟΣ, Δρ. Πολιτικός Μηχανικός, ΠΑΝΓΑΙΑ ΣΥΜΒΟΥΛΟΙ ΜΗΧΑΝΙΚΟΙ Ε.Π.Ε. editor@hssmge.gr, ctsatsanifos@pangaea.gr
Β' Αντιπρόεδρος	:	Μιχάλης ΠΑΧΑΚΗΣ, Πολιτικός Μηχανικός mpax46@otenet.gr
Γενικός Γραμματέας	:	Γιώργος ΜΠΕΛΟΚΑΣ, Δρ. Πολιτικός Μηχανικός, Επίκουρος Καθηγητής ΤΕΙ Αθήνας gbelokas@teiath.gr, gbelokas@gmail.com
Ταμίας	:	Γιώργος ΝΤΟΥΛΗΣ, Πολιτικός Μηχανικός, ΕΔΑΦΟΜΗΧΑΝΙΚΗ Α.Ε.- ΓΕΩΤΕΧΝΙΚΕΣ ΜΕΛΕΤΕΣ Α.Ε. gdoulis@edafomichaniki.gr
Έφορος	:	Γεώργιος ΓΚΑΖΕΤΑΣ, Δρ. Πολιτικός Μηχανικός, Ομότιμος Καθηγητής Ε.Μ.Π. gazetas@central.ntua.gr, gazetas50@gmail.com
Μέλη	:	Ανδρέας ΑΝΑΓΝΩΣΤΟΠΟΥΛΟΣ, Δρ. Πολιτικός Μηχανικός, Ομότιμος Καθηγητής ΕΜΠ aanagn@central.ntua.gr
		Παναγιώτης ΒΕΤΤΑΣ, Πολιτικός Μηχανικός, ΟΜΙΛΟΣ ΤΕΧΝΙΚΩΝ ΜΕΛΕΤΩΝ Α.Ε. otmate@otenet.gr
		Μαρίνα ΠΑΝΤΑΖΙΔΟΥ, Δρ. Πολιτικός Μηχανικός, Αναπληρώτρια Καθηγήτρια Ε.Μ.Π. mpanta@central.ntua.gr
Αναπληρωματικά Μέλη	:	Χρήστος ΣΤΡΑΤΑΚΟΣ, Πολιτικός Μηχανικός, ΝΑΜΑ Α.Ε. stratakos@namalab.gr
		Βάλια ΞΕΝΑΚΗ, Δρ. Πολιτικός Μηχανικός, ΕΔΑΦΟΜΗΧΑΝΙΚΗ Α.Ε. vxenaki@edafomichaniki.gr
Εκδότης	:	Χρήστος ΤΣΑΤΣΑΝΙΦΟΣ, Δρ. Πολιτικός Μηχανικός, ΠΑΝΓΑΙΑ ΣΥΜΒΟΥΛΟΙ ΜΗΧΑΝΙΚΟΙ Ε.Π.Ε. editor@hssmge.gr, ctsatsanifos@pangaea.gr

ΕΕΕΕΓΜ

Τομέας Γεωτεχνικής
ΣΧΟΛΗ ΠΟΛΙΤΙΚΩΝ ΜΗΧΑΝΙΚΩΝ
ΕΘΝΙΚΟΥ ΜΕΤΣΟΒΙΟΥ ΠΟΛΥΤΕΧΝΕΙΟΥ
Πολυτεχνειούπολη Ζωγράφου
15780 ΖΩΓΡΑΦΟΥ

Τηλ. 210.7723434
Τοτ. 210.7723428
Ηλ-Δι. secretariat@hssmge.gr ,
geotech@central.ntua.gr
Ιστοσελίδα www.hssmge.org (υπό κατασκευή)

«ΤΑ ΝΕΑ ΤΗΣ ΕΕΕΕΓΜ» Εκδότης: Χρήστος Τσατσανίφος, τηλ. 210.6929484, τοτ. 210.6928137, ηλ-δι. ctsatsanifos@pangaea.gr, editor@hssmge.gr, info@pangaea.gr

«ΤΑ ΝΕΑ ΤΗΣ ΕΕΕΕΓΜ» «αναρτώνται» και στην ιστοσελίδα www.hssmge.gr